Quasi-analytical modelling of advective-diffusive transport in porous media

By

Damien Paul Verrall, BSc, BE *JCU*

A thesis submitted to James Cook University

for the degree of

Doctor of Philosophy

School of Engineering and Physical Sciences

December 2015

Typeset in LaTeX 2_ε.

Except where acknowledged in the customary manner, the material presented in this thesis is, to the best of my knowledge, original and has not been submitted in whole or part for a degree at any university.

Damien Paul Verrall, BSc, BE *JCU*

Acknowledgements

This thesis would not have been possible without the help of many people. The following list of acknowledgements is probably deficient, and if I have neglected anyone, I apologise.

First and foremost I would like to thank my parents, Paul and Marie, without whose support and encouragement this thesis could never have been written.

In particular, I thank Wayne Read, my primary supervisor. His guidance, suggestions and advice during my candidature has been invaluable. Again, this thesis could not have been written without him.

For a multitude of reasons I have had various associate supervisors for short periods during my candidature. All have been helpful in some way. Thank you to Kumar Narayan, Graeme Sneddon and Ron White.

Finally, I would like to thank all my friends and family for their encouragement over the years. In particular, thank you to Leonie Mynott, who went beyond encouragement and proofread this thesis.

List of publications

- Verrall, D. P., Read, W. W. & Narayan, K. A. (2009). Predicting salt advection in groundwater from saline aquaculture ponds. *Journal of Hydrology, 364*(3-4), 201–206.

- Verrall, D. P., Read,W.W. & Narayan, K. A. (2009). Computational aspects of accurately modelling salt advection beneath aquaculture ponds. *Proceedings of the 13th biennial computational techniques and applications conference, CTAC-2006* (Vol. 48, pp. C1075–C1089). ANZIAM J.

- Verrall, D. P. & Read, W. W. (2012). Predicting diffusion in aquifers beneath saline ponds. *Journal of Hydrology, 475*, 150–157.

- Verrall, D. P. & Read, W. W. Equations for predicting contamination from leaky ponds through saturated unconfined aquifers. (In preparation)

- Verrall, D. P. & Read, W. W. (2015). A quasi-analytical approach to the advection-diffusion-reaction problem, using operator splitting. *Applied Mathematical Modelling.* (In press)

- Verrall, D. P. & Read, W. W. Split analytical operator technique as applied to the pond problem. (In preparation)

Statement of contribution of others

Chapter No.	Details of publication on which chapter is based	Nature and extent of the intellectual input of each author, including the candidate
2	Verrall, D. P., Read, W. W. & Narayan, K. A. (2009). Predicting salt advection in groundwater from saline aquaculture ponds. *Journal of Hydrology, 364* (3-4), 201–206.	The main idea in this paper originated with Read. It was the seed for the Ph.D topic explored in this thesis. Verrall wrote the first draft of the paper, with a subsequent partial rewrite performed by Read. Verrall performed all subsequent drafts with additional editorial input from Read and Narayan. Verrall developed the figures.
3	Verrall, D. P., Read,W.W. & Narayan, K. A. (2009). Computational aspects of accurately modelling salt advection beneath aquaculture ponds. *Proceedings of the 13th biennial computational techniques and applications conference, CTAC-2006* (Vol. 48, pp. C1075–C1089). ANZIAM J.	The main idea in this paper originated with Verrall. Verrall wrote all drafts of the paper with revision and editorial input from Read and Narayan. Verrall developed the figures.

TABLE 1: Statement of contribution of others. *(Continued over...)*

Chapter No.	Details of publication on which chapter is based	Nature and extent of the intellectual input of each author, including the candidate
4	Verrall, D. P. & Read, W. W. (2012). Predicting diffusion in aquifers beneath saline ponds. *Journal of Hydrology, 475*, 150–157.	The main idea in this paper originated from discussions between Verrall and Read. Verrall wrote all drafts of the paper with revision and editorial input from Read. Verrall developed the figures.
5	Verrall, D. P. & Read, W. W. Equations for predicting contamination from leaky ponds through saturated unconfined aquifers. (In preparation)	The idea in this paper is a logical extension of the work in the previous chapters/papers. Verrall wrote all drafts of the paper with revision and editorial input from Read. Verrall developed the figures.
6	Verrall, D. P. & Read, W. W. (2015). A quasi-analytical approach to the advection-diffusion-reaction problem, using operator splitting. *Applied Mathematical Modelling.* (In press)	The main idea in this paper originated from Verrall. Verrall wrote all drafts of the paper with revision and editorial input from Read. Verrall developed the figures.
7	Verrall, D. P. & Read, W. W. Split analytical operator technique as applied to the pond problem. (In preparation)	The idea in this paper is a logical extension of the work in the previous chapter/paper. Verrall wrote all drafts of the paper with revision and editorial input from Read. Verrall developed the figures.

TABLE 1: Statement of contribution of others.

Abstract

This thesis formulates mathematical modelling techniques to investigate groundwater contamination from a leaky saline pond situated above a freshwater aquifer. This problem has received little attention from researchers, but given the increasing prevalence of land based aquaculture, and the fact that saline ponds can be considered a proxy for other types of contaminated ponds, for example, tailings dams, it's a scenario that deserves more consideration. Unfortunately, it's also a problem that (currently) cannot be solved mathematically using analytical techniques. As such, it falls to numerical methods when a solution is required. However, although numerical methods will always give a solution, problems such as truncation error and numerical diffusion often cast doubt on the result. Therefore, this thesis will instead explore combined analytical/numerical techniques (or quasi-analytical techniques) as a potential alternative.

The major transport processes in groundwater contamination are advection and diffusion. These processes are coupled, with each affecting the evolution of the other through time. However, depending on the problem, often one of these processes can be ignored. This is the initial approach taken in this thesis. Given a leaky contaminated pond, separate quasi-analytical solutions are devised for the individual processes of advection and diffusion. These then form the basis of two additional quasi-analytical techniques, which solve for contaminant transport via combined advection-diffusion. Using the above techniques, mathematical experimentation also revealed general empirical equations which simplify the modelling of contaminant transport beneath leaky contaminated ponds.

Contents

List of tables

List of figures

1

Introduction

1.1 Rationale

As the title suggests, this thesis concerns the modelling of advective-diffusive transport in porous media, or (perhaps) more succinctly: predicting groundwater flow and contamination. Groundwater resources comprise more than 98% of the world's liquid fresh water, with lakes and streams (which are often fed by groundwater) being the remainder (Bouwer, 2000). Therefore, understanding groundwater flow and contamination is crucial for the management of these resources. Indeed, many countries are acutely dependent on groundwater for agricultural, municipal and industrial purposes, and in these circumstances contamination can be catastrophic. Unfortunately, groundwater is easily contaminated by a variety of means, and often happens unseen and unsuspected. Over-use of chemical fertilisers, leakage of hazardous substances from storage containers, or bacterial contamination from septic tanks are just a few examples of the ways in which groundwater contamination occurs (Fetter, 2001). The (typically) long residence time of water in groundwater systems often means that by the time contamination is discovered, the problem is well beyond any short term remediation.

A groundwater contaminant often of interest is salt. Lateral seawater intrusion is a common occurrence in coastal aquifers worldwide and has received much attention (Bear, 1999), while in Australia, salt mobilised from underground deposits by a rising water table degrades valuable farmland, leading to a corresponding impact on local communities (for a qualitative description refer to Bennett (1998)). However, recently concern has arisen over another source of salt contamination: the placement of aquaculture farms in close proximity to traditional farmland. In particular, when the aquaculture (saltwater) ponds are placed above a freshwater aquifer being used for irrigation, fears of groundwater contamination are inevitable (Bristow et al., 2006).

Leakage from aquaculture ponds, and the resultant environmental effects have been largely overlooked by researchers. However, the increasing prevalence of land based

aquaculture requires that this potential source of contamination be investigated. Indeed, a saline aquaculture pond can be regarded as a proxy for other types of contaminated ponds (for example, tailings dams) sitting above freshwater aquifers. The lack of research in this area is therefore all the more surprising. Liu et al. (2003) have shown seepage from saltwater fish ponds above a freshwater aquifer to be a major source of contamination, while Simmons and Narayan (1998) have numerically modelled salt transport from saline disposal basins in the Murray-Darling basin. However, these studies did not investigate salt transport throughout the aquifer. Given a leaky saline pond, how long will it be before it pollutes other areas, or will it pollute those areas at all? Questions like these need to be answered, and accurately, in order to avoid the economic and environmental consequences of a vital groundwater reservoir and surrounding land becoming unusable. However, to answer these questions we must have an adequate understanding of the transport processes that occur in these aquifers. Once contaminant transport phenomena are understood, and predictable, costly environmental and economic consequences can be avoided or minimised, and the process of rehabilitating already contaminated aquifers can begin.

1.2 Problem description and background

This thesis will investigate the case of leaky contaminated ponds sitting above a freshwater aquifer. As mentioned, this scenario has received little attention from researchers, but is an ever increasing situation, be it from land based aquaculture, or tailings dams, or any other non-freshwater pond. Whatever the contaminant, the techniques developed in this thesis are equally applicable. However, for consistency, the contaminant used throughout this thesis will be salt, ostensibly leaking from an aquaculture pond. A simple schematic can be seen in Figure 1.1.

Contaminant transport through groundwater predominately occurs in two ways: advection and hydrodynamic dispersion. Advection, simply put, is the movement of a contaminant within a fluid, via the fluid's bulk motion. For example, silt dumped in a fast moving river would be advected downstream. Hydrodynamic dispersion, on

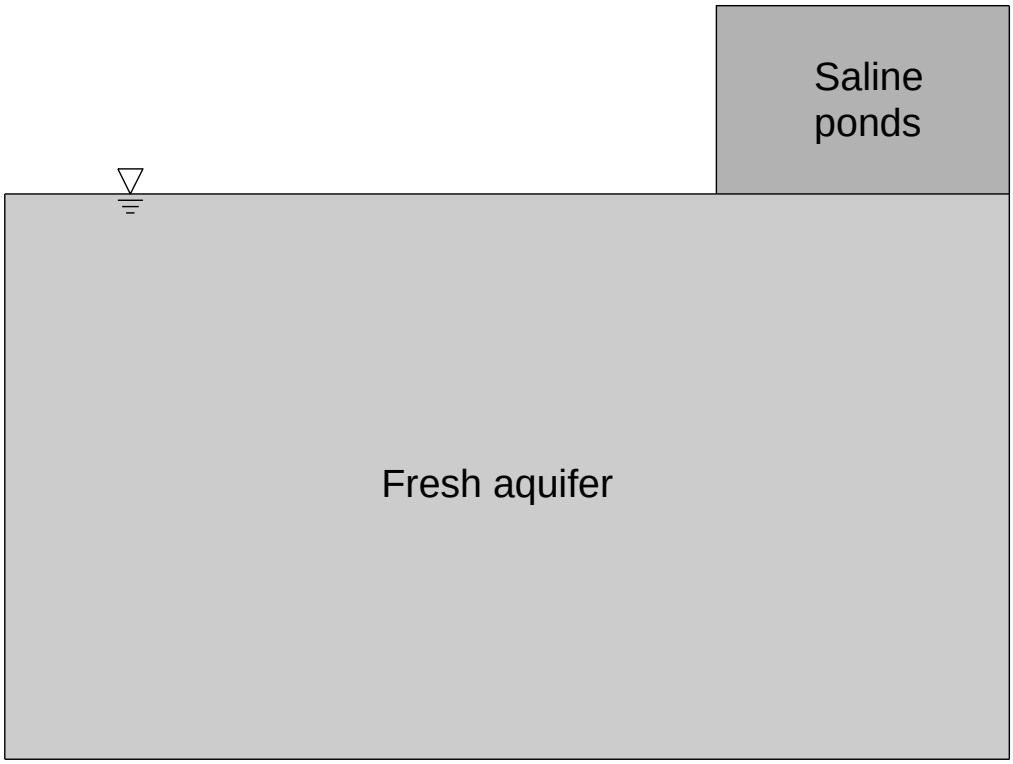

FIGURE 1.1: Schematic of domain being considered throughout this thesis.

the other hand, is more complicated; it results from the combined processes of molecular diffusion (the random molecular movement of individual contaminant particles) and mechanical dispersion (the mixing of advected groundwater and its contaminant constituents, caused by the vastly different paths two initially adjacent contaminant particles can take through the porous media). Typically, mechanical dispersion is more important than molecular diffusion, but as advection reduces to zero, mechanical dispersion disappears, and molecular diffusion must be considered in isolation. (In practice, mechanical dispersion is often assumed to be negligible for low advective flow rates.) However, although functionally different, hydrodynamic dispersion and pure molecular diffusion are treated mathematically the same way; that is, the same equation governs both processes. The difference between the two arises through different 'diffusion' coefficients. We refer the reader to Bear (1979) for an in-depth treatment.

In this thesis, the governing equation is solved non-dimensionally, and the appropriate coefficient for either hydrodynamic dispersion or pure molecular diffusion can potentially be substituted for dimensional results (at least, that is, when the coefficients can be approximated as constants, such as in this work). Mathematically, for the sake of simplicity and consistency, the term 'diffusion' will cover both processes herein. This thesis assumes advection and diffusion to be the major transport mechanisms in the domain of Figure 1.1, with other possible transport, for example, density driven flow, assumed to be negligible.

Mathematically, we're interested in solving the advection-diffusion equation,

$$\frac{\partial C}{\partial t} = \nabla \cdot (D \nabla C) - \nabla \cdot (\mathbf{u} C), \tag{1.1}$$

where C is the concentration (of whatever solute/contaminant is being modelled), D is the diffusion coefficient, and $\mathbf{u}$ is the bulk velocity of the solvent (groundwater). (In the generalised form of equation (1.1), the terms D and $\mathbf{u}$ may vary with space, time, or the concentration C.) Typically, there are two approaches to solving the above equation: analytical methods and numerical methods.

When available, analytical methods are superior. They are easily applied to different values of parameters and inputs, and the relative influence of the parameters can be readily shown (Bear, 1979). However, for most problems of practical interest, analytical solutions quickly become impractical or impossible; either the required mathematical techniques are unfamiliar to the practitioner, or the problem has some complexity that analytical methods cannot accommodate. For example, irregularly shaped domains, variable boundary conditions, non-uniform flow fields, and multiple spatial dimensions, or some combination thereof, all increase the difficulty involved in finding an analytical solution; and although some solutions exist for the above examples, typically they are special cases. As such, it generally falls to numerical methods when a solution is required for a problem with any complexity. Nevertheless, analytical methods are widely used for simple domains, as coarse approximations of complex domains, or as test problems for validating numerical methods.

There are many numerical methods available for solving partial differential equations such as that in equation (1.1). However, in the field of groundwater modelling the main techniques employed fall into one of two categories: finite difference methods or finite element methods. Both types replace the partial differential equation with an approximating set of algebraic equations (which are then solved simultaneously) (Strang, 1986), however, each have relative advantages and disadvantages. For example, finite difference methods are generally more intuitive and easier to formulate, whereas finite element methods are more flexible and can accommodate more complex domains. Nonetheless, a major benefit of both types of method is that they can be implemented in generic groundwater modelling software. As such, practitioners with minimal mathematical background can (relatively) safely extract solutions for complex problems (Bear, 1979). Two such software packages are MODFLOW (USGS, 2005) (based on finite difference methods) and SUTRA (Voss and Provost, 2002) (based on finite element methods).

For the domain of Figure 1.1 the modelling of combined advection-diffusion is (currently) beyond purely analytical techniques. As such, numerical methods become the default option. However, the grid resolution needed to accurately resolve the flow field can be a major stumbling block for the above techniques. The large aspect ratios (that is, length to depth) common in groundwater systems pose fundamental problems for the transport equation (1.1) when solving numerically (Reddy and Trefethen, 1994). Nevertheless, as stated above, numerical solutions are typically the best option available for domains with any complexity. However, this thesis will explore an alternative methodology. Rather than an either/or approach, it will take analytical techniques as far as practicable, and only then resort to numerical methods. In this manner, it is hoped to improve upon existing numerical results by removing at least some of the limitations of numerical methods (for example, truncation error caused by discretisation), and possibly imbue some of the advantages of analytical methods. Therefore, the ultimate goal of this thesis is a combined analytical/numerical technique (henceforth described as a quasi-analytical technique) to solve the advection-diffusion equation (1.1) in the domain of Figure 1.1. If this can be achieved, then any techniques

developed may also be more widely applicable.

1.3 Scope and structure of the thesis

This document is a thesis by publication. Therefore, each of the main chapters (2, 3, 4, 5, 6 and 7) were originally written as standalone articles for submission to journals or peer reviewed conference proceedings. Details can be found in the list of publications. These chapters/articles are presented in a linear fashion (that is, each builds upon the work of the previous ones), and therefore (ideally) should be read in the order in which they appear. Additionally, note that some chapters will vary slightly from the original articles. In general, introductory background information that was repeated between articles (where it could be sensibly removed) has been merged into Sections 1.1 and 1.2 of this thesis, some minor improvements to the text have been made, and some variable/parameter names have been renamed for consistency. Finally, it should be noted that there is no standalone literature review in this document. The relevant background literature is presented and discussed as needed within each chapter.

In general, contaminant transport through the domain is a coupled process, with advection and diffusion being inseparable from each other. That is, each process occurs simultaneously with the other, and therefore each affects the evolution of the other through time. However, depending on the domain in question, one or the other can often be neglected. This is a common technique to reduce the complexity of a problem. In order to proceed, this thesis will tackle each process separately. Each process, advection and diffusion, will be solved using quasi-analytical techniques, with combined advection-diffusion building on these solutions. The below descriptions of each chapter gives a broad overview of the scope and structure of this thesis.

1.3.1 Chapter 2: Advection

In Chapter 2, the problem of contaminant transport due to advection is tackled. That is, we assume the advection process is dominant and diffusion can be ignored. The flow field of the domain of Figure 1.1 is found analytically, and a simple numerical technique

is used to find isochrones (advection fronts) for a couple of different contamination scenarios. From these results, simple equations are empirically derived to predict the advection front location as a function of time.

1.3.2 Chapter 3: Modified advection

In Chapter 3, an improved numerical method is employed to find the advection isochrones revealed in Chapter 2. This chapter can be viewed as an extension to the work of Chapter 2.

1.3.3 Chapter 4: Diffusion

The results from Chapter 2 show that for the domain of Figure 1.1, although initially the major source of contamination, at some point in time advection becomes a stagnant process. In Chapter 4 this result is used as a constant concentration condition when modelling the progress of diffusion throughout the rest of the domain. This condition precludes an analytic solution, therefore a quasi-analytical technique is formulated. The result is advection and diffusion combined within the domain where and when each is dominant. From these results, simple equations are empirically derived to predict the diffusion front, which, combined with those from Chapter 2, allow the rapid modelling of combined advection-diffusion within the domain.

1.3.4 Chapter 5: Generalised equations for advection and diffusion

Chapter 5 is a generalisation and expansion of the simplified equations derived in Chapters 2 and 4. These equations may prove useful for the rapid modelling of combined advection-diffusion within the domain of Figure 1.1. They can accommodate different parameters of hydraulic conductivity, diffusivity, porosity, aquifer depth and pond height, as well as variable thresholds of contamination. The major limiting assumptions are that there is no density driven flow, the hydraulic conductivity is constant throughout the domain, and the domain can be approximated as rectangular.

1.3.5 Chapter 6: Combined advection-diffusion-reaction

In Chapter 4, a combined advection-diffusion solution is found that depends on each transport process being dominant at different times. While this may be true for the leaky pond domain in Figure 1.1, this will not be the case for most other situations. Chapter 6 explores a more robust technique for combining the above quasi-analytical solutions of contaminant transport. However, it should be noted that while the method formulated in this chapter was developed using the leaky pond domain, for publication it was decided to simplify the problem for explanatory and demonstrative purposes. That is, this chapter departs from the leaky pond problem as the example considered, in preference of a simpler domain. In so doing, it was discovered that as well as solving for advection and diffusion, the technique can be extended to reaction as well. That is, using the method described in this chapter, it's easy to incorporate a possible reaction process (or chemical decay) of the contaminant.

1.3.6 Chapter 7: Combined advection-diffusion for the leaky pond problem

In this chapter, the technique described in Chapter 6 is applied to the familiar leaky pond problem. The results represent the realisation of the ultimate goal of this thesis, that is, a quasi-analytical technique to solve the advection-diffusion equation in the domain of Figure 1.1.

1.3.7 Chapter 8: Comparison of quasi-analytical techniques

This chapter was not written as an article. It is a comparison of the techniques in Chapters 5 and 7. We assume results from the quasi-analytical technique of Chapter 7 to be accurate, and test similar results from the simplified equations of Chapter 5 against them.

1.3.8 Chapter 9: Discussion

The Discussion incorporates an overview of the thesis, suggestions for future work, and some final remarks.

2

Advection

2.1 Introduction

This chapter deals with the transport of contaminant via the process of advection. As stated in Section 1.2, the domain of interest is a saline pond sitting above a freshwater aquifer. We are interested in advection away from the source, caused by the potential of the pond height. In addition, we consider the situation (as may occur near the coast) that the fresh groundwater sits above a deeper saltwater layer. In this case the influence of the saline ponds can cause salt water from the deeper layer to rise, also contaminating the fresh groundwater.

Modelling the advection and diffusion of salt through an aquifer is a difficult problem to solve accurately in the best of circumstances. There are fundamental problems associated with the transport equation that preclude even moderately accurate solutions over the large aspect ratios (that is, length to depth) that are common in groundwater flows (Reddy and Trefethen, 1994). For these larger aspect ratios the main features of these flows appear to be advection with some lateral diffusion and negligible longitudinal diffusion. In this chapter, we assume that diffusion is negligible compared to advection and concentrate on accurately determining the breakthrough front as salt is advected through the aquifer.

One of the major computational stumbling blocks for numerical schemes is the grid resolution necessary to accurately resolve the flow field. However, analytic series solutions for the flow field avoid this problem as they provide continuous, accurate solutions for the entire solution domain (Powers et al., 1967; Read, 1996a,b; Read and Volker, 1993). These solutions provide potential functions, stream functions and velocity fields continuously throughout the solution domain, and can be used to calculate equi-potentials, streamlines and velocity contours accurately and efficiently. The velocity field can be integrated to provide accurate isochrones (or breakthrough curves) with relatively little computational effort. This method has been used by Philip (1984) to determine isochrones in unsaturated soil profiles of infinite depth.

In this chapter we provide simple models of advection from saltwater ponds to surrounding areas, and from the lower saltwater layer of the aquifer up to the water

table. We also provide solutions for the isochrones (breakthrough curves), and from these results find simple formulas to predict when these isochrones affect the area away from the ponds. Although these results are for specific examples, the models can be applied to any similar problems that satisfy the same underlying assumptions.

This chapter is organised as follows. Section 2.2 provides an overview of the examples considered. Section 2.3 presents the mathematical model to be used, with model results being presented in Section 2.4. Finally, we discuss these results and draw appropriate conclusions in Section 2.5.

2.2 Hydrogeology and model boundaries

This chapter models aquaculture ponds placed near traditional farmland, and within coastal proximity. We assume that the coastal aquifer in the region has a depth of 40 m, beneath which a confining layer of bedrock exists. Since we are near the coast, we assume the bottom three quarters of the aquifer is affected by salt water intrusion, leaving the top ten meters of groundwater useful for irrigation. Figure 2.1 shows a schematic of the above situation. Assuming the worst case scenario, that is, unlined (or damaged) ponds that allow salt water to discharge freely into the ground, we wish to model how contamination of the irrigable fresh water within the aquifer might occur.

Before we can model the flow within the aquifer, we first require the boundary conditions of our model. Since the base of the aquifer is bedrock, the bottom boundary can be considered impermeable. We make the right boundary of the model a vertical line through the center of the aquaculture ponds, and hence a line of symmetry which can be regarded as impermeable also. For simplicity we make the left boundary impermeable as well, but place it far enough away that the flow within the aquifer is not affected. Finally, the top boundary is the free surface of the aquifer water table, but there is a smooth transition to the free surface of the aquaculture ponds, the height of which provides the driving potential of the saltwater contamination.

To keep our model relatively simple, the following additional assumptions are made. The hydraulic conductivity of the aquifer is assumed constant (which is valid providing

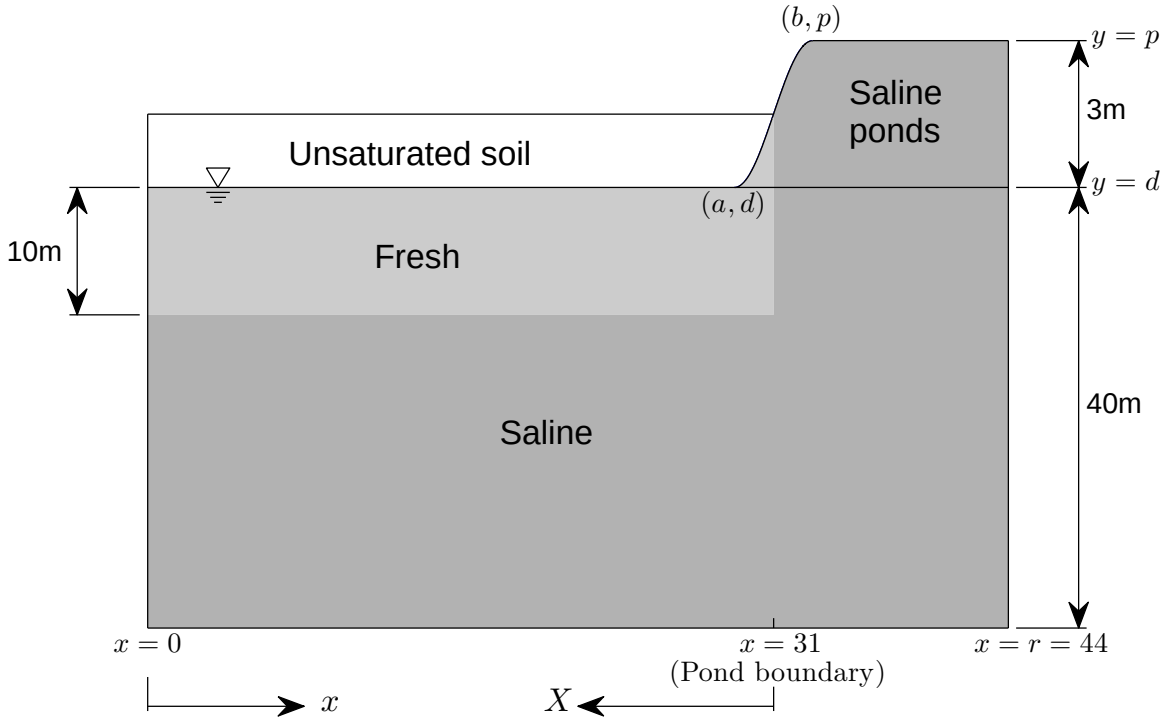

FIGURE 2.1: Sketch of domain being considered.

that any actual soil heterogeneity is small), and since we are near the sea, we set this parameter to that of sandy loam (0.864 m/d) (Arunakumaren et al., 2000). Also, the water table below the traditional farmland is horizontal, therefore giving a constant hydraulic head downstream boundary condition. Finally, we assume hydrodynamic dispersion to be negligible.

2.3 Mathematical model of salt transport

In view of the discussion in Section 2.2, we can model the seepage from the aquaculture ponds by assuming the aquifer is horizontal and of uniform depth, with constant hydraulic conductivity K_*. Figure 2.1 shows a schematic of the soil horizon (Note that all coordinates are dimensionless, while the actual physical lengths are shown as dimensional). Inside the saturated flow boundary, we assume the seepage velocity

$\mathbf{u}_* = (u_*, v_*)$ satisfies Darcy's law

$$\mathbf{u}_* = -K_* \nabla_* \phi_*(x_*, y_*), \tag{2.1}$$

where $\phi_*(x_*, y_*)$ is the hydraulic head. (Note that asterisk subscripts represent dimensional variables. These will later be dropped when the problem is non-dimensionalised.) Upon invoking the continuity condition, we obtain Laplace's equation for the saturated flow domain,

$$\nabla_*^2 \phi_*(x_*, y_*) = 0. \tag{2.2}$$

Along the impermeable aquiclude $y_* = 0$ and the vertical side boundaries at $x_* = 0,\ r_*$, the seepage velocity is zero:

$$v_*(x_*, 0) = -K_* \frac{\partial}{\partial y_*} \phi_*(x_*, 0) = 0, \tag{2.3}$$

$$u_*(0, y_*) = -K_* \frac{\partial}{\partial x_*} \phi_*(0, y_*) = 0, \tag{2.4}$$

$$u_*(r_*, y_*) = -K_* \frac{\partial}{\partial x_*} \phi_*(r_*, y_*) = 0. \tag{2.5}$$

Along the water table, the hydraulic head is equal to the elevation of the water table for $0 \leq x_* \leq a_*$ with a smooth transition to the height of the water in the ponds $b_* \leq x \leq r_*$. We achieve a smooth transition by using a cubic spline, with the hydraulic head and the derivative of the head equal at $x_* = a_*$ and $x_* = b_*$. Noting that the elevation of the water table is d_*, the height of the ponding is p_*, and the gradient along the water table and the top of the pond is zero, the hydraulic head on the upper boundary is

$$\begin{aligned} \phi_*(x_*, d_*) &= h_*^t(x_*) \\ &= \begin{cases} d_*, & 0 \leq x_* \leq a_* \\ \alpha_3(x_*^3 - a_*^3) + \alpha_2(x_*^2 - a_*^2) & \\ \qquad +\alpha_1(x_* - a_*) + \alpha_0, & a_* < x_* \leq b_* \\ p_*, & b_* < x_* \leq r_* \end{cases}, \end{aligned} \tag{2.6}$$

where

$$\begin{aligned} \alpha_3 &= -2\frac{p_* - d_*}{(b_* - a_*)^3}, & \alpha_2 &= 3\frac{(b_* + a_*)(p_* - d_*)}{(b_* - a_*)^3}, \\ \alpha_1 &= -6\frac{a_* b_* (p_* - d_*)}{(b_* - a_*)^3}, & \alpha_0 &= d_*. \end{aligned} \tag{2.7}$$

(The mathematical details are given in Appendix A.1.) The smooth transition is a small region included to eliminate the discontinuity between the pond and the water table which would otherwise introduce Gibbs phenomenon into the solution. It affects only the smallest advection fronts which are of little interest to this chapter. (Note, the effects of the smooth transition are investigated more thoroughly in Chapter 5.) In fact, a smooth transition between water levels is arguably a more realistic situation than a discontinuity. The boundary value problem is now fully defined and can be solved. Once the hydraulic head is available throughout the aquifer, we can calculate the stream function and the pore velocity.

The stream function $\psi_*(x_*, y_*)$ is related to the hydraulic head by the Cauchy-Riemann equations,

$$\frac{\partial \psi_*}{\partial y_*} = K_* \frac{\partial \phi_*}{\partial x_*}, \qquad \frac{\partial \psi_*}{\partial x_*} = -K_* \frac{\partial \phi_*}{\partial y_*}. \tag{2.8}$$

The stream function is a scalar field that quantifies the mass flux throughout the aquifer. Note that with this definition the mass flux is positive in the clockwise direction.

The pore velocity $\mathbf{U}_*(x_*, y_*)$ is related to the seepage velocity by the porosity σ, where $0 < \sigma < 1$ and σ is assumed constant, by

$$\mathbf{u}_* = \sigma \mathbf{U}_*. \tag{2.9}$$

Hence,

$$\mathbf{U}_* = (U_*, V_*) = -\frac{K_*}{\sigma} \left(\frac{\partial \phi_*}{\partial x_*}, \frac{\partial \phi_*}{\partial y_*} \right). \tag{2.10}$$

At this point we non-dimensionalise the problem using the hydraulic conductivity

K_*, and the depth of the aquifer d_*. That is,

$$x_* = d_* x, \;\; y_* = d_* y, \;\; a_* = d_* a, \;\; b_* = d_* b, \;\; r_* = d_* r, \;\; p_* = d_* p, \tag{2.11}$$

$$h^t_*(x_*) = d_* h^t(x), \;\; \phi_*(x_*, y_*) = d_* \phi(x, y), \;\; \psi_*(x_*, y_*) = d_* K_* \psi(x, y), \tag{2.12}$$

$$t_* = \frac{\sigma d_*}{K_*} t, \;\; \mathbf{u}_* = K_* \mathbf{u}, \;\; \mathbf{U}_* = \frac{K_*}{\sigma} \mathbf{U}. \tag{2.13}$$

There are three points to note here. First, throughout the dimensionless boundary value problem, dimensionless parameters replace their dimensional counterparts simply by removing the subscript asterisk. Second, the coefficients α_i of the cubic in the equations of (2.7) are the same for the dimensionless variables, with the asterisk subscripts removed, and noting that $d_* = d_* d \Rightarrow d = 1$. That is, the dimensionless depth d of the aquifer is $d = 1$. Finally, the dimensionless pore velocity $\mathbf{U}$ has been scaled by the (dimensionless) porosity σ.

2.3.1 Series solution for the hydraulic head and stream function

Using the classic method of separation of variables (Carrier et al., 1966), a series solution for the hydraulic head $\phi(x, y)$ can be obtained. (Note that this solution presumes a hydrostatic head distribution above $y = d$.) Truncating this series after $N+1$ terms, the series approximation is given by

$$\phi(x, y) = \sum_{n=0}^{N} A_n \cosh \frac{n\pi y}{r} \cos \frac{n\pi x}{r}. \tag{2.14}$$

This series satisfies the bottom and side boundary conditions exactly with the remaining boundary condition, equation (2.6), used to evaluate the series coefficients $A_n, \; n = 0, 1, \ldots, N$. This is a standard cosine series, with

$$A_0 = \frac{1}{r} \int_0^r h^t(x) \, dx, \tag{2.15}$$

$$A_n = \frac{2}{r} \int_0^r h^t(x) \cos \frac{n\pi x}{r} \, dx, \quad n \neq 0. \tag{2.16}$$

These integrals can be evaluated quickly and accurately using quadrature; see, for example, Trefethen (2000).

The series solution for the stream function $\psi(x, y)$ that corresponds to $\phi(x, y)$ is easily obtained using the Cauchy-Riemann equations (2.8). Choosing the impermeable boundary along $x = 0$, $y = 0$ and $x = r$ as the zero for ψ, then

$$\psi(x, y) = -\sum_{n=1}^{N} A_n \sinh \frac{n\pi y}{r} \sin \frac{n\pi x}{r}. \tag{2.17}$$

The value of the stream function at any point (x, y) in the domain is the mass flux between the impermeable boundary and the point (x, y).

2.3.2 Isochrones

Once the series solution for the hydraulic head $\phi(x, y)$ has been determined, the pore velocity field, $\mathbf{U} = (U, V)$, can be calculated by differentiating the series. That is,

$$\mathbf{U} = (U, V) = -\left(\frac{\partial \phi}{\partial x}, \frac{\partial \phi}{\partial y}\right). \tag{2.18}$$

The pore velocity at any point is also given by

$$\mathbf{U} = \left(\frac{dx}{dt}, \frac{dy}{dt}\right), \tag{2.19}$$

where now the location at which the pore velocity is calculated is parameterised using (non-dimensional) time t as a parameter. That is, $x \equiv x(t)$, $y \equiv y(t)$. Thus from equations (2.18) and (2.19), the time t taken for a neutrally buoyant particle to be advected along a stream line from (x_0, y_0) to $(x(t), y(t))$ is

$$t = \int_{x_0}^{x(t)} \frac{dx}{U} = -\int_{x_0}^{x(t)} \frac{dx}{\partial \phi / \partial x} \tag{2.20}$$

$$= \int_{y_0}^{y(t)} \frac{dy}{V} = -\int_{y_0}^{y(t)} \frac{dy}{\partial \phi / \partial y}. \tag{2.21}$$

We can use this result to determine isochrones, or the breakthrough curve, for

the salt water as it is transported away from the aquaculture ponds. By rearranging equations (2.20) and (2.21), the distances $(\Delta x, \Delta y)$ a particle is advected in the x and y directions in a small time interval Δt are given (approximately) by

$$\Delta x \approx -\frac{\partial \phi}{\partial x}\Delta t, \tag{2.22}$$

$$\Delta y \approx -\frac{\partial \phi}{\partial y}\Delta t. \tag{2.23}$$

Consider at time $t = t_0$ a discrete set of $I > 0$ points $(x_{i,0}, y_{i,0}),\ i = 1, \ldots, I$. Then, for any time $t_J = t_0 + J\Delta t,\ J > 0$, we can calculate the approximate location of the advection front $(x_{i,J}, y_{i,J})$ by calculating the intermediate points $(x_{i,j}, y_{i,j}),\ j = 1, \ldots, J-1$ using the difference equations

$$x_{i,j} \approx x_{i,j-1} - \left(\frac{\partial \phi}{\partial x}\right)_{i,j-1} \Delta t, \tag{2.24}$$

$$y_{ij} \approx y_{i,j-1} - \left(\frac{\partial \phi}{\partial y}\right)_{i,j-1} \Delta t, \tag{2.25}$$

where

$$\left(\frac{\partial \phi}{\partial x}\right)_{i,j} = \left(\frac{\partial \phi(x,y)}{\partial x}\right)_{\substack{x=x_{i,j} \\ y=y_{i,j}}}, \tag{2.26}$$

$$\left(\frac{\partial \phi}{\partial y}\right)_{i,j} = \left(\frac{\partial \phi(x,y)}{\partial y}\right)_{\substack{x=x_{i,j} \\ y=y_{i,j}}}. \tag{2.27}$$

For sufficiently small Δt (that is, sufficiently large J), this converges to the advection front at time t_J. Using this algorithm, we can predict the advection of solutes from *any* initial location in the flow domain. In particular, we can determine the isochrones of solutes advected from the water table immediately below the aquaculture ponds $(b \leq x \leq r)$. We can also determine the advection of solutes from the saline water that is assumed to lie 10 metres below the water table under the traditional farmland.

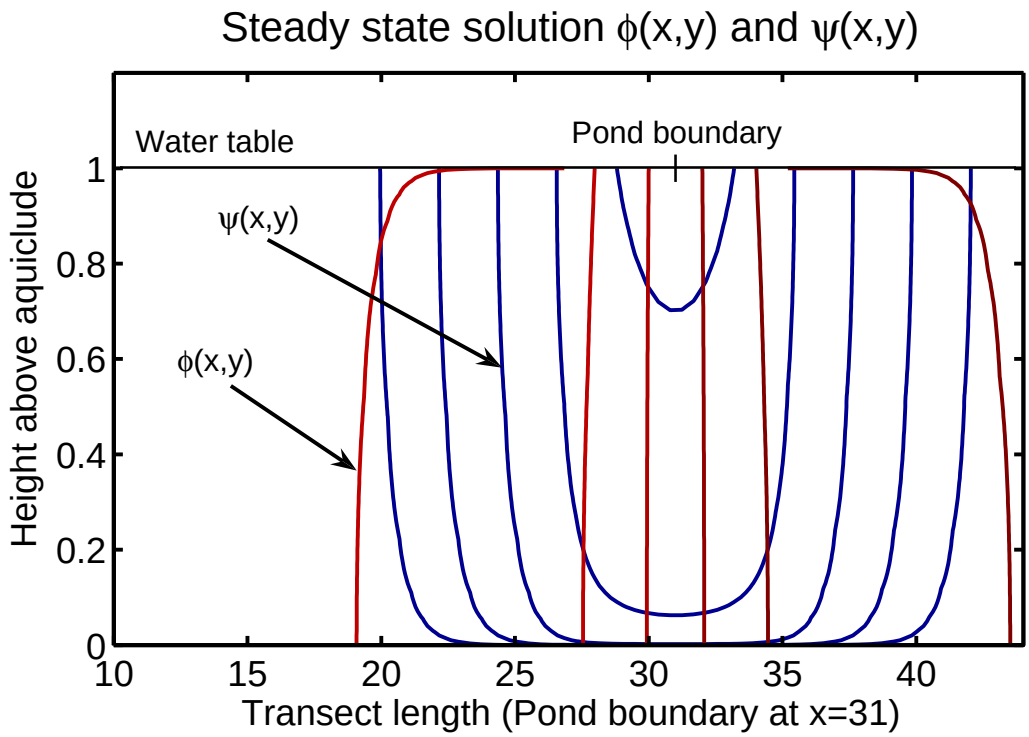

FIGURE 2.2: Steady state solution of $\phi(x, y)$ and $\psi(x, y)$.

2.4 Model results

Given the parameters described in Section 2.2, we solve for the stream and potential functions of Section 2.3.1. Figure 2.2 shows the orthogonal functions $\phi(x, y)$ and $\psi(x, y)$ which represent the hydraulic head at any point in the domain, and the flow path at any point in the domain, respectively. We refer to these while solving the isochrone problems in the following subsections.

2.4.1 Model 1: Advection from aquaculture ponds

The first situation modelled is that of salt water contaminating the water table directly from the aquaculture ponds. Given that any salt water escaping into the aquifer would be replenished, we model the pond height as being maintained at a constant value, and set this hydraulic potential as being 3 m. That is, the surface of the ponds are 3 m above the water table. Setting the contaminant location to be at the top of the water table directly beneath the ponds, and scaling our dimensionless parameters

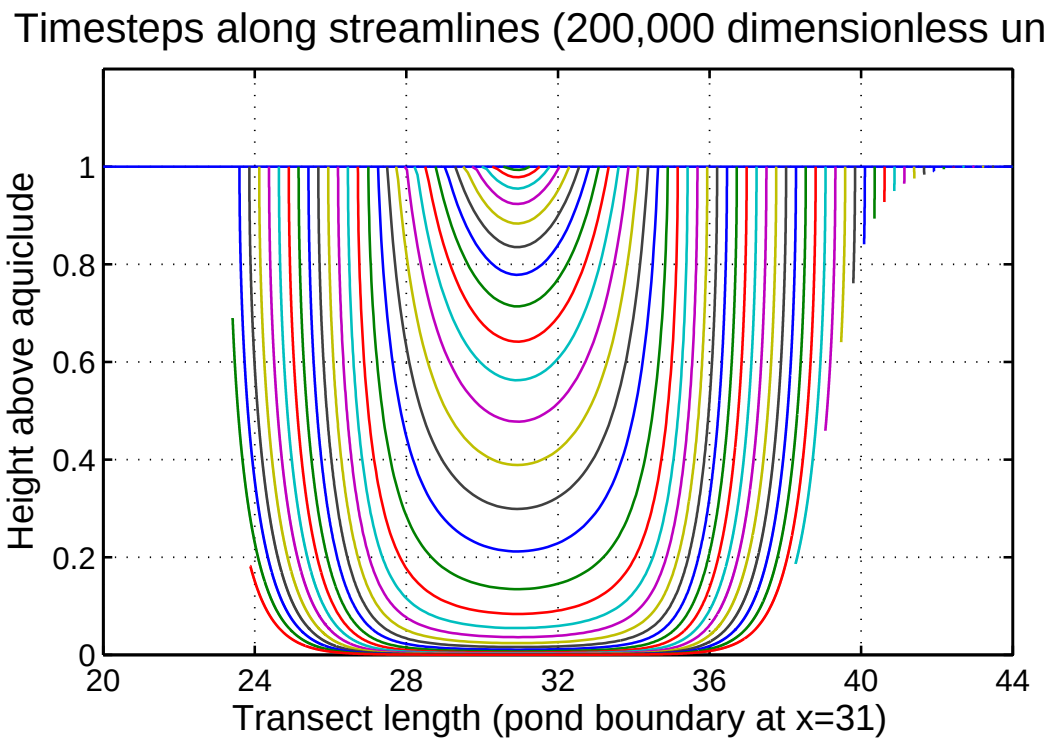

Figure 2.3: Final extent of travel along streamlines for Model 1.

with an aquifer depth of $d_* = 40$ m (as indicated by (2.11)), we now utilise equations (2.24) and (2.25) to track the advection of salt from 3,000 points directly beneath the pond. This salt traces out streamlines (or parts thereof) as they are advected through the aquifer until they reach the surface of the water table downstream of the ponds.

Figure 2.3 shows the results of the model after 200,000 dimensionless time units (7,610 years). For clarity, the plot is restricted to 50 starting points, and reveals the extent that contaminated water at the bottom of the ponds will travel along the relevant streamlines for the time period specified. From this figure we observe that the longer the distance between the start and end of each streamline (beginning and ending at the water table), the less progress has been made by the advection front along that streamline. Darcy's law says that the velocity is proportional to the change in hydraulic head per unit distance. A close inspection of the equi-potentials in Figure 2.2 reveals that the change in hydraulic head becomes smaller further from the aquaculture ponds, which implies that the velocity is decreasing with distance. This decrease in velocity results in slower advection along the streamline.

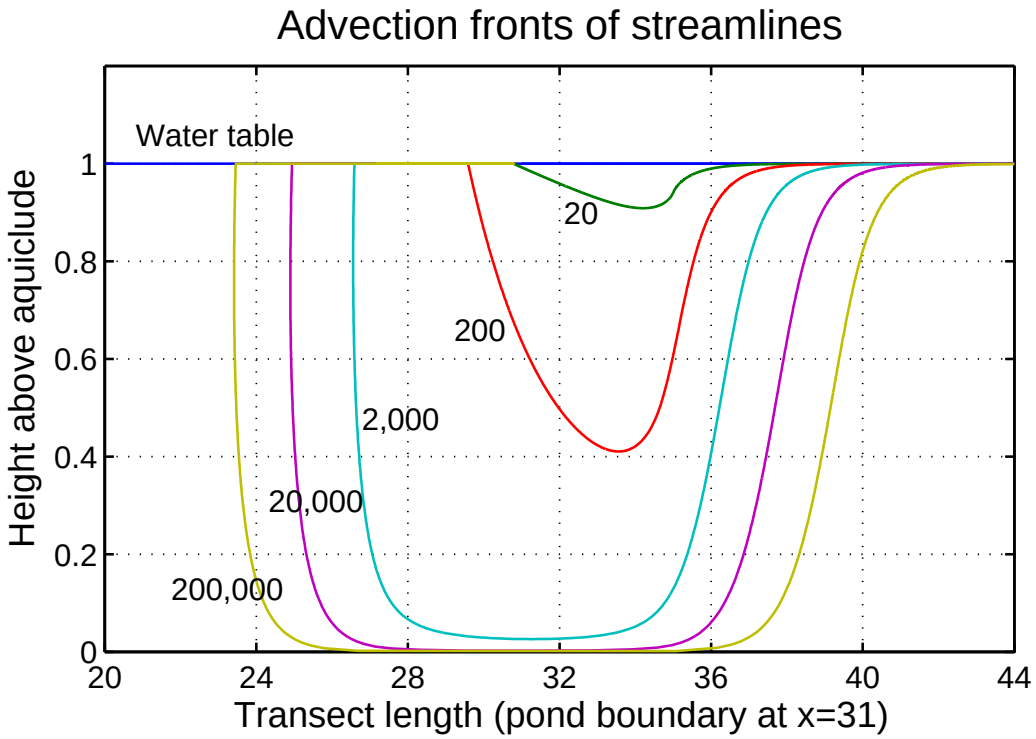

FIGURE 2.4: Advection fronts for Model 1.

The final location of contaminant advection is represented by the ends of each streamline in Figure 2.3. By joining the ends of these streamlines, we create a new curve representing the advection front of the saltwater contaminant. Doing this for intermediate times as well produces Figure 2.4, which represents the advection fronts (or isochrones) in increasing powers of ten between 20 and 200,000 time units.

As the salt water progresses along the streamlines with each incremental time step, eventually it will break through the water table at a point downstream of the ponds. By recording the time and location that this occurs for a large number of points, we can plot the advance of the saltwater front along the water table at any given time. This introduces a new variable, X, the dimensionless distance (scaled similarly to equation (2.11)) from the pond boundary along the water table. Note that X is positive from right to left as seen in Figure 2.1. Figure 2.5 shows a semi-log plot of the breakthrough points versus time for a number of data values. We ignore the points close to the pond boundary ($X < 5$) as they are affected by the non-linearity introduced to the model by our smooth transition. Fitting the rest of the data points

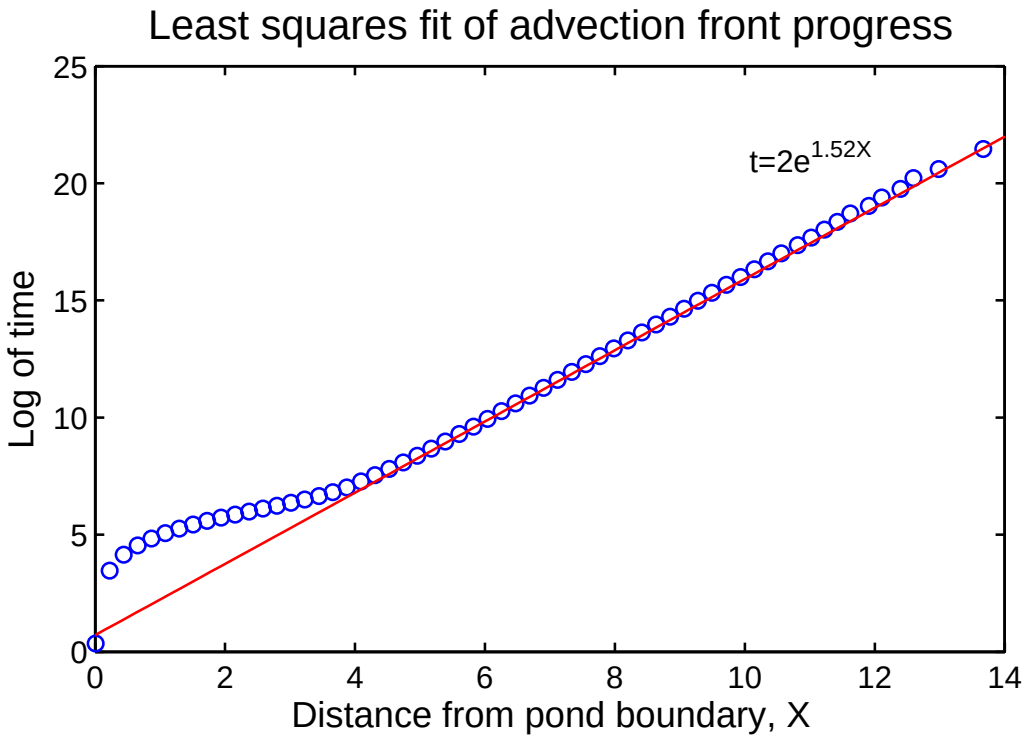

Figure 2.5: Breakthrough curve for Model 1.

using the method of Least Squares, the following 'contamination equation' is obtained:

$$t = 2e^{1.52X}, \tag{2.28}$$

where X is the dimensionless distance from the pond boundary, and t is the dimensionless time at emergence. It gives us a simple equation to find the progress of the salt without needing to rerun the model. We note that the plot only shows values for $X < 14$. Beyond this point the velocities are so slow the advection front progress cannot be calculated. We take this to mean there is no flow in this region ($X > 14$).

To find the *actual* contaminant progress using the above equation, we need to substitute in the relevant dimensional values from equation (2.11) and solve:

$$t_* = \frac{2\sigma d_*}{K_*} e^{(\frac{1.52}{d_*})X_*}, \tag{2.29}$$

where X_* is the dimensional distance in metres, and t_* is the dimensional time in seconds.

Using aquifer hydraulic conductivity $K_* = 0.864$ m/d (10^{-5} m/s), $d_* = 40$ m, and a typical value of $\sigma = 0.3$, equation (2.29) reveals that after 23.6 years the advection front has progressed 150 metres. To progress to 300 metres requires 7,610 years, which in Figure 2.4 is the curve represented by 200,000 dimensionless time units.

2.4.2 Model 2: Advection from lower saline layer

The second situation considered is that of contamination coming from the saline water 10 metres below the water table. For the most part, this is similar to the previous model, with the constant pond height assumption still valid, and salt water from the ponds escaping into the aquifer. This model's only difference is the initial location of the contaminant, in this case located 10 m below the water table, a dimensionless distance of 0.25.

Figure 2.6 plots the extent of travel along each streamline after 200,000 dimensionless time units (7,610 years). For clarity we restrict the number of starting points in the plot to 50, but the model was actually run from 500 such points. We note that the same streamlines in Figure 2.3 which emerged most rapidly are the same to do so in Figure 2.6, while those that had barely progressed below the water table (Figure 2.3) have also not moved significantly from their starting points (Figure 2.6). Again, Darcy's law explains the reason this occurs, as the whole process is driven by the hydraulic gradient which is greatest near the pond boundary, and decreases the further we move away.

To produce the advection fronts of this model, we repeat the steps described in Section 2.4.1. By joining the final location of travel along each streamline for particular time periods, Figure 2.7 is produced. These are the advection fronts in increasing powers of ten between 20 and 200,000 dimensionless time units.

We can plot the time and location that salt water emerges at the water table in the same way we did for the first model. Figure 2.8 shows a semi-log plot of the breakthrough location versus time for a number of data values. We ignore the breakthrough points close to the pond boundary ($X < 4$) due to the non-linearity introduced by our smooth transition. As indicated in the previous model, as the distance from the

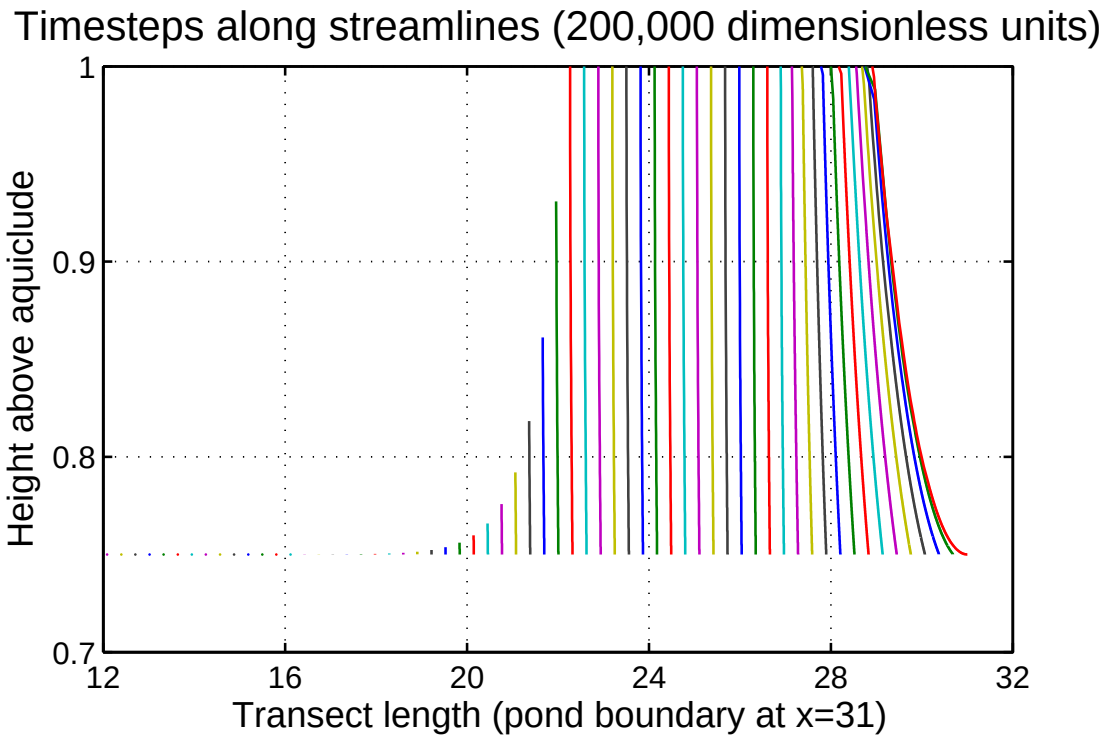

Figure 2.6: Final extent of travel along streamlines for Model 2.

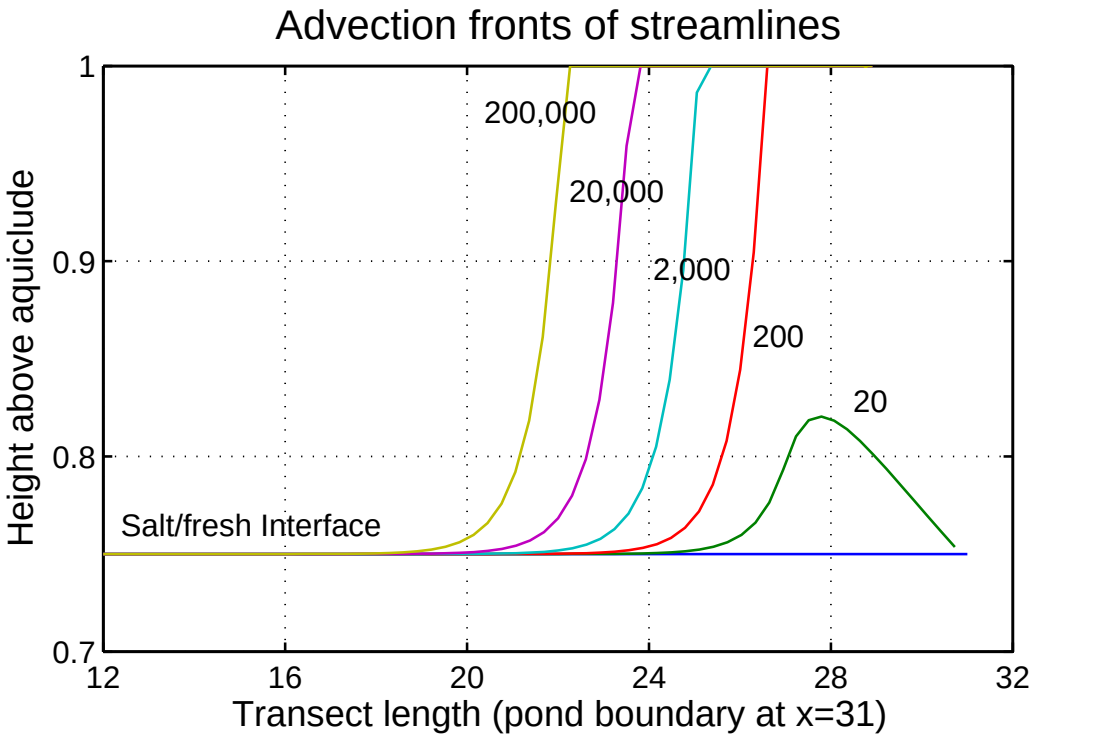

Figure 2.7: Advection fronts for Model 2.

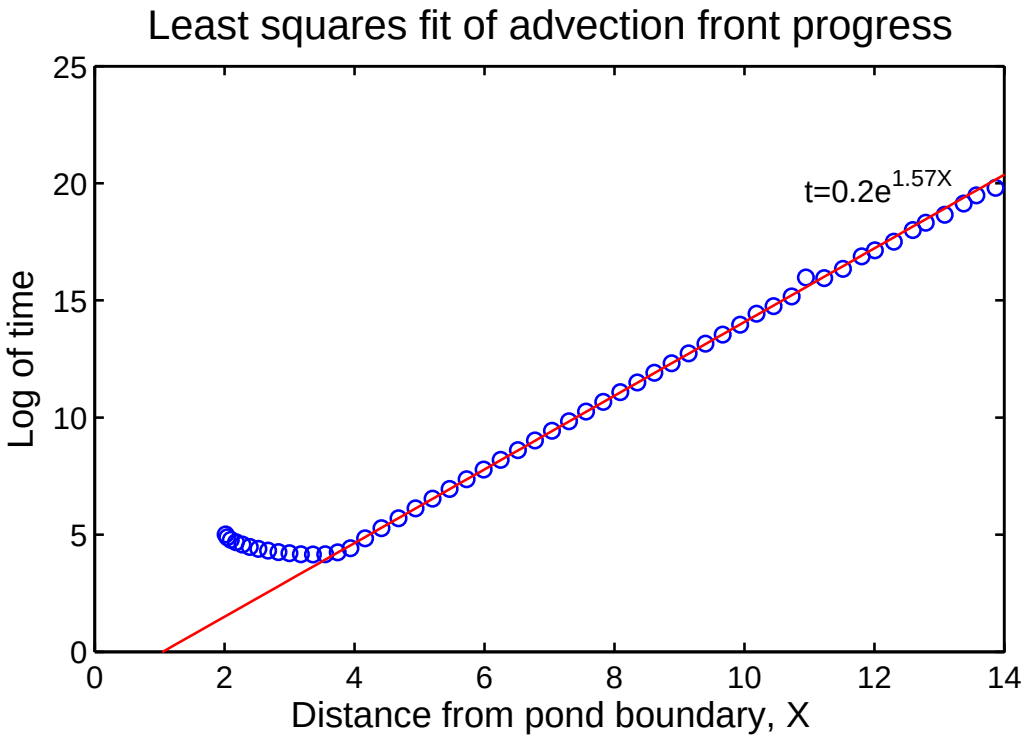

FIGURE 2.8: Breakthrough curve for Model 2.

pond boundary increases ($X > 14$), the velocities become so slow the advection front progress cannot be calculated without machine error. Fitting the section $4 < X < 14$ using the method of Least Squares reveals a second 'contamination equation':

$$t = 0.2e^{1.57X}, \tag{2.30}$$

where X and t represent the same parameters as equation (2.28).

To find the dimensional values, substitution from equation (2.11) reveals:

$$t_* = \frac{0.2\sigma d_*}{K_*} e^{(\frac{1.57}{d_*})X_*}, \tag{2.31}$$

where X_* is the dimensional distance in metres, and t_* is the dimensional time in seconds.

Using $K_* = 0.864$ m/d (10^{-5} m/s), $d_* = 40$ m, and $\sigma = 0.3$, we find that after 7.6 years the advection front has progressed 175 metres. To progress to 350 metres requires 7,610 years, which is the curve represented by 200,000 dimensionless time units

in Figure 2.7.

2.5 Discussion and conclusions

In this chapter a simple method has been developed to find advection fronts of groundwater systems, with specific application to an aquaculture farm on a coastal aquifer system. The method relies on knowledge of the potential and stream functions of the area, in this chapter derived through a series solutions approach, but not necessarily limited to this technique. Numerical schemes may prove useful in providing these functions when they are too difficult to solve analytically. However, in practice the random errors of numerical solutions are amplified when the numerically evaluated stream function or hydraulic potential is differentiated to obtain the velocity field, and this may affect the accuracy and efficiency of the method presented in this chapter. Currently, little is known about the performance of these methods on numerical data. Once these functions are known, it is a relatively straightforward process to find advection fronts for any time required. This adds an extra dimension (and importance) to the ever increasing number of analytic solutions for the potential and stream functions of varying geometries.

The models developed in this chapter show the progression of the advection front as it moves outward from the aquaculture ponds to adjacent areas. Although it is evident from the stream function (Figure 2.2) that contamination of the surrounding land will occur, until now it has been difficult to predict when this will happen. But from Section 2.4 we can see that for the models in question, contamination of the usable groundwater will occur exponentially slowly, in accordance with equations (2.29) and (2.31), depending on the contamination source. For example, from equation (2.29) we see that for the advection front to progress 300 metres from the pond boundary requires 7,610 years. But from equation (2.31), 300 metres requires only 990 years. This simple comparison is indicative of the general case that arrival of salt water from below will more rapidly cause problems for the surrounding land. But even so, from Section 2.4.2 we see that the exponential nature of the contamination means that although salt

water will emerge within 7.6 years up to 175 metres from the pond boundary, for the advection front to travel as far again will require a further 7,600 years. So anyone judging the ongoing extent of contamination based on the initial progress of the salt may be dramatically overestimating the final impact to the environment.

The figures above imply some significant conclusions. It could be argued that the large time period for any significant contamination to occur makes concerns over salt-water seepage from the aquaculture ponds unfounded, given the relatively short lifespan of any such operation. However, it is important to note that the results above are based on a uniform (mean) hydraulic conductivity of 0.864 m/d (10^{-5} m/s) throughout the domain. Equations (2.29) and (2.31) show that K_* is inversely proportional to the travel time t_*, but in a typical soil profile K_* can vary by many orders of magnitude via small pockets of clay and coarse sand, even though macroscopically the soil is homogeneous. So even though the mean estimate of advection front progress may be accurate, locally the contaminant location could vary quite significantly. Additionally, if the heterogeneity within the soil profile is large (for example, such as layers of different soil types), our assumption of constant hydraulic conductivity will break down, and the mean estimate of advection front progress will no longer be valid. However, recently there has been some (as yet unpublished) progress (at local workshops and seminars) in the solution of the analytic functions for non-uniform hydraulic conductivity, meaning that any local variation may soon be calculable.

3

Modified advection

3.1 Introduction

The quasi-analytical technique presented in Chapter 2 incorporated a simple numerical method as part of the solution scheme. However, it was found that for very large isochrones, extracting results could be time consuming, particularly when solutions are sought using a laptop or PC. As such, this chapter presents an efficient and accurate alternative for the numerical component of the aforementioned quasi-analytical technique.

Figure 3.1 represents a soil profile taken from an aquaculture farm in the North Queensland region, where saline ponds sit above a freshwater aquifer 40 meters deep. Given the worst case scenario of salt water leaking freely into the groundwater beneath, we determine the contaminant advection fronts using two different techniques. The first technique, based on Euler's method, is a more traditional approach for solving time-dependent problems numerically; that is, we integrate along the closed form solution of the streamlines using a small discrete time step. This technique has an advantage in simplicity, but can be slow to extract a solution, especially for low flow domains, or large isochrones. For this reason, we present a second method (also based on Euler's method) which uses a small discrete spatial step, or natural parameterisation. The second technique has improved accuracy and is significantly quicker, but introduces some complexity which we discuss.

3.2 Original methodology

Read (1996a,b) describes the method of series solutions in some detail. For our example (Figure 3.1), we non-dimensionalise the domain using the depth as our scaling factor. These non-dimensional parameters (shown in brackets) constitute the domain of consideration in the rest of this article. Using the method described in Read (1996a,b), we truncate after $N+1$ terms to obtain a potential function $\phi(x, y)$ and a stream function $\psi(x, y)$,

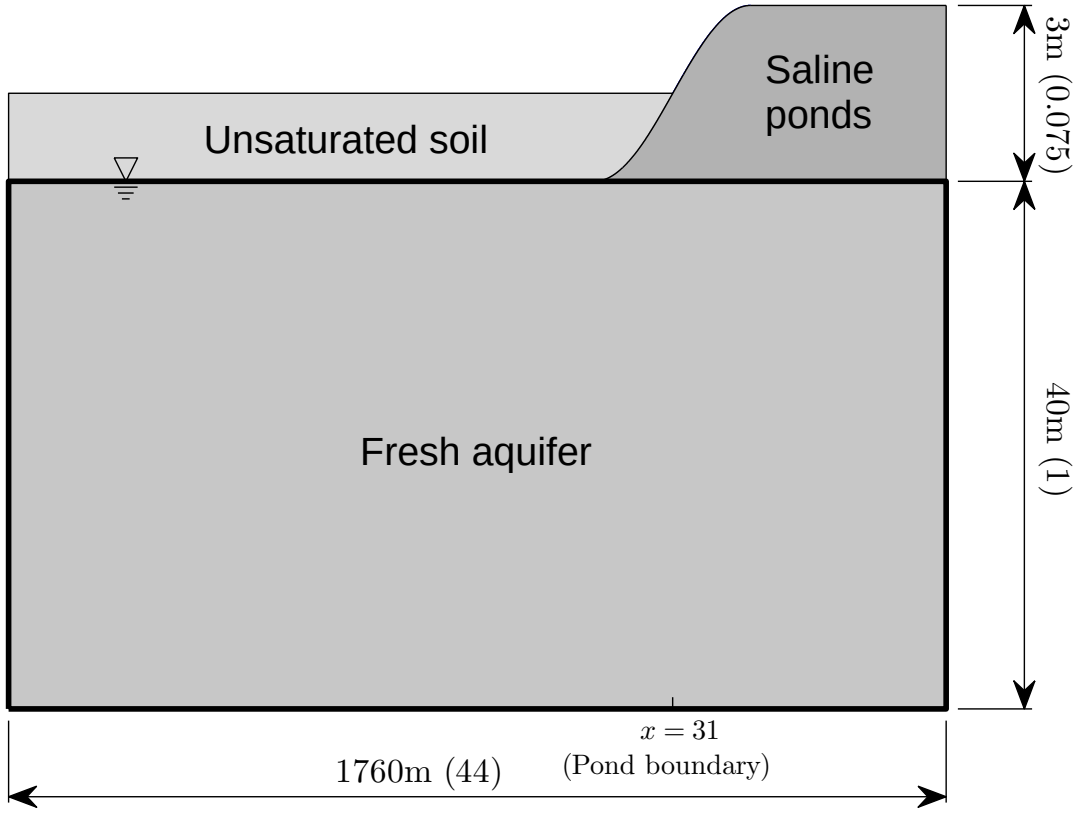

Figure 3.1: Saline ponds above freshwater aquifer (bracketed terms are dimensionless).

$$\phi(x,y) = \sum_{n=0}^{N} A_n \cosh\frac{n\pi y}{r}\cos\frac{n\pi x}{r}, \tag{3.1}$$

$$\psi(x,y) = -\sum_{n=1}^{N} A_n \sinh\frac{n\pi y}{r}\sin\frac{n\pi x}{r}, \tag{3.2}$$

where

$$A_0 = \frac{1}{r}\int_0^r h^t(x)\,dx, \tag{3.3}$$

$$A_n = \frac{2}{r}\int_0^r h^t(x)\cos\frac{n\pi x}{r}\,dx, \quad n \neq 0. \tag{3.4}$$

The partial derivatives of equations (3.1) and (3.2) (that is, the fluid velocity) satisfy the bottom and side (impermeable) boundary conditions exactly (to machine

precision), with the remaining boundary condition ($h^t(x)$) used to evaluate the series coefficients $A_n, n = 0, 1, ..., N$.

From the series solution of the hydraulic head $\phi(x, y)$, we find the seepage velocity $\mathbf{u}_*$ (that is, the macroscopic velocity averaged over the void and solid area) from Darcy's equation,

$$\mathbf{u}_* = -K_* \nabla \phi(x, y), \tag{3.5}$$

where K_*, the hydraulic conductivity, is a scalar. To find the pore velocity $\mathbf{U}_*$ (that is, the actual flow velocity through the void space) from equation (3.5), we simply divide through by the soil porosity σ (also a scalar),

$$\mathbf{U}_* = -\frac{K_*}{\sigma} \nabla \phi(x, y). \tag{3.6}$$

We non-dimensionalise equation (3.6) with the scaling factor K_*/σ and separate the directional components to get an expression for the velocity field $\mathbf{U} = (U, V)$,

$$\mathbf{U} = -\left(\frac{\partial \phi}{\partial x}, \frac{\partial \phi}{\partial y} \right). \tag{3.7}$$

The velocity at any point is also

$$\mathbf{U} = \left(\frac{dx}{dt}, \frac{dy}{dt} \right), \tag{3.8}$$

where the location at which the pore velocity is calculated is parameterised using time t. That is, x and y are no longer independent variables, but are now time dependent, $x \equiv x(t),\ y \equiv y(t)$. Thus, from equations (3.7) and (3.8), the time t taken for a neutrally buoyant particle to be advected along a streamline from (x_0, y_0) to $(x(t), y(t))$ is

$$t = \int_{x_0}^{x(t)} \frac{dx}{U} = -\int_{x_0}^{x(t)} \frac{dx}{\partial \phi / \partial x}, \tag{3.9}$$

$$= \int_{y_0}^{y(t)} \frac{dy}{V} = -\int_{y_0}^{y(t)} \frac{dy}{\partial \phi / \partial y}. \tag{3.10}$$

We use this result to determine isochrones for the salt water as it is transported away from the aquaculture ponds. By rearranging equations (3.9) and (3.10), the distances $(\Delta x, \Delta y)$ a particle is advected in the x and y directions in a small time interval Δt is

$$\Delta x \approx -\frac{\partial \phi}{\partial x}\Delta t, \tag{3.11}$$

$$\Delta y \approx -\frac{\partial \phi}{\partial y}\Delta t. \tag{3.12}$$

Consider at time $t = t_0$ a discrete set of $I > 0$ points $(x_{i,0}, y_{i,0}),\ i = 1, \ldots, I$. Then, for any time $t_J = t_0 + J\Delta t,\ J > 0$, we calculate the approximate location of the advection front $(x_{i,J}, y_{i,J})$ by calculating the intermediate points $(x_{i,j}, y_{i,j}),\ j = 1, \ldots, J-1$ using the difference equations

$$x_{i,j} \approx x_{i,j-1} - \left(\frac{\partial \phi}{\partial x}\right)_{i,j-1} \Delta t, \tag{3.13}$$

$$y_{i,j} \approx y_{i,j-1} - \left(\frac{\partial \phi}{\partial y}\right)_{i,j-1} \Delta t, \tag{3.14}$$

where

$$\left(\frac{\partial \phi}{\partial x}\right)_{i,j} = \left(\frac{\partial \phi(x,y)}{\partial x}\right)_{\substack{x=x_{i,j}\\ y=y_{i,j}}}, \tag{3.15}$$

$$\left(\frac{\partial \phi}{\partial y}\right)_{i,j} = \left(\frac{\partial \phi(x,y)}{\partial y}\right)_{\substack{x=x_{i,j}\\ y=y_{i,j}}}. \tag{3.16}$$

For sufficiently small Δt (that is, sufficiently large J), this converges to the advection front at time t_J. Using this algorithm, we predict the advection of solutes from any initial location in the flow domain. In particular, we determine the isochrones of solutes advected from the water table immediately below the saline ponds. Choosing an isochrone of $t_J = 200,000$ dimensionless units, Figure 3.2 shows the extent of the advection along each streamline. We have then joined these final advection locations to create the advection front, or isochrone.

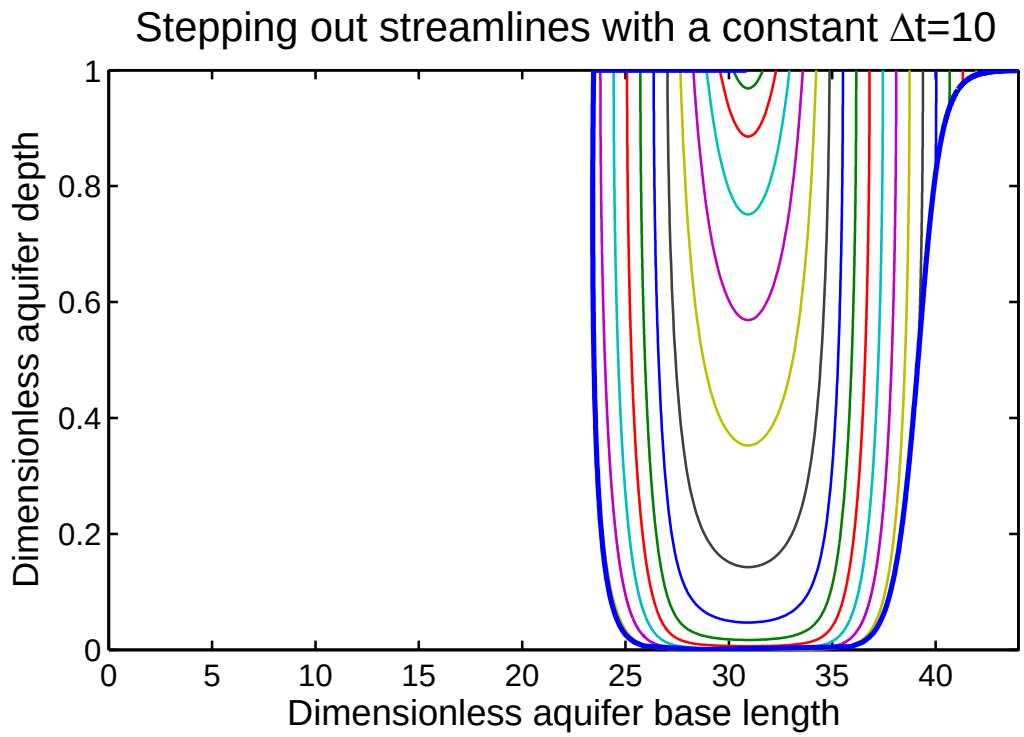

FIGURE 3.2: Δt solution scheme giving isochrone at $t_J = 200,000$.

3.3 Problems

The above methodology is inherently simple, but for the example considered, the large aspect ratio and relative small potential results in extremely low flow velocities in part of the domain. As we see from equations (3.11) and (3.12), a low velocity will result in small spatial increments $(\Delta x, \Delta y)$. If this happens, then even for a large isochrone value (as in Figure 3.2), we observe that the final location of the advection front has moved little from its initial location (observe the area near the right boundary of Figure 3.2). Although this is not a problem when solving for particular isochrones, solving for the time to reach a particular location can be problematic. If the location is in the low velocity part of the domain, then the solution output time may be extremely high. If we want to solve for the entire domain (that is, for salt water to move everywhere within the domain), then the time required to produce a solution may be excessive.

3.4 Modified methodology

For the most part, our modified methodology is similar to that of the original. From Section 3.2, we follow the procedure described to equations (3.9) and (3.10). It is after this point that the modified method diverges.

From the original methodology, we observe that in the low velocity part of the domain our solution progresses extremely slowly. If we could get a consistent rate of progress throughout the domain at every iteration, this should result in a faster solution output time. Rather than calculating the distance we move along a streamline for a set Δt, we set Δs as the length we *will* move along the streamline, and find the time it takes to do so. That is,

$$\Delta s = \sqrt{(\Delta x)^2 + (\Delta y)^2} = \text{constant}. \tag{3.17}$$

Equation (3.7) defines the velocity field ($\mathbf{U} = (U, V)$) everywhere within the domain. We define W as the speed along Δs, therefore,

$$W = \|\mathbf{U}\| = \sqrt{U^2 + V^2}. \tag{3.18}$$

We also know

$$W \approx \frac{\Delta s}{\Delta t}. \tag{3.19}$$

So, rearranging and solving equations (3.11),(3.12) and (3.19),

$$\Delta x \approx \left(\frac{U}{W}\right)\Delta s, \tag{3.20}$$

$$\Delta y \approx \left(\frac{V}{W}\right)\Delta s, \tag{3.21}$$

$$\Delta t \approx \frac{\Delta s}{W}. \tag{3.22}$$

Stepping along each streamline by Δs will mean consistent progress at each iteration, even in the low flow part of the domain. However, unlike the original method where the time at any iteration (j) was found from the equation ($t_j = t_0 + j\Delta t$), now the

time varies, not only for each iteration, but for each streamline in an iteration. For the modified methodology, as well as recording Δx and Δy as in the original method, from equation (3.22) we need to record Δt.

Consider at time $t = t_{i,0}$ a discrete set of $I > 0$ points $(x_{i,0}, y_{i,0}),\ i = 1, \ldots, I$. For a given number of iterations (J), we now determine our progress through the domain, both spatially and temporally $(x_{i,J}, y_{i,J}, t_{i,J})$, by calculating the intermediate values $(x_{i,j}, y_{i,j}, t_{i,j}),\ j = 1, \ldots, J-1$ using the difference equations

$$x_{i,j} \approx x_{i,j-1} + \left(\frac{U_{i,j-1}}{W_{i,j-1}}\right)\Delta s, \tag{3.23}$$

$$y_{i,j} \approx y_{i,j-1} + \left(\frac{V_{i,j-1}}{W_{i,j-1}}\right)\Delta s, \tag{3.24}$$

$$t_{i,j} \approx t_{i,j-1} + \left(\frac{\Delta s}{W_{i,j-1}}\right), \tag{3.25}$$

where

$$U_{i,j} = -\left(\frac{\partial \phi(x,y)}{\partial x}\right)_{\substack{x=x_{i,j}\\ y=y_{i,j}}}, \tag{3.26}$$

$$V_{i,j} = -\left(\frac{\partial \phi(x,y)}{\partial y}\right)_{\substack{x=x_{i,j}\\ y=y_{i,j}}}, \tag{3.27}$$

$$W_{i,j} = \sqrt{(U_{i,j})^2 + (V_{i,j})^2}. \tag{3.28}$$

Given a sufficiently small Δs (that is, sufficiently large J), the advection location on any streamline will converge at time $t = t_{i,J}$ (each value of i represents a separate streamline). But unlike the original methodology, our values of $t_{i,J}$ are not the same, and this introduces some complexity into our scheme. Let's take the previous example of solutes advected from the water table immediately below the saline ponds. Choosing an isochrone of $200,000$ dimensionless units, we now have to find the values of i, j where $t_{i,j} = 200,000$.

We found the simplest method was to let the scheme iterate through j, with a stopping condition that for all i, $t_{i,j} > 200,000$. The ends of the streamlines in Figure 3.3 show when this stopping condition is met. We now must find the values of

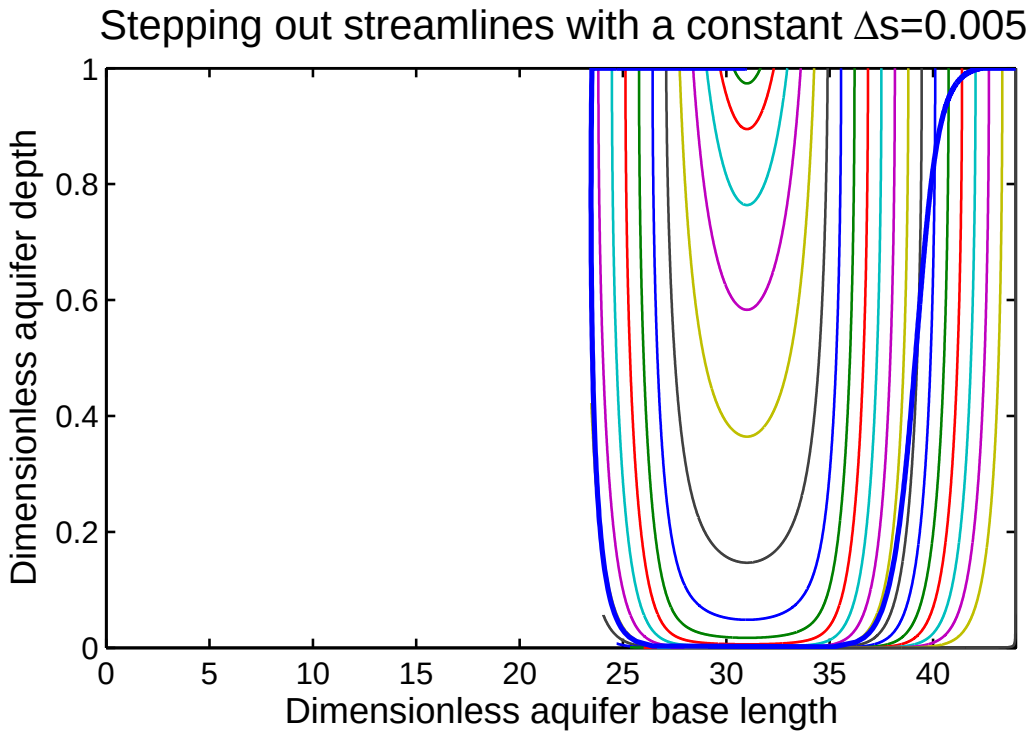

Figure 3.3: Δs solution scheme giving isochrone at $t = 200,000$.

$t_{i,j} = 200,000$, but this is complicated by the discrete nature of Δt. We may not find even one set of i, j values where $t_{i,j} = 200,000$, so we must find the closest such values on each streamline and interpolate. Using these values of i, j, we find the corresponding values of $x_{i,j}, y_{i,j}$, and applying the same interpolation ratios, we produce the isochrone for $t = 200,000$ seen in Figure 3.3.

3.5 Comparison

The constant time step approach is an intuitive method, but when dealing with low velocity domains such as Figure 3.1, we found the time taken to produce a solution was excessive. To produce satisfactorily accurate results for the example considered in this chapter (Figure 3.2), we needed to run the scheme overnight using a standard PC (Intel Pentium 4 CPU 3.40GHz, 1.00GB RAM, Matlab). The constant spatial step approach was developed in response to our need for faster solution output times. Keeping all other parameters equal, but changing to a constant spatial step, the example in this

chapter (Figure 3.3) achieved a seven fold reduction in solution output time, from 11 hours to 95 minutes.

Of course, faster solutions can be achieved using the constant time step approach, simply by choosing a larger value of Δt and allowing our accuracy to suffer. To show that the increase in speed of the constant spatial step method is not achieved by a corresponding decrease in accuracy, we compare the two methods to the analytic solution. For both methods, we step through the domain incrementally using the characteristics of the flow field at each point to calculate the location of the next point. If our schemes are accurate, the paths stepped out in this fashion correspond to streamlines derived from the stream function (equation (3.2)) starting at the same points. We judge whether our values of Δt or Δs are sufficiently small by finding the corresponding deviation from the analytic result.

For each of our methods, we take the final point of every streamline which emerges at the water table for an isochrone of $200,000$, and compare it with the final point as found from the analytic solution. Figure 3.4 is a plot of the deviation of each of these streamlines for the examples in this chapter, that is, $\Delta t = 10$ and $\Delta s = 0.005$. We see that the Δs method not only gives a seven fold improvement in solution output time, but is approximately an order of magnitude more accurate as well.

3.6 Discussion

The constant spatial step method was developed to reduce the time required to solve isochrones in low velocity flow domains. Since we are generally interested in the physical location of a contaminant as it progresses through a domain, the fact that this method is consistent in its progress at any point is a big advantage over the constant time step method. A constant time step will require a certain number of iterations to solve for a particular isochrone, but in the low velocity part of the domain the physical progress of the contaminant may be infinitesimal compared with the progress elsewhere. However, the constant spatial step method can potentially solve even large isochrones in this low velocity area in a single iteration. For this reason the constant spatial step method is

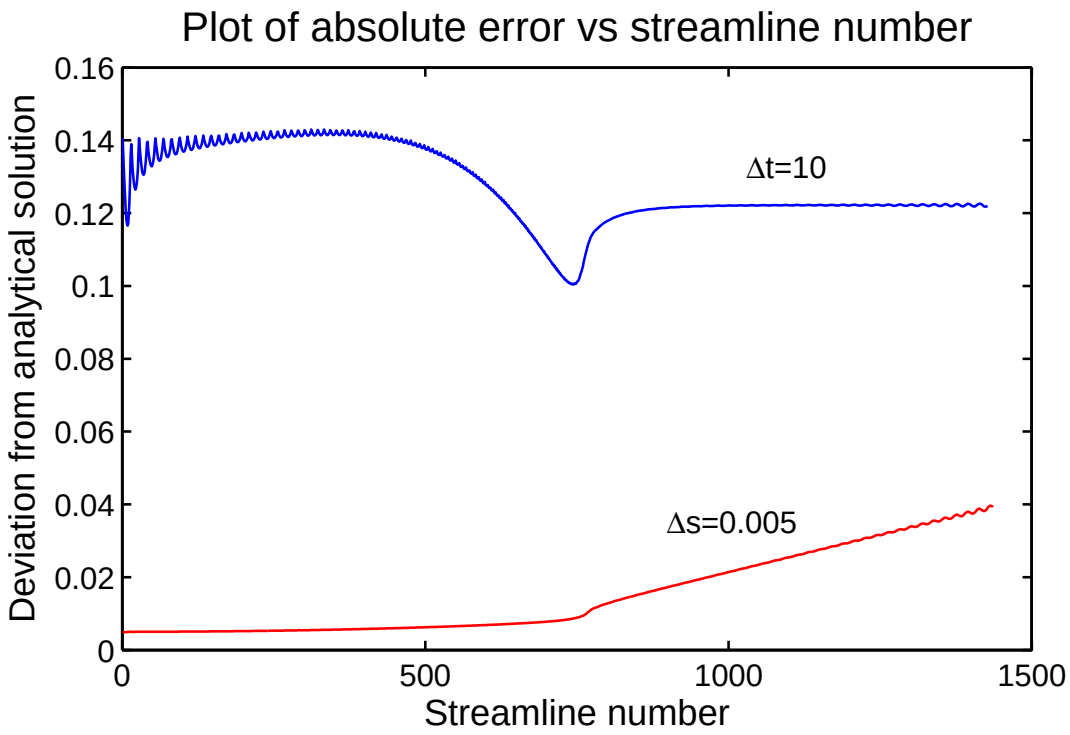

Figure 3.4: Deviation of $\Delta t = 10$ and $\Delta s = 0.005$ from the analytical solution.

not constrained to a certain number of iterations for any particular isochrone, but will produce a solution in the number of iterations required to step to the final physical location.

For the examples considered in this chapter, $\Delta t = 10$ and $\Delta s = 0.005$ were chosen as they represent the maximum values at which the accuracy of the solutions started to decay. For $\Delta t = 10$, exactly $20,000$ iterations were required to solve for the isochrone at $t = 200,000$, while just $3,173$ iterations were required for $\Delta s = 0.005$ for the same isochrone. We calculated many other isochrones in this same flow domain for varying Δt and Δs values, with the constant spatial step method significantly more efficient in every case. (Note, the errors were similar for both methods.)

The relative improvements in time and accuracy of the constant spatial step method will vary based on the isochrone being solved, the values of Δs and Δt, and the characteristics of the velocity field throughout the domain. For some situations there may be little advantage in using the constant spatial step method at all. But as we have shown, when dealing with domains where any part of the velocity field is small, the

constant spatial step method should perform significantly better.

In this chapter we have compared two different methods for integrating along streamlines to find the advection front of possible groundwater contaminants. Although different in their application, both techniques are based on simple Euler forward integration. For the purposes of this chapter, this simple integration technique was sufficient, but future investigation of other numerical integration methods may yet yield more accurate and/or faster results.

4

Diffusion

4.1 Introduction

Contaminant transport via advection from a leaky saltwater pond into an underlying freshwater aquifer has previously been analysed by Verrall et al. (2009b) (Chapter 2). Contamination near the pond edge was shown to occur rapidly, but as the distance from this boundary increased, the time taken for salt to arrive at any particular point slowed exponentially. A dimensionless 'contamination equation' was deduced to predict the movement of salt away from the pond. This equation showed that the initial burst of outward movement from the saltwater pond quickly slowed to such an extent that it was no longer calculable as movement at all. This is a somewhat surprising finding, but this research only considered the role of advection in the transport of salt contamination. Given the rapid decay in the speed of the advection process, a natural question to ask is *How long does it take the salt to be transported to the adjacent farmlands once diffusion takes over?*

To answer this question, we extend the analysis carried out in Chapter 2 by considering diffusive transport as the dominant process, once the advective component has become negligible. We analyse the problem by dividing the transport process into two distinct phases. First, salt is advected into the aquifer (ignoring any diffusive effects), until the discharge velocity becomes negligible. This creates a contaminated region that forms the source for the diffusion process, the size and shape of this region being one of the results of Chapter 2. Second, at the boundaries of this region the discharge velocity is small, therefore advection is ignored and diffusion takes over as the dominant transport process. That is, the problem this chapter investigates is contaminant transport through the domain once diffusion becomes dominant. Section 4.2 describes this domain in greater detail. Note that advection still plays a significant role in the process. Advection replenishes salt that diffuses through the domain, therefore transforming the problem to one of diffusion from a region of constant concentration within the aquifer. (We examine this idea in more detail in Section 4.4.)

In this chapter, we will solve for the general diffusion problem using analytic series solutions. The analytic method will be modified to allow for the salt advection from the

aquaculture ponds, by iteratively updating a region of solute in the aquifer. This quasi-analytical method incorporates the accuracy of an analytical solution, while maintaining the robustness of a numerical scheme. Using this technique, we find where diffusion becomes the dominant mode of transport, as well as determining the overall time frame for contamination to any point within the freshwater aquifer.

This chapter is organised as follows. In Section 4.2 we provide an overview of the example considered, with the mathematical model presented in Section 4.3. The relationship between advection and diffusion is analysed in Section 4.4, and results of the model are presented in Section 4.5. Finally, we discuss these results and draw appropriate conclusions in Section 4.6.

4.2 Hydrogeology and model boundaries

In this chapter, the problem that we solve is modelled on aquaculture ponds situated near the coast and adjacent to farmland. We assume that the coastal aquifer in the region has a depth of 40 metres and lies above an aquiclude of impermeable bedrock. A leaky saltwater pond, 3 metres high, is situated above the aquifer. The left side boundary is impermeable, well beyond the area of interest, while the right side boundary lies beneath the edge of the ponds. There is no diffusion across this boundary as it is spanned by a region $R(x, y)$ that (for the situations of interest to this chapter) extends to the bottom of the aquifer and is maintained at a constant maximum concentration. Therefore, the right side boundary can be treated as zero flux. Figure 4.1 shows a schematic of the solution domain.

The domain of consideration has been modified slightly from the original problem (Chapter 2) where advection was analysed. In this chapter, the left boundary has been extended well past the farmland, so that any edge effects are negligible. For the advection problem, the location of the left boundary had little or no effect on the advection of the solute. However, edge effects can be important for diffusive processes, because the concentration of solute increases as the left boundary is moved closer to the source. For the aquaculture ponds and farmland being modelled in this chapter, the

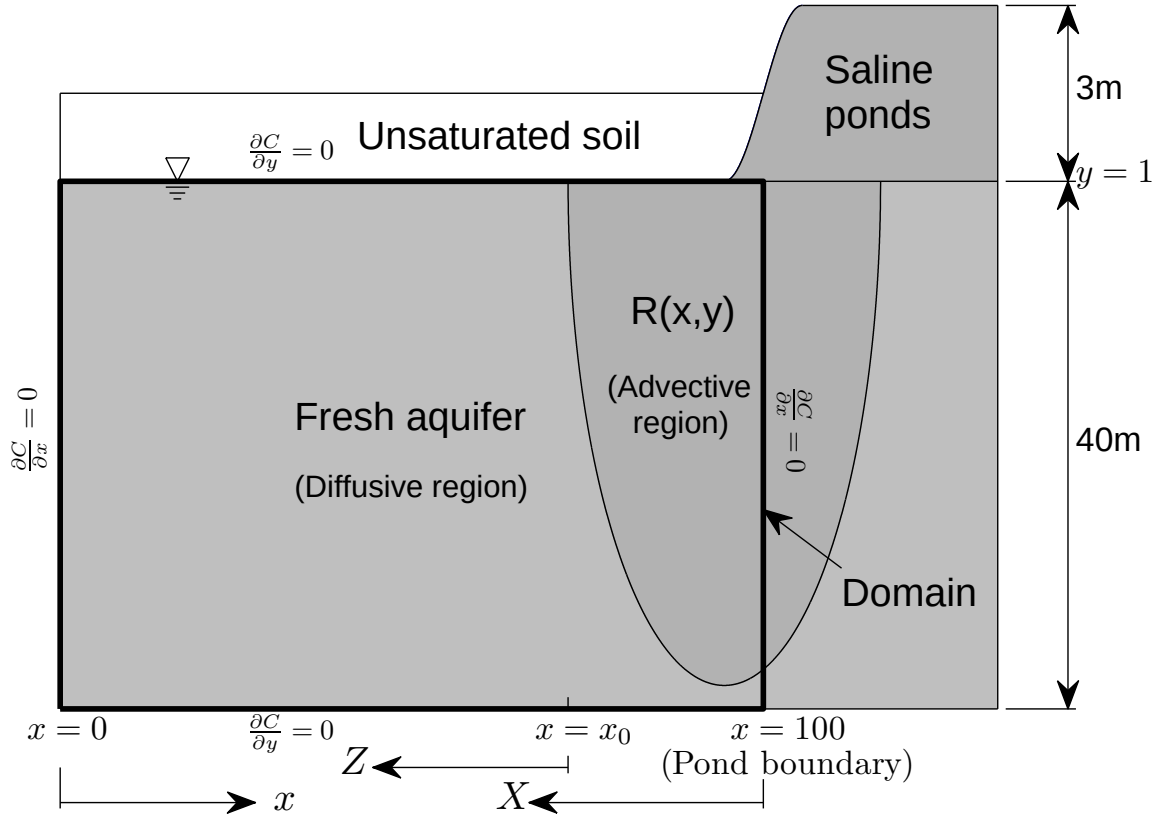

FIGURE 4.1: Domain considered throughout this chapter.

left boundary is situated well beyond any possible edge effects. Also in this chapter, the right boundary has been shifted from beneath the centre of the saline ponds to beneath the edge of the saline ponds. This was done for reasons of simplicity, that is, so the region of higher concentration $R(x, y)$ spanned the boundary, allowing for a zero flux boundary condition. The top boundary is the surface of the water table, and as such represents an air/water interface. There is no diffusion across this surface or the impermeable bottom and side boundaries.

In this chapter we are interested in the breakthrough front of salt diffusion, taken as the point when the concentration has reached 50% of the concentration in the saltwater ponds. That is, the diffusion front is said to have moved only when the salt concentration at any point has reached 50% of the initial contaminant concentration level. The source boundary for diffusion is taken as the final location of the advection

front, $R(x, y)$. Outside the final location of the advection front, diffusion is assumed faster than advection. Inside the advection front, advection is assumed to be faster than diffusion, and solute is replaced as quickly as it diffuses. (Refer to Section 4.4 for more details.) The region $R(x, y)$ is treated as a source of constant strength, with solute concentration maintained at the same level as that in the ponds. Any excess salt that is not diffused away from this region is transported through to the soil surface.

Outside the advection region, the process is considered purely diffusive, with any solute movement a consequence of molecular diffusion. An important consideration here is the location where this change from advection to diffusion occurs—we examine and validate this process in Section 4.4. In the diffusion region, the diffusive processes are assumed isotropic and due to molecular diffusion only, so the diffusion coefficients in the lateral and longitudinal directions are equal and constant (Hunt, 1983).

4.3 Mathematical model of salt transport

The problem is formulated mathematically as follows. Inside the aquifer,

$$\frac{\partial}{\partial x_*}\left(D_{x_*}\frac{\partial C_*}{\partial x_*}\right) + \frac{\partial}{\partial y_*}\left(D_{y_*}\frac{\partial C_*}{\partial y_*}\right) = \frac{\partial C_*}{\partial t_*}, \tag{4.1}$$

where $C_*(x_*, y_*, t_*)$ is the concentration of solute at any point (x_*, y_*) in the aquifer at time t_*. (Note that asterisk subscripts represent dimensional variables. These will later be dropped when the problem is non-dimensionalised.) Assuming there is no diffusion across impermeable boundaries or the water table, the boundary conditions are

$$D_{x_*}\frac{\partial}{\partial x_*}C_*(0, y_*, t_*) = D_{x_*}\frac{\partial}{\partial x_*}C_*(s_*, y_*, t_*) = 0, \tag{4.2}$$

$$D_{y_*}\frac{\partial}{\partial y_*}C_*(x_*, 0, t_*) = D_{y_*}\frac{\partial}{\partial y_*}C_*(x_*, d_*, t_*) = 0, \tag{4.3}$$

where s_* and d_* are the length and depth of the domain, respectively. The initial condition at $t_* = 0$ is then

$$C_*(x_*, y_*, 0) = \begin{cases} C_*^0, & x_*, y_* \in \mathrm{R}_*(x_*, y_*), \\ 0, & \text{elsewhere} \end{cases}, \tag{4.4}$$

with the general solution

$$C_*(x_*, y_*, t_*) = \begin{cases} C_*^0, & x_*, y_* \in \mathrm{R}_*(x_*, y_*), \\ C_*(x_*, y_*, t_*), & x_*, y_* \notin \mathrm{R}_*(x_*, y_*) \end{cases}, \tag{4.5}$$

where $\mathrm{R}_*(x_*, y_*)$ is the region in the aquifer to be maintained at constant concentration C_*^0, the concentration of solute in the ponds. That is, the region $\mathrm{R}_*(x_*, y_*)$ is the area within the aquifer where advection is dominant. Unfortunately, this constant source region $\mathrm{R}_*(x_*, y_*)$ cannot be incorporated into the partial differential equation (4.1) as a source term, as the solute concentration in the aquifer would increase without bound, since there is no solute flux across any of the boundaries. In fact, the boundary of this region intersects the original rectangular boundary to form an irregular boundary with a constant concentration along it (refer to Figure 4.1). This means the problem is not amenable to the usual analytic series techniques. However, also note that we can solve this problem directly when this condition collapses to an initial condition, as in equations (4.1)–(4.4).

We non-dimensionalise the problem in terms of the depth of the aquifer, d_*, the initial concentration of the ponds, C_*^0, and (noting that $D_{x_*} = D_{y_*} = D_*$) the diffusivity, D_*:

$$s_* = d_* s, \quad x_* = d_* x, \quad y_* = d_* y, \quad C_* = C_*^0 C, \quad t_* = \frac{d_*^2}{D_*} t_{\mathrm{D}}. \tag{4.6}$$

(Note, t_{D} is non-dimensional time, scaled for diffusion parameters.) In terms of the non-dimensional variables x, y, C, t_{D}, the diffusion equation (4.1) becomes

$$\nabla^2 C(x, y, t_{\mathrm{D}}) = \frac{\partial C(x, y, t_{\mathrm{D}})}{\partial t_{\mathrm{D}}}, \tag{4.7}$$

with the boundary conditions in equations (4.2) and (4.3),

$$\frac{\partial C}{\partial x}\,|_{x=0,s} = 0, \qquad \frac{\partial C}{\partial y}\,|_{y=0,1} = 0, \tag{4.8}$$

and the initial condition in equation (4.4),

$$C(x,y,0) = \begin{cases} 1, & x,y \in \mathrm{R}(x,y), \\ 0, & \text{elsewhere} \end{cases}, \tag{4.9}$$

where $R(x,y)$ is the region of constant concentration in the non-dimensional problem.

4.3.1 Series solution for initial solute distribution

As noted in Section 4.3, the diffusion problem detailed in equations (4.7), (4.8) and (4.9) is amenable to analytic series methods, and the solution form can be obtained using separation of variables (see Appendix A.2 for details). Truncating after $m = M$, $n = N$ terms, the series expansion is

$$C(x,y,t_{\mathrm{D}}) = \sum_{m=0}^{M}\sum_{n=0}^{N} a_{mn}\cos\left(\frac{m\pi x}{s}\right)\cos\left(n\pi y\right)e^{-\lambda_{mn}^2 t_{\mathrm{D}}}, \tag{4.10}$$

where $\lambda_{mn}^2 = m^2\pi^2/s^2 + n^2\pi^2$ and a_{mn} are the series expansion coefficients. The series coefficients can be obtained from an orthogonality relationship,

$$a_{mn} = \int_0^s\int_0^1 C(x,y,0)\cos\left(\frac{m\pi x}{s}\right)\cos(n\pi y)\,dy\,dx, \tag{4.11}$$

or by using a (theoretically equivalent) collocation/discrete least squares approach (Trefethen, 2000):

$$C(x_i,y_j,0) = \sum_{m=0}^{M}\sum_{n=0}^{N} a_{mn}\cos\left(\frac{m\pi x_i}{s}\right)\cos(n\pi y_j) \tag{4.12}$$

at $M'N'$ collocation points $(x_i,y_j),\ i = 0,\ldots,M';\ j = 0,\ldots,N'$, where $M' \geq M+1$, $N' \geq N+1$. ($M' = M+1,\ N' = N+1$ for a 'pure' collocation or pseudo-spectral

approach.) In this case, the solution process devolves into solving a matrix equation,

$$X^{\mathrm{T}} C Y^{\mathrm{T}} = \left(X^{\mathrm{T}} X\right) A \left(Y Y^{\mathrm{T}}\right), \tag{4.13}$$

where, for $i = 0, \ldots, M'$, $j = 0, \ldots, N'$, $m = 0, \ldots, M$, $n = 0, \ldots, N$,

$$[X]_{im} = \cos(m\pi x_i/s), \qquad [Y]_{nj} = \cos(n\pi y_j), \tag{4.14}$$

$$[C]_{ij} = C(x_i, y_j), \qquad [A]_{mn} = a_{mn}. \tag{4.15}$$

This is the approach used in this chapter, with equally spaced collocation points x_i, y_j, as evaluating the integrals in equation (4.11) is significantly more computationally expensive than the collocation approach.

Once the solution for the diffusion equation (4.7) has been obtained, the isochrones of concentration at any (fixed) time t_{D} can be obtained by solving the implicit equation

$$C(x, y, t_{\mathrm{D}}) = c^0, \tag{4.16}$$

where c^0 is a constant with $0 < c^0 \leq 1$, and is the concentration along the isochrone. In this chapter, we are interested in the breakthrough front where the concentration is 50% ($c^0 = 0.5$) of the saline pond concentration.

4.3.2 Quasi-analytical technique

The series solution in equation (4.10) is obtained for the initial condition of equation (4.9), however, the solution is only correct at $t_{\mathrm{D}} = 0$. Once $t_{\mathrm{D}} > 0$, the concentration of solute will drop below 1, as the diffusive effects start to take place. As $t_{\mathrm{D}} \to \infty$, the concentration of solute throughout the aquifer approaches a constant value less than 1, and this obviously violates the constant source requirement as stated in Section 4.2.

To overcome this difficulty, we apply the series solution technique to the problem iteratively. Diffusing for a short time step (that is, a fraction of the required time

period) gives a small amount of transport away from the initial distribution, as well as a small reduction in concentration of that initial distribution. The result of the outward diffusive transport is kept to define the initial condition outside of $R(x, y)$, but the initial distribution of solute is reset to the original concentration, and then the series solution is obtained for the new problem. By repeating this process using very small time steps, we satisfy the requirement of $C(x, y, t_{\mathrm{D}}) = C^0$ where $x, y \in \mathrm{R}(x, y)$, and solve the problem for an arbitrary time period.

To choose the time step used for each iteration, simply choose an arbitrary value, for example, $\delta t_{\mathrm{D}} = 10$, and measure the overall reduction in the mean concentration of the source region $R(x, y)$. This time step is then adjusted until the percentage decrease in concentration in $R(x, y)$ is less than a predefined tolerance. If the decrease in concentration is greater than the tolerance, the value of δt_{D} is reduced and the process repeated until a suitable time step is obtained. In this chapter we used a value of $\delta t_{\mathrm{D}} = 0.0391$, which corresponds to a tolerance level of 10% of the source concentration in $R(x, y)$ (that is, the total quantity of salt within $R(x, y)$ never dipped below 90% of the initial level). Some experimentation revealed that smaller values of the tolerance did not significantly affect the results, although the computational cost increased markedly.

4.4 Advection versus diffusion

We model the progress of the solute as a two stage process: advection then diffusion. In the first stage, solute is advected from the saline ponds to form a stagnant region, $R(x, y)$, of contamination. That is, the potential gradient from the ponds to the aquifer can only force contaminated water so far, before fluid flow effectively stops. Within this stagnant region, $R(x, y)$, if solute is removed, it gets replenished via advection. In the second stage, contamination via diffusion becomes the dominant process away from this stagnant region. Depending on the properties of the aquifer, the limits of $R(x, y)$ will change. The first stage was solved in Chapter 2, with one of the results being an equation for the contaminant breakthrough curve along the water table. The second

stage can be solved using the quasi-analytical scheme described in Section 4.3.2. Using this method, an equation for the 50% breakthrough curve along the water table can be found. In the following subsections the process for finding the diffusion breakthrough curve is provided, the relationship between the advection and diffusion time scales is determined, and the method used to determine the extent of the stagnant region, $R(x, y)$, is detailed.

4.4.1 Predicting the advective and diffusive contamination velocities

Chapter 2 found an empirical relationship for the progress of advective contamination through the domain,

$$t_{\mathrm{A}} = 2e^{1.52X}, \quad 5 \leq X \leq 14, \tag{4.17}$$

where t_{A} is the dimensionless time (scaled for advection parameters) needed to progress the dimensionless distance X from the pond boundary along the water table. In the zone $X < 5$, the results leading to the above equation were influenced by smoothing the water table at the pond boundary. Note that X is positive from right to left as seen in Figure 4.1, and that the advection process had effectively stopped when $X \geq 14$. Equation (4.17) can be differentiated w.r.t. time, and rearranged to give the rate of progress of advective contamination along the water table (which for lack of a better term we will refer to as the advective contamination velocity) u_{A}:

$$u_{\mathrm{A}} = \frac{1}{\frac{dt_{\mathrm{A}}}{dX}} = \frac{e^{-1.52X}}{3.04}, \quad 5 \leq X \leq 14. \tag{4.18}$$

Given a constant concentration region $R(x, y)$ of solute, the quasi-analytical scheme of Section 4.3.2 is used to determine a solution for the concentration $C(x, y, t_{\mathrm{D}})$ throughout the aquifer at any time $t_{\mathrm{D}} > 0$. This solution can be used to determine I coordinates $(Z_i, t_{\mathrm{D}i}),\ i = 1, \ldots, I$ of the 50% breakthrough curves of salt contamination along the water table (Z is the dimensionless distance along the water table from $R(x, y)$, and is positive from right to left as seen in Figure 4.1). Some experimentation revealed the

best fit for this empirical relationship is a quadratic of the form

$$t_{\mathrm{D}} = a_R Z^2 + b_R Z + c_R, \tag{4.19}$$

where t_{D} is the dimensionless time (scaled for diffusion parameters) needed to progress the distance Z from the boundary of $R(x, y)$. That is, if the boundary of the advection zone $R(x, y)$ starts on the water table at $x = x_0$, then any point Z_i on the breakthrough curve has $x-$coordinate $x_i = x_0 - Z_i$. Differentiating equation (4.19) w.r.t. time, re-arranging, and substituting $Z = 0$, gives the rate of progress of diffusive contamination along the water table (which again, for lack of a better term we will refer to as the diffusive contamination velocity) u_{D} at the boundary of $R(x, y)$:

$$u_{\mathrm{D}} = \frac{dZ}{dt_{\mathrm{D}}} = \frac{1}{b_R}. \tag{4.20}$$

However, this diffusive contamination velocity, u_{D}, is unrealistic as it occurs at a discontinuity. That is, mathematically there is a step change in concentration from the advection region, $R(x, y)$, to the rest of the domain, when clearly this is not the case in reality. This discontinuity creates two problems: firstly, the concentration change from $C^0 = 1$ to $C(x, y, 0) = 0$ means the concentration gradient is infinite; and secondly, the analytic series solution suffers from Gibbs phenomenon (a mathematical artifact resulting in oscillatory behaviour near the discontinuity). However, both can be dealt with by smoothing the transition zone so the concentration changes smoothly from $C^0 = 1$ to $C(x, y, 0) = 0$. We initially used a Gaussian spatial filter to smooth the concentration gradient at the discontinuity. This type of filter is designed to give no overshoot to a step function input, while minimising the rise and fall time. In our case, the smooth transition zone corresponded to approximately 2% of the length of the domain. The modified initial concentration $\hat{C}(x, y, 0)$ was given by

$$\hat{C}(x_i, y_j, 0) = \sum_{i=1}^{K} \sum_{j=1}^{L} w_{ij} C(x_i, y_j, 0), \tag{4.21}$$

with the weights,

$$w_{ij} = \frac{1}{2\pi\theta^2} e^{-(\frac{x^2+y^2}{2\theta^2})}, \tag{4.22}$$

where θ is the standard deviation. Note, we limited the transition zone on each side of the discontinuity to three standard deviations, where $\theta = 0.3$ dimensionless units (giving a total transition length for this domain of 72 m). This smoothed initial distribution removed the Gibbs phenomenon and the sharp discontinuity in the transition zone, and gave good results.

However, there is a more natural way to introduce a smooth transition between $C^0 = 1$ and $C(x, y, 0) = 0$, using the original (discontinuous) series solution. The series solution is allowed to diffuse for the same period of time required for advection to create the stagnant region $R(x, y)$, and this is then used as the initial solution for the quasi-analytical scheme. That is, the series solution for the concentration is obtained using the original (discontinuous) initial conditions, and then the solution at a later time (that corresponds to the time taken for advection to create $R(x, y)$) is used as the 'smoothed' initial condition. This process provides smooth initial solutions that do not suffer from Gibbs phenomenon and work as well, or better, than the filtering technique previously described. It is this method that will be used throughout the remainder of this chapter. Note that the coefficients of equation (4.19) are reevaluated after this smoothing has been applied.

4.4.2 Advection and diffusion time scales

To combine the models (or results) of advection and diffusion (Sections 2.3 and 4.3, respectively), the dimensionless advection and diffusion time scales have to be related. That is, although both models are dimensionless, each were non-dimensionalised (temporally) using different parameters, resulting in different scaling factors (similar in concept to the difference between the dimensionless terms *parts per million* and *parts per billion*). To relate these non-dimensional time scales, we simply convert each back to the common reference value of dimensional time, and solve. (Note that as the spatial scaling is the same for both processes, that is, the depth of the aquifer d_*, there is no

spatial adjustment required to combine the models.)

For the domain of Figure 4.1, to solve for real (dimensional) time, t_*, for pure advection, Section 2.3 provides the following equation (given in terms of the non-dimensional advection time t_{A}),

$$t_* = t_{\mathrm{A}} \frac{\sigma d_*}{K_*}, \tag{4.23}$$

where σ is the porosity, d_* is the depth, and K_* is the hydraulic conductivity. To combine separate solutions of advection and diffusion, equation (4.23) must equate to the real time for diffusion t_*, given in terms of the dimensionless diffusion time t_{D},

$$t_* = t_{\mathrm{A}} \frac{\sigma d_*}{K_*} = t_{\mathrm{D}} \frac{d_*^2}{D_*}. \tag{4.24}$$

Rearranging, this becomes

$$t_{\mathrm{D}} = \frac{D_* \sigma}{K_* d_*} t_{\mathrm{A}} = \alpha t_{\mathrm{A}}, \tag{4.25}$$

where

$$\alpha = \frac{D_* \sigma}{K_* d_*} = \frac{\frac{D_*}{d_*}}{\frac{K_*}{\sigma}}. \tag{4.26}$$

The parameter α is the ratio of the dimensionless diffusion time scale to the dimensionless advection time scale. However, it is also a combination of the physical parameters of the aquifer. In this sense, α can be regarded as characteristic of the aquifer. Therefore, the location within the domain where diffusion becomes the dominant transport process will vary depending on this characteristic value. In the next section we determine a relationship between α and the location where diffusion becomes dominant. (As an aside, given that hydraulic conductivity, K_*, has the same units as velocity (m/s), it is interesting to note the similarity of equation (4.26) to expressions of the (inverse) Péclet number.)

4.4.3 Advection–diffusion boundary

For each α value there corresponds an $X-$coordinate (or $x-$coordinate) that delineates the point on the water table beyond which the diffusive contamination velocity is faster than the advective contamination velocity; that is, where diffusion is the dominant

transport process. This relationship can be obtained by considering the end result of advection, $R(x, y)$, for any arbitrary time period. The intersection of $R(x, y)$ with the water table gives the position, X_0, which will be the transition point between the advective region ($R(x, y)$) and the diffusive region ($X > X_0$) for some (as yet undetermined) value of α. For this particular α, X_0 is therefore also the point on the water table where the rate of diffusive contamination (4.20) is the same as the rate of advective contamination (4.18). Recalling that these rates of contamination are defined using different time scales, t_{A} and t_{D}, then, using equation (4.25) and the chain rule,

$$u_{\mathrm{A}} = \alpha u_{\mathrm{D}}. \tag{4.27}$$

Substituting for u_{A} and u_{D},

$$\frac{e^{-1.52X_0}}{3.04} = \frac{\alpha}{b_R}. \tag{4.28}$$

Hence,

$$\alpha = b_R \frac{e^{-1.52X_0}}{3.04}, \quad 5 \leq X_0 \leq 14, \tag{4.29}$$

or, given a known value of α,

$$X_0 = \frac{\ln\left(\frac{3.04}{b_R}\alpha\right)}{-1.52}, \quad 5 \leq X_0 \leq 14. \tag{4.30}$$

A given set of aquifer parameters allows for the calculation of the characteristic value α (from equation (4.26)). Substituting α into equation (4.30) gives the location on the water table, $X = X_0$, that delineates the advective and diffusive regions of the domain. That is, up to X_0, diffusion can be ignored and an advection only simplification is sufficient. Beyond X_0, further advection can be ignored and a diffusion only simplification (from a constant concentration source) is sufficient. If the time for contamination to reach $X > X_0$ is required, then the time for advection to X_0 is simply added to the time for diffusion (greater than X_0). It is important to note that straddling this point, X_0, will be a two-mode region of some thickness wherein the relative rates of advective and diffusive contamination are comparable in magnitude. However,

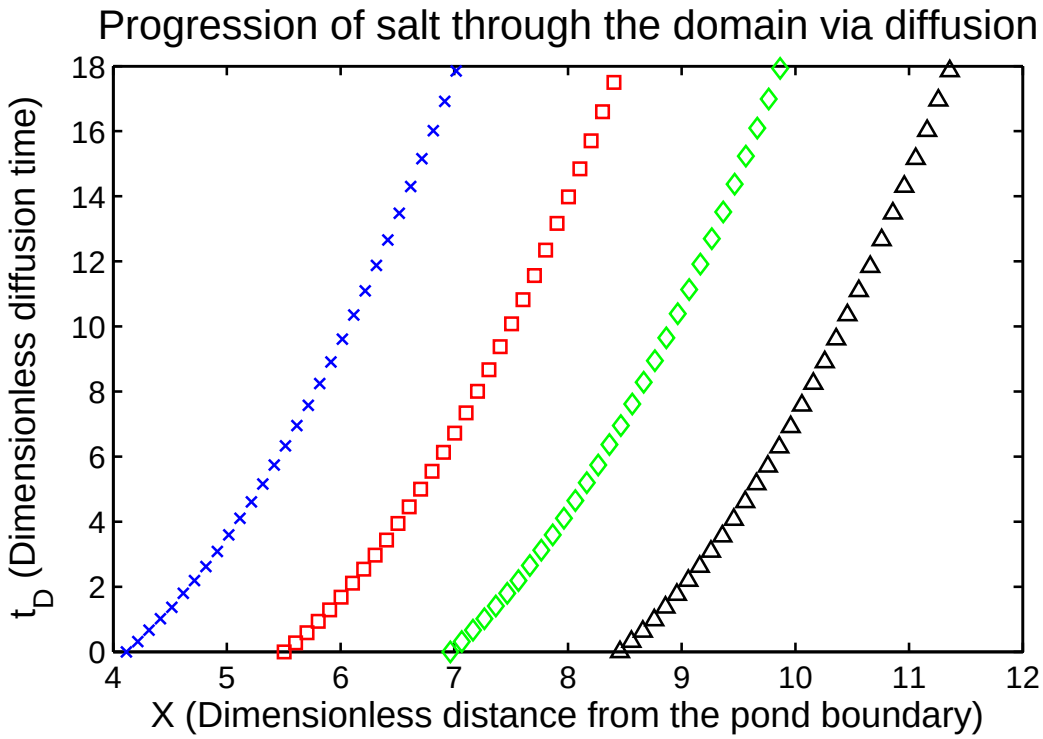

Figure 4.2: Diffusion for different $R(x, y)$.

given the exponential decay of the advective velocity, we will ignore this two-mode region on the expectation that it is small in comparison to the rest of the domain.

4.4.4 Evaluating the quadratic coefficients

The coefficients of equation (4.19) (in particular b_R) need to be known before equations (4.29) or (4.30) can be determined. Rather surprisingly, the diffusion curve (and hence the quadratic) is virtually the same for all the different constant concentration regions $R(x, y)$. Figure 4.2 shows a plot of the diffusion time t_{D} versus the distance X from the pond boundary for four different sized regions $R(x, y)$. These vary from a small region close to the pond boundary, to a large region well away from the pond boundary. The root-mean-square error between the fitted quadratic equations and the model output for each of the curves of Figure 4.2 is less than 2×10^{-3}.

The similarity of the diffusion curves of Figure 4.2 can be seen even more clearly when superimposed upon each other, that is, with the origin moved from the pond boundary to the edge of $R(x, y)$ (the coordinate system changed from X to Z), as in

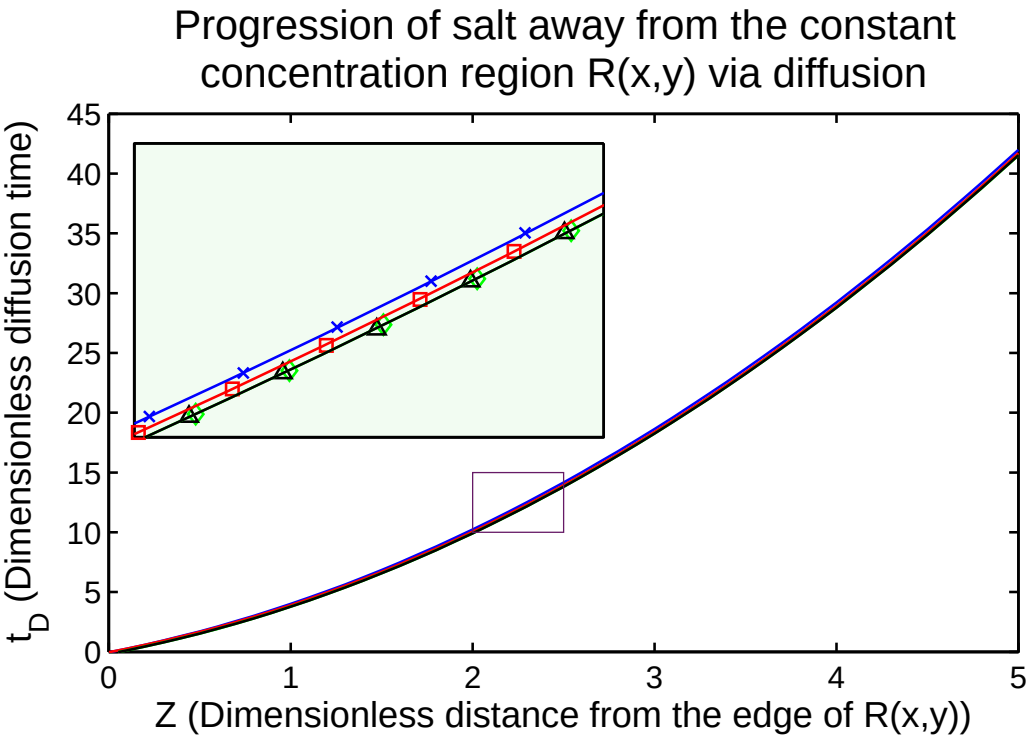

FIGURE 4.3: Superimposed diffusion curves for different $R(x, y)$. Note the excellent quadratic fit to the data points.

Figure 4.3. Averaging these curves gives the following quadratic (which deviates from the curves of Figure 4.2 by less than 1%):

$$t_{\mathrm{D}} = 1.10Z^2 + 2.84Z. \tag{4.31}$$

As different regions $R(x, y)$ lead to the same equation, it is natural to then compare equation (4.31) with the result for one-dimensional ($1D$) diffusion. Ignoring the depth y of the aquifer, and solving analytically for a boundary of constant concentration (which is readily found; see, for example, Farlow (1993)) reveals a $1D$ breakthrough curve along the water table of

$$t_{\mathrm{D}} = 1.10Z^2 + 2.90Z. \tag{4.32}$$

This equation is almost identical to the two-dimensional ($2D$) case, with any difference possibly attributable to the numerical error associated with the time step δt_{D}.

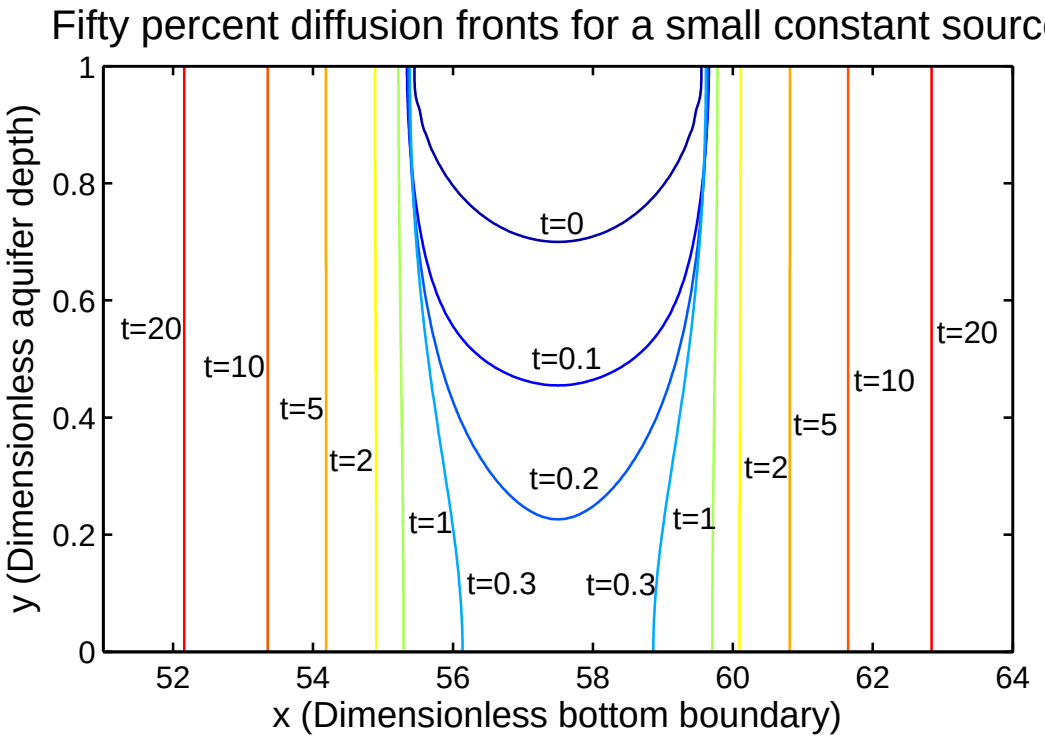

Figure 4.4: Diffusion fronts of a small region $R(x, y)$, demonstrating the rapid transformation from $2D$ to $1D$.

The implication is that the rate of diffusion along the water table is basically a one-dimensional process, even when the source $R(x, y)$ (and the aquifer geometry) is clearly $2D$ in shape.

We include Figure 4.4 to better demonstrate the diffusion process from a constant concentration source. This figure is modified slightly from the original problem description, with the region $R(x, y)$ being smaller, and rather than spanning the boundary as before, it is placed near the middle of the domain. We present this figure to demonstrate the rapid transformation from $2D$ to $1D$, and to give the reader a feel for the evolution of the concentration profile.

Another important conclusion from this section is that the quadratic coefficients (and b_R in particular) are not dependent on the location, size or shape of the region $R(x, y)$ and thus the subscript R can be dropped when referring to them. Therefore, taking $b = 2.84$ from equation (4.31) and substituting into equation (4.29) gives

$$\alpha(X) = 0.93e^{-1.52X}, \quad 5 \leq X \leq 14. \tag{4.33}$$

4.5 Results

Before any results can be generated, the number of terms in the series solution need to be provided (M and N in equation (4.10)). In this chapter, values of $M = 1,000$ and $N = 200$ were used, with $M' = M + 1$ and $N' = N + 1$ collocation points to determine the series coefficients. The solution was obtained efficiently and accurately at each step of the iterative process, with root-mean-square errors (evaluated in between collocation points) of the order of 10^{-5} or better.

The techniques described in the preceding sections of this chapter allow the progress of salt (by advection, then diffusion) from the pond through the soil to be predicted, once the soil parameters are specified. First, the time taken for advection (to create the constant concentration region, $R(x, y)$) is calculated. Then, the time taken for diffusion (ignoring any advection during the diffusion process) outside $R(x, y)$ is calculated. We consider an aquifer with the following physical parameters: hydraulic conductivity $K_* = 10^{-5}$ m/s; depth $d_* = 40$ m; and porosity $\sigma = 0.3$. This is the example used in Chapter 2 to demonstrate the progress of salt contamination via advection in a typical coastal (sandy-loam) aquifer. Additionally, a value of diffusivity, D_*, is required. Chapter 2 showed that transport due to advection slows exponentially as distance from the pond boundary increases. Since we are interested in the area where the discharge velocity approaches zero, the hydrodynamic dispersion coefficient reduces to the molecular diffusion coefficient. For salt (NaCl) in water, this value is approximately $D_* = 2 \times 10^{-9}$ m^2/s (Stoessell and Hanor, 1975).

Solving for equation (4.26) with the above parameter values gives $\alpha = 1.5 \times 10^{-6}$, with equation (4.33) revealing that diffusion becomes the dominant mode of transport at $X = 8.77$ dimensionless units from the pond boundary. Chapter 2 was only interested in contamination up to 300 m ($X = 7.5$) from the pond boundary, therefore, diffusion need not be considered at all in that case. Clearly, as diffusion is still the minor contributor of contamination to $X = 7.5$, Chapter 2 seems justified in ignoring its effects. However, to demonstrate the role diffusion plays within the domain, we consider a point 500 m ($X = 12.5$) from the pond boundary. To reach $X = 8.77$

dimensionless units via advection takes 46,851 years (equations (4.17) and (4.23)), while the remaining $Z = 3.73$ dimensionless units requires an additional 656,961 years (equations (4.24) and (4.31)) via diffusion. Figure 4.5 shows the movement of salt contamination along the water table for this example. Salt progresses along the advection curve (dotted line) to $X = 8.77$, where it then continues along the diffusion curve (solid line). The total time of 703,812 years via advection and diffusion is approximately 5% of the 13,583,128 years required if advection were the only transport process.

For the domain of Figure 4.1, we compared the above results to a similar model in the standard numerical groundwater modelling package, SUTRA (Voss and Provost, 2002). The SUTRA model began from when contamination first entered the aquifer, and therefore had to develop both the advective and diffusive regions. Tracking the 50% concentration levels along the water table (in SUTRA) over time produced the labelled curve (grey line) in Figure 4.5. In comparing the SUTRA results to the quasi-analytical results, the curves have the same basic shape and are in general agreement, differing by a maximum of 8% for dimensionless distances up to $X = 16$ from the pond boundary. The SUTRA model indicates greater contamination, likely for the following reasons: firstly, the quasi-analytical model in this chapter neglects the two-mode region near X_0 (described in Section 4.4.3); and secondly, the possibility of numerical diffusion, a problem that most numerical techniques suffer from when solving for the large aspect ratios dealt with here (Reddy and Trefethen, 1994).

4.6 Discussion and conclusions

The domain of Figure 4.1 describes a similar situation to that modelled in Chapter 2, that is, saltwater aquaculture ponds sitting above a freshwater aquifer. This situation has received little attention from researchers, with anecdotal evidence (Arunakumaren et al., 2000) suggesting that salt contamination from said ponds can be serious and immediate. Chapter 2 showed that although contamination from leaky saltwater ponds is indeed immediate, the ongoing extent of such contamination (via advection) reduces exponentially. This leaves contamination via diffusion to be considered.

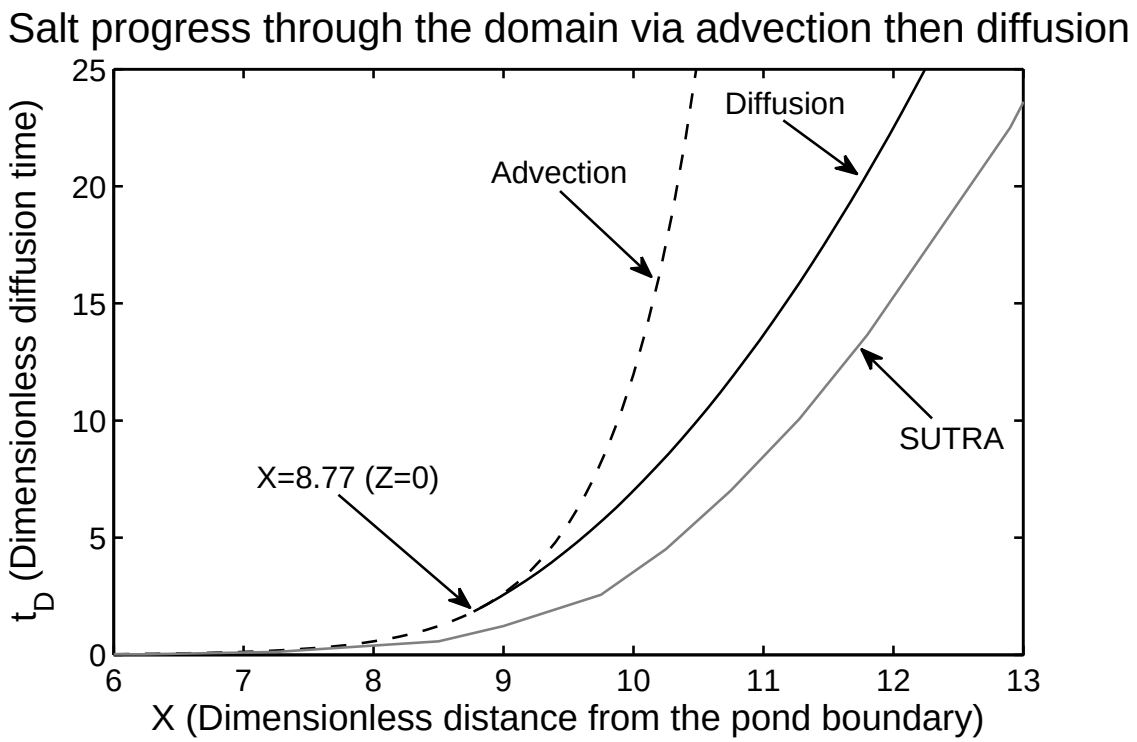

FIGURE 4.5: The progress of salt along the water table via advection then diffusion.

The techniques described in Sections 2.3 and 4.3 are easily mated, with each solution contributing to the final result where it is dominant. Figure 4.4 shows that the progress of diffusive transport through time (from a constant concentration advective source), rapidly degenerates (in comparison to the distance travelled) to a $1D$ system, endorsing the simple $1D$ models typically used to approximate large aspect ratio domains. However, the techniques developed herein can also quantify the relative contributions of advection and diffusion. The quasi-analytical $2D$ modelling method is a potential alternative to many domains that would otherwise require orthodox numerical techniques.

Chapter 2 supplied the equation for advective progress (4.17), while this chapter derived the equations for 50% diffusive progress (4.31 or 4.32), and the location where diffusion becomes dominant (4.29). There is potential for these dimensionless equations to allow for the rapid calculation (perhaps in the field) of contaminant progress from a leaky pond to its surrounds (as demonstrated in Section 4.5). To this end, we include Appendix A.3. Having established in Section 4.4.4 that a $1D$ analysis is a

valid simplification of this particular $2D$ system, Appendix A.3 contains the curves for a range of varying percentage diffusion fronts (1% to 90%), calculated using a $1D$ analysis.

The equations (4.31 or 4.32) and (4.29) derived in this chapter are necessarily dependent on the advective contamination equation (4.17) obtained from Chapter 2. Unfortunately, equation (4.17) only corresponds to a single ratio of pond height to aquifer depth. A range of equations (or better still, a general equation) corresponding to multiple (pond height to aquifer depth) ratios is required to obtain the general solution for a leaky pond of any height, sitting above an aquifer of any depth, with any aquifer properties.

In Section 4.5 we considered only the 50% diffusion front when calculating contamination to 500 m ($X = 12.5$) from the pond boundary. However, the speed at which diffusive contamination spreads through an aquifer varies, based on the concentration of the solute that is considered harmful. For instance, in absolute terms, if a 1% level of the concentration of the ponds is considered harmful, this diffusive contamination front will progress more rapidly than if a 50% contamination level is considered harmful. This is easily seen in the difference between different percentage diffusion curves in Figure A.1 (Appendix A.3). In addition, at the 1% level, diffusion will take over from advection (as the dominant transport mechanism) sooner than the 50% level. We recalculate the example in Section 4.5 using the general equation in Appendix A.3. Assuming a 1% diffusion front as sufficient for contamination, the reworked example in Section 4.5 takes 92,362 years to reach 500 m from the pond boundary, or approximately 13.1% of the time for the 50% diffusion front.

To get an idea of the general applicability (to different soil types) of the procedure outlined in this chapter, we assume the scaling parameter $d_* = 40$ m and the porosity $\sigma = 0.3$ to be those of a typical aquifer. From equation (4.33), the limits of X allow for $5.39\times10^{-10} \leq \alpha \leq 4.70\times10^{-4}$. Assuming the molecular diffusivity, $D_* = 2\times10^{-9}$ m^2/s, to be relatively constant across a range of soil types, substituting into equation (4.26) gives a range of hydraulic conductivity values $3.19 \times 10^{-8} \leq K_* \leq 2.78 \times 10^{-2}$ (m/s). These encompass the majority of the spectrum of soil types encountered in groundwater

modelling, from well sorted sand (or sand and gravel) to layered clay (Bear, 1972).

There are a couple of important points to note regarding the methodology used in this chapter. Firstly, the original quadratic of diffusion progress (equation (4.19)) was found using the X rather than the Z coordinate system, that is, in relation to the fixed pond boundary rather than the edge of the variably sized constant source region $R(x, y)$. This is significant in that it allows the simultaneous solution of α, and the amount of 'smoothing' during the advection phase. We have used the Z coordinate system in this chapter for simplicity, and to better demonstrate that diffusion away from the constant source region (equation (4.31)) is not dependent on the size of $R(x, y)$.

Secondly, two methods were described in this chapter (Section 4.4.1) to achieve a smooth transition from $R(x, y)$ to the rest of the domain; these being a Gaussian spatial filter, and utilising diffusion. However, the amount of smoothing affects the concentration gradient at the edge of $R(x, y)$, which in turn affects the calculation of the parameter α. Since diffusive effects cannot be separated from the advection process (just ignored if practical to do so), it was found to be more effective, and efficient, to incorporate smoothing via diffusion.

The idea that advection replenishes any solute that diffuses into the domain is (perhaps) non-intuitive. Let's reconsider this idea in light of the results of this chapter. Assuming advection replenishes solute as quickly as it diffuses, thus providing the constant concentration source used in this chapter, then this situation provides the largest driving potential possible for the diffusion process. That is, the concentration gradient from X_0 into the rest of the domain is at its highest. Therefore, contamination from the constant concentration source will progress further into the domain than it would from a diminishing source over the same time period. However, Figure 4.5 shows that the quasi-analytical method presented in this chapter does not progress as far as the comparative SUTRA model (likely for the reasons stated at the end of Section 4.5). Given that a diminishing source would differ still more from the SUTRA model, our stated assumption that advection replenishes solute as quickly as it diffuses seems reasonable. It seems to give good results at any rate.

This chapter has presented a quasi-analytical modelling technique to address the

problem of irregularly shaped constant strength sources for $2D$ diffusion. The model was compared to a similar one in the numerical groundwater modelling package SUTRA, with good agreement. The equations derived along the way allow for calculation of the relative contributions of advection and diffusion from a leaky pond, but for the domain considered in this chapter, the conclusion can only be that diffusion is irrelevant (even using a 1% concentration contour) in practical terms. However, this chapter has only considered advection and diffusion, with the inherent assumptions of contaminant neutral buoyancy (no density driven flow), and constant hydraulic conductivity (no preferential flow channels). These limiting assumptions were necessary, but will undoubtedly cause deviation from the real system being modelled.

5

Generalised equations for advection and diffusion

5.1 Introduction

In this chapter we present equations for predicting groundwater contamination, via advection and diffusion, from a leaky pond above a freshwater aquifer. The equations are derived from quasi-analytical mathematical models (Verrall and Read, 2012; Verrall et al., 2009b) (Chapter 2 and Chapter 4), and attempt to reduce the analysis of the above situation to a few simple relations that can be solved rapidly, without further need of the original models. In this sense, the equations presented may be regarded as a transfer function; that is, a simple description of the model output for any given input.

Groundwater modelling usually involves simplifications and assumptions. Often the complexities of the domain are simply not known, and/or the governing equations can't be solved without simplifying the domain parameters. The equations presented in this chapter are no exception, with the major assumptions being the same as the underlying models, that is, constant hydraulic conductivity, no density driven flow, and a rectangular domain. However, if the above assumptions are reasonable, then the equations presented are applicable to a pond of any height sitting above an aquifer of any depth.

The simple equations presented in this chapter will not contain the detail available from the underlying models. However, the advantage achieved is that of speed of solution and simplicity of application. Assuming these relations are a good approximation, some potential applications might be: a quick reference for assessing numerical models; an alternative when the complete mathematical model is unavailable or impractical, for example, in the field or when results are sought by those without the requisite modelling experience; or as a transfer function for use within a decision support system (DSS). (A DSS is "a metadiscipline, which integrates knowledge and practices across multiple scientific fields (for example, hydrology, ecology, economics, various social sciences)" (Jakeman et al., 2011). That is, it is a computer-based information system used for the rapid evaluation of "what if?" scenarios. As such, if the runtime of a groundwater model within a DSS is too long, it will not be useful (Anderson et al., 2015). In such

cases, transfer functions become the preferred option.)

This chapter is organised as follows. Section 5.2 presents the equations relevant to advection, with Section 5.3 presenting those relevant to diffusion. Section 5.4 contains the results of an example used for demonstration purposes, and finally, a discussion is presented in Section 5.5.

5.2 Advection

The situation of interest in this chapter can be seen in Figure 5.1. Figure 5.1 is a generic representation of a leaky contaminated pond sitting above a saturated freshwater aquifer. Inside the saturated flow domain, we assume the seepage velocity $\mathbf{u}_* = (u_*, v_*)$ satisfies Darcy's law,

$$\mathbf{u}_* = -K_* \nabla_* \phi_*(x_*, y_*), \tag{5.1}$$

where $\phi_*(x_*, y_*)$ is the hydraulic head. (Note that asterisk subscripts represent dimensional variables. These will later be dropped when the problem is non-dimensionalised.) Combining Darcy's law and the continuity condition results in the saturated flow equation (Laplace's equation) for the domain of Figure 5.1,

$$\nabla_*^2 \phi_*(x_*, y_*) = 0. \tag{5.2}$$

We leave the details for modelling the domain in Figure 5.1 to Chapter 2. However, in brief, Chapter 2 used a quasi-analytical technique to find advection fronts (isochrones) for advective contaminant transport through an unconfined aquifer, away from leaky raised ponds. Using series solutions, a closed form solution was derived for the saturated flow equation, thereby providing the potential function, stream function and velocity field. Then, it was a simple matter to numerically step along the streamlines (starting from immediately below the contaminated ponds) for any predefined upper time limit. In this manner, a relationship was found for the time and location each streamline emerged at the water table. It is this relationship which is the focus of this section.

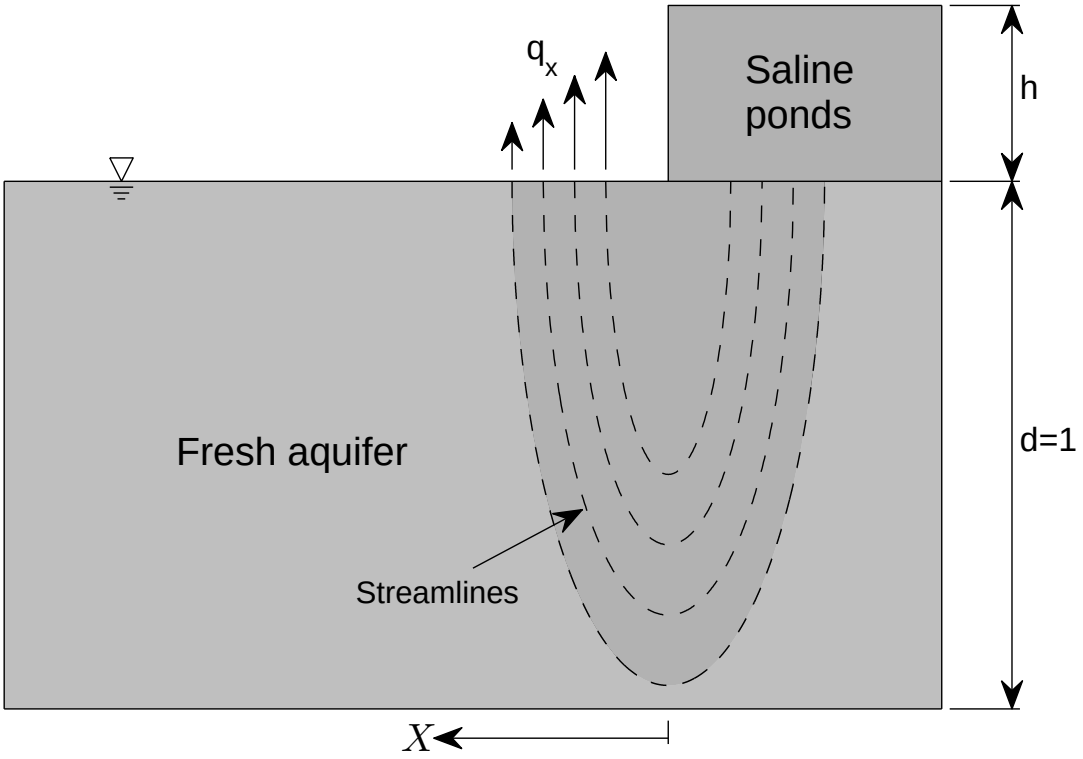

FIGURE 5.1: Sketch of domain being considered.

To proceed, we first non-dimensionalise the domain parameters. This is done to present a general solution that can be used for any number of similar cases; that is, the parameters in Figure 5.1 can take on any value we choose. According to Chapter 2, the problem is non-dimensionalised using the hydraulic conductivity, K_*, and the depth of the aquifer, d_*, therefore,

$$d_* = d_* d, \quad h_* = d_* h, \quad X_* = d_* X, \tag{5.3}$$

$$t_* = \frac{\sigma d_*}{K_*} t_{\mathrm{A}}, \quad \mathbf{u}_* = K_* \mathbf{u}, \quad \mathbf{U}_* = \frac{K_*}{\sigma} \mathbf{U}, \tag{5.4}$$

where h_* is the height of the pond above the water table, X_* is the distance from the pond boundary, $\mathbf{U}_*$ is the pore velocity, σ is the porosity, and t_* is time. Dimensional numbers have an asterisk subscript, while their non-dimensional equivalents do not. We will be working with the non-dimensional parameters, with any conversions achieved

using equations (5.3) and (5.4) above. It should be noted that dimensionless time is represented by t_{A}, with the subscript denoting advection. The reason for this will become clear in Section 5.3.

5.2.1 One-dimensional advection simplification

We are interested in the empirical contamination equation found in Chapter 2,

$$t_{\mathrm{A}} = 2e^{1.52X}, \quad X \geq 5, \tag{5.5}$$

for determining the progress of contamination along the water table, X, as measured from the pond boundary ($X = 0$). This equation wasn't derived, but simply found by recording the time and location each streamline emerged on the water table when integrated numerically. Streamlines start immediately below the ponds and plunge deep into the aquifer before reemerging vertically at the water table (a schematic representation of this process can be seen in Figure 5.1). The horizontal movement of contamination, as quantified by equation (5.5), is the result of solute progressively emerging from adjacent vertical streamlines at the water table. It should be noted the above equation is only applicable to a single ratio of pond height to aquifer depth of 3/40, but given the simplicity of equation (5.5), it seems reasonable there should exist a general version of this equation that incorporates any ratio of pond height to aquifer depth.

However, before we proceed there is an additional point to be addressed. Chapter 2 applied a smooth transition between the water table and the pond surface, in order to remove Gibbs phenomenon (a mathematical artifact). Upon further investigation, it was found that the length of this transition zone affects the coefficients in equation (5.5). To solve for the closed form solution of our domain, while minimising Gibbs phenomenon (and therefore allowing for solutions of domains with smaller transition zones), we now incorporate Lanczos smoothing (Hamming, 1977). This is a correction factor applied to each coefficient of the series solution, that smooths the high frequency ripples of Gibbs phenomenon. This allows the reduction of the transition zone to 2%

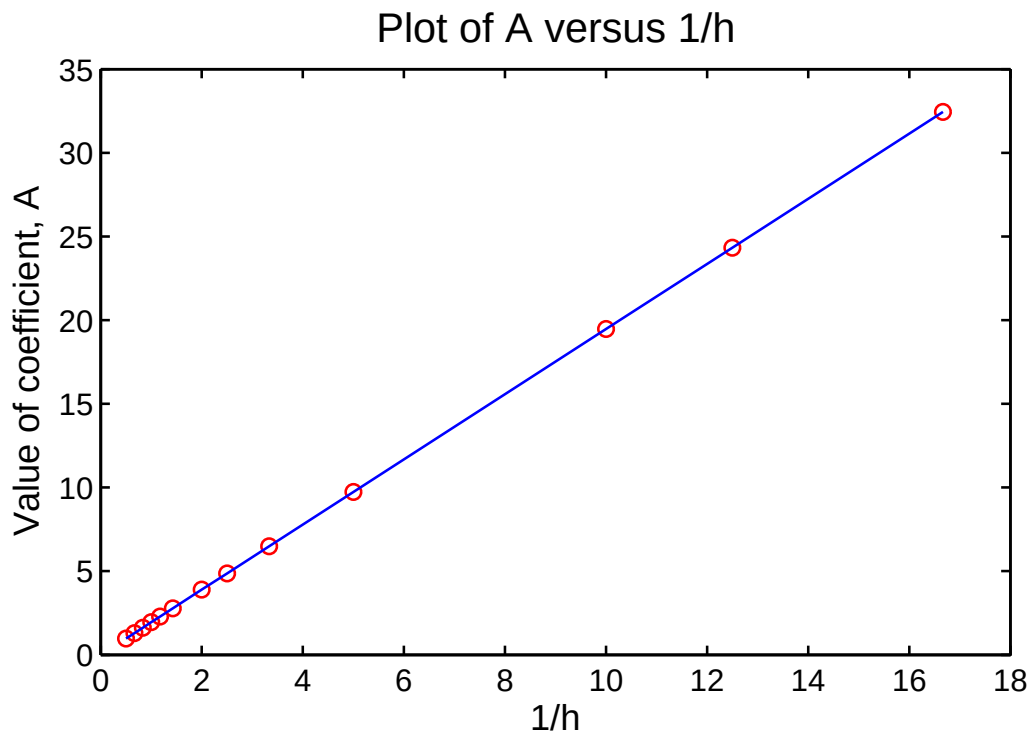

FIGURE 5.2: Plot showing that the height of the ponds is inversely proportional to the value of the coefficient A.

of the depth of the aquifer. Further reduction of this region is not required as any additional change in the coefficients of equation (5.5) is minor beyond this point. Further analysis of the transition region can be found in Appendix A.4.

We follow the technique described in Chapter 2, and apply it to multiple ratios of pond height, h, to aquifer depth, $d = 1$. If we assume the general equation will likely have the same form as equation (5.5), that is,

$$t_{\mathrm{A}} = Ae^{BX}, \tag{5.6}$$

then the height of the pond must be incorporated into the coefficients A and/or B. Analysing the relationships for A and B against various values of h reveals that B is independent of h, but agreeably, $A \propto 1/h$. Figure 5.2 shows this relationship between A and $1/h$.

Given a transition zone of 2% of the aquifer depth, and taking the coefficients of A and B at $h = 1$, the general equation for contaminant progress (as seen at the water

table) through an unconfined aquifer from leaky ponds is

$$t_{\mathrm{A}} = \frac{1.93}{h}\, e^{1.58X}, \quad X \geq 1. \tag{5.7}$$

Now that we know when contamination will occur at any point, $X \geq 1$, along the water table, how much contamination will occur at that point? As part of the model, Chapter 2 defined the velocity field throughout the domain of Figure 5.1. In analysing the vertical velocity component at the water table, again, a simple relationship was found to exist, this time of the form

$$q_x = M e^{-NX}, \tag{5.8}$$

where q_x represents the vertical component of the seepage velocity $\mathbf{u}$ at the water table, that is, the specific discharge at X. Running models for various pond heights, h, and plotting the coefficients, M and N, against these heights, revealed that N is independent of h, while $M \propto h$. Therefore, taking the coefficients of M and N at $h = 1$, the general equation giving the mass flux at the water table is

$$q_x = 1.03\, h\, e^{-1.58X}, \quad X \geq 1. \tag{5.9}$$

As is evident from equation (5.9), q_x reduces exponentially as the distance from the pond boundary increases.

Equations (5.7) and (5.9) allow the modelling of advective contaminant progress through the general domain of Figure 5.1. Even though flow within the domain isn't horizontal, the flow field is such that contaminant progress at the water table is a good representation of contamination in the vertical column of the aquifer below. As such, the two-dimensional ($2D$) domain can be satisfactorily represented by the above one-dimensional ($1D$) equations. This can be regarded as similar to the 'hydraulic approach', often employed in groundwater problems (Bear, 1979). That is, in the hydraulic approach the thickness of the aquifer is ignored and flow is assumed to be horizontal, therefore reducing the problem to $1D$. But this assumption generally fails close

to a source or sink, as the flow in these regions is demonstrably *not* horizontal. However, in our case the $1D$ equations are empirical, and represent contaminant progress only; they are derived from the complete flow equation (5.2), without this assumption of horizontal flow. Therefore, equations (5.7) and (5.9) are valid close to the pond source, and can be regarded as representing an apparent $1D$ transport of contaminant, rather than the real $2D$ flow of contaminated water. Differentiating and inverting equation (5.7) gives the final result of this section, the apparent velocity of advective contaminant transport along the water table,

$$u_{\mathrm{A}} = \frac{1}{\frac{dt_{\mathrm{A}}}{dX}} = \frac{h}{3.05}\, e^{-1.58X}, \quad X \geq 1. \tag{5.10}$$

An examination of equation (5.10) reveals that advective contamination along the water table is exponentially slowing. Chapter 2 found that eventually advective contamination became so slow as to be incalculable. Given this result, at some point diffusion must take over as the dominant transport mechanism.

5.3 Diffusion

Chapter 4 found that transport within the domain of Figure 5.3 could be modelled as a two stage process: advection then diffusion. That is, the aquifer can be separated into two distinct regions: an advective region, where advective processes dominate and diffusion can be ignored; and a diffusive region, where diffusive processes dominate and advection can be ignored. We leave the details to Chapter 4, but briefly, it was found that diffusion within the domain of Figure 5.3 could be modelled as a $1D$ process with a constant concentration boundary condition. It is $1D$ because the aspect ratio (that is, length to depth) is high; and it has a constant strength boundary condition because any solute that doesn't diffuse (from the advective contamination already within the aquifer) is transported through to the soil surface via advection and is replaced by full strength contaminated water from the pond. Using this $1D$ diffusion simplification, and the $1D$ advection simplification (5.10), we will find where diffusion takes over as

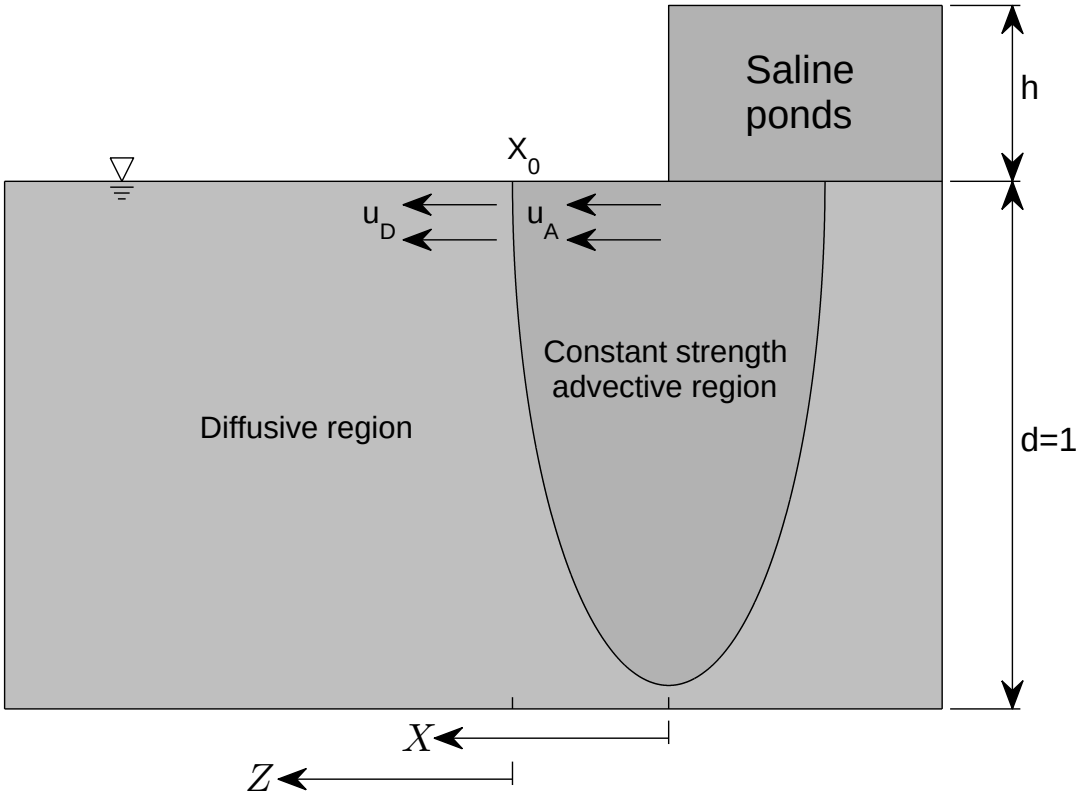

Figure 5.3: Schematic of advective and diffusive regions within the domain.

the dominant transport process, therefore delineating the regions.

To proceed, we must again non-dimensionalise some parameters. For the diffusion problem, Chapter 4 used the same spatial scaling as that used in the advection problem, the depth of the aquifer d_*. In addition, the following scaling was also used:

$$t_* = \frac{d_*^2}{D_*} t_{\mathrm{D}}, \quad C_* = C_*^0 C, \tag{5.11}$$

where C_*^0 is the initial concentration of the ponds, and D_* is the diffusivity. Note that dimensionless time is represented by t_{D}, with the subscript denoting scaling for diffusion.

However, an examination of equations (5.4) and (5.11) reveals a problem. In this chapter we wish to combine the (dimensionless) results of advection and diffusion, but time is scaled differently for each process. (This is analogous to comparing the terms

parts per million and *parts per billion*; although each is dimensionless, they differ by a factor of $1,000$.) We need to relate the different time scales by converting each back to the common reference value of dimensional time,

$$t_* = \frac{\sigma d_*}{K_*} t_{\mathrm{A}} = \frac{d_*^2}{D_*} t_{\mathrm{D}}. \tag{5.12}$$

Rearranged, this becomes

$$t_{\mathrm{D}} = \frac{D_* \sigma}{K_* d_*} t_{\mathrm{A}} = \alpha t_{\mathrm{A}}, \tag{5.13}$$

where

$$\alpha = \frac{D_* \sigma}{K_* d_*}. \tag{5.14}$$

The dimensionless parameter α is the ratio of the dimensionless diffusion time scale to the dimensionless advection time scale. However, it is also a combination of the physical parameters of the aquifer. In this sense, α can be regarded as characteristic of the aquifer. Therefore, the location within the domain where diffusion becomes the dominant transport process will vary depending on this characteristic value. We will return to this idea in Section 5.3.2. (As an aside, given that hydraulic conductivity, K_*, has the same units as velocity (m/s), it is interesting to note the similarity of equation (5.14) to expressions of the (inverse) Péclet number.)

5.3.1 One-dimensional diffusion simplification

An analytical solution for $1D$ diffusion with a constant concentration boundary condition is relatively easy to find (for example, Farlow (1993)). This solution can be used to determine breakthrough curves for any threshold concentration level (for example, 1% of the concentration of the ponds) along the water table, for any given time. Chapter 4 found that the best fit for this relationship is a quadratic of the form

$$t_{\mathrm{D}} = a_\infty Z^2 + b_\infty Z, \tag{5.15}$$

where Z is a displaced X coordinate system. That is, as yet we don't know where diffusion takes over as the dominant transport mechanism, but wherever that is becomes the point $Z = 0$. (The reason for the subscript in the coefficients a_∞ and b_∞ will become clear below.)

Differentiating and inverting the above equation (similarly to (5.10)) gives the apparent velocity of diffusive contaminant transport along the water table,

$$u_{\mathrm{D}} = \frac{1}{2a_\infty Z + b_\infty}. \tag{5.16}$$

Therefore, at the point where diffusion becomes dominant, $Z = 0$,

$$u_{\mathrm{D}} = \frac{1}{b_\infty}. \tag{5.17}$$

However, this diffusive contamination velocity is unrealistic as it occurs at a discontinuity. That is, mathematically there is a step change in concentration from advection (where $C = 1$) to the rest of the domain (where $C = 0$). This creates an infinite concentration gradient when $t_{\mathrm{D}} = 0$, which doesn't exist in reality; diffusive processes occurring during the advection phase will smooth any concentration boundary between the two regions. To overcome this problem, we modify equation (5.15). This equation has the inherent assumption that diffusion begins only when advection ends, but as we have just stated, this is not a realistic scenario. Therefore, let's make the point $(Z = Z', t_{\mathrm{D}} = \alpha t'_{\mathrm{A}})$ the new origin of the Z coordinate system, where $t_{\mathrm{D}} = \alpha t'_{\mathrm{A}}$ is the total (scaled) time advection occurs until diffusion takes over, and Z' is not yet known. That is, equation (5.15) is still used to predict diffusion, but we assume diffusion has been occurring simultaneously with advection, and shift along the diffusion curve accordingly. Effectively, equation (5.15) must be shifted down by $\alpha t'_{\mathrm{A}}$, and in the negative direction by Z'. As Z' is unknown, we solve for it by shifting the curve down and equating to zero,

$$a_\infty Z^2 + b_\infty Z - \alpha t'_{\mathrm{A}} = 0. \tag{5.18}$$

Now, when diffusion takes over as the dominant transport mechanism at $t_{\mathrm{D}} = \alpha t'_{\mathrm{A}}$, the diffusive contamination velocity along the water table must equal the advective contamination velocity along the water table. The advective and diffusive contamination velocities are defined using the advection and diffusion time scales, respectively, so applying the chain rule we find

$$u_{\mathrm{A}} = \alpha u_{\mathrm{D}}. \tag{5.19}$$

Hence,

$$\frac{e^{-BX}}{AB} = \frac{\alpha}{2a_\infty Z + b_\infty}, \tag{5.20}$$

or from equation (5.6),

$$\frac{1}{Bt'_{\mathrm{A}}} = \frac{\alpha}{2a_\infty Z + b_\infty}, \tag{5.21}$$

$$\alpha t'_{\mathrm{A}} = \frac{2a_\infty Z + b_\infty}{B}. \tag{5.22}$$

Substituting into equation (5.18),

$$a_\infty Z^2 + b_\infty Z - \frac{2a_\infty Z + b_\infty}{B} = 0, \tag{5.23}$$

$$a_\infty Z^2 + \left(b_\infty - \frac{2a_\infty}{B}\right) Z - \frac{b_\infty}{B} = 0. \tag{5.24}$$

Using the quadratic formula,

$$Z' = \left(\frac{-b_\infty}{2a_\infty} + \frac{1}{B}\right) \pm \sqrt{\left(\frac{b_\infty}{2a_\infty}\right)^2 + \left(\frac{1}{B}\right)^2}. \tag{5.25}$$

We know that Z' must be positive, so observing that the terms outside the radical sign are the same as the squared terms inside, from Pythagoras' theorem,

$$Z' = \left(\frac{-b_\infty}{2a_\infty} + \frac{1}{B}\right) + \sqrt{\left(\frac{b_\infty}{2a_\infty}\right)^2 + \left(\frac{1}{B}\right)^2}. \tag{5.26}$$

To shift the curve (5.15) in the negative direction,

$$t_{\mathrm{D}} = a_{\infty}(Z + Z')^2 + b_{\infty}(Z + Z'). \tag{5.27}$$

Therefore, making the point $(Z = Z', t_{\mathrm{D}} = \alpha t'_{\mathrm{A}})$ the new origin, gives the new contamination equation (with smoothing incorporated),

$$t_{\mathrm{D}} = aZ^2 + bZ, \tag{5.28}$$

where

$$a = a_{\infty}, \tag{5.29}$$

$$b = b_{\infty} + 2a_{\infty}Z'. \tag{5.30}$$

There is an important point here: diffusive smoothing is not dependent on the characteristic parameter α, which is (perhaps) a little surprising. Changing the aquifer properties, and therefore α, doesn't affect the value of Z', because Z' is dimensionless and α is simply a scaling parameter. Differing values of α are reflected in differing values of dimensional time t_*.

The quadratic coefficients of equation (5.28) vary according to the threshold concentration fronts considered harmful. That is, diffusive contamination progresses through the domain at different speeds, depending on the concentration level being tracked. Treating these quadratic coefficients as a function of concentration, C, the following relationship was found (where a_{∞} was found similarly to Chapter 4, $b_{\infty} = 0$, and each are substituted into equations (5.29) and (5.30)),

$$t_{\mathrm{D}} = a(C)Z^2 + b(C)Z, \quad 0.01 \leq C \leq 0.9, \tag{5.31}$$

where

$$a = e^{65.654\,C^5 - 147.446\,C^4 + 129.625\,C^3 - 53.062\,C^2 + 13.972\,C - 2.662}, \tag{5.32}$$

$$b = 2aZ'. \tag{5.33}$$

5.3.2 Where does diffusion become dominant?

Diffusion takes over when the apparent diffusive velocity equals the apparent advective velocity,

$$u_{\mathrm{A}} = \alpha u_{\mathrm{D}}. \tag{5.34}$$

Substituting for u_{A} (from equation (5.10)) and u_{D} (from equation (5.17), but replacing b_∞ with b),

$$\frac{h}{3.05}\, e^{-1.58X} = \frac{\alpha}{b}. \tag{5.35}$$

Given a known value of α,

$$X_0 = \frac{\ln\left(\frac{3.05\,\alpha}{b\,h}\right)}{-1.58}, \tag{5.36}$$

A given set of aquifer parameters allows for the calculation of α (from equation (5.14)). Substituting α into equation (5.36) gives the location on the water table, $X = X_0$, that delineates the advective and diffusive regions of the domain. That is, up to X_0, diffusion can be ignored and an advection only simplification is sufficient. Beyond X_0, further advection can be ignored and a diffusion only simplification (from a constant concentration source) is sufficient. If the time for contamination to reach $X > X_0$ is required, then the time for advection to X_0 is simply added to the time for diffusion (greater than X_0).

5.4 Results

To demonstrate the use of the equations presented in this chapter, we consider the following example. Assume an aquifer has the following properties: $K_* = 10^{-2}$ m/s, $D_* = 2 \times 10^{-9}$ m^2/s, $d_* = 5$ m, $\sigma = 0.3$, and the height of the contaminated ponds is

$h_* = 3$ m. How long does it take for (minimum) 1% contamination to reach 50 m from the pond boundary? In addition, assuming a (dimensionless) unit width of the aquifer (that is, into the page of Figure 5.1), what quantity of contaminated pond water exits the water table during this time?

We first non-dimensionalise the problem using equations (5.3), (5.4) and (5.11). Solving for equation (5.14) reveals the characteristic dimensionless variable $\alpha = 1.2 \times 10^{-8}$, with substitution into equation (5.36) giving $X = 9.566$ (dimensionless units from the pond boundary) as the point at which diffusion becomes the dominant transport process. Therefore, the actual time for advection to reach $X = 9.566$ is then found from equations (5.4) and (5.7): $t_* = 50.161$ years. From $X = 9.566$ to $X = 10$ ($Z = 0$ to $Z = 0.434$) diffusion is the dominant process, so substitution into equations (5.11), (5.28) and (5.31) yields the actual time for diffusion: $t_* = 39.816$ years. Adding these values of t_* means that (minimum 1%) contamination reaches $X = 10$ (50 m) from the pond boundary in 89.977 years. Figure 5.4 shows the movement of contamination through the aquifer for the above example. Contamination progresses along the advection curve (dotted line) to $X = 9.566$, where it then continues along the diffusion curve (solid line).

Now we require the quantity of contaminated pond water exiting the water table over this period. At any particular point in time t_ρ, advective contamination has progressed to $X = X_\rho$ on the water table. Integrating equation (5.9) between $X = 1$ and $X = X_\rho$ gives an average flux, Q_x, of contaminated outflow (at $t = t_\rho$ only) between these points,

$$Q_x = \int_1^{X_\rho} q_x \, dX \tag{5.37}$$

$$= 1.03\, h \int_1^{X_\rho} e^{-1.58X} \, dX \tag{5.38}$$

$$= \frac{1.03\, h}{1.58} \left(e^{-1.58} - e^{-1.58\, X_\rho} \right). \tag{5.39}$$

Now, over the given period the point $X = X_\rho$ varies as a function of time. This value of X_ρ can be found for any time by rearranging equation (5.7). The above equation of

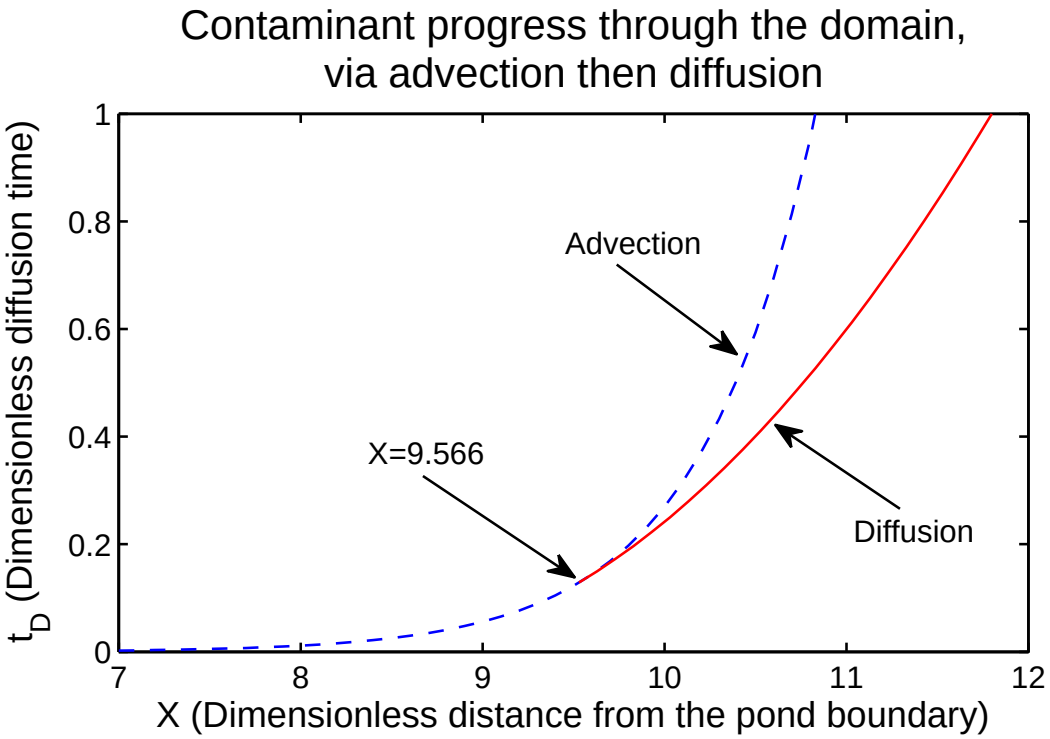

FIGURE 5.4: The progress of contamination through the aquifer via advection then diffusion.

average flux can therefore be changed to a function of time,

$$Q_x = 0.652\, h\, e^{-1.58} - \frac{1.26}{t_\rho}. \tag{5.40}$$

Integrating equation (5.40) over the period $t_\rho = \tau_0$ to $t_\rho = \tau_1$ will give the total volume, $\overline{Q}$ (for an aquifer of unit width), of contaminated pond water exiting the water table (for $X \geq 1$),

$$\overline{Q} = \int_{\tau_0}^{\tau_1} Q_x \, dt_\rho \tag{5.41}$$

$$= 0.652\, h\, e^{-1.58}\, t_\rho \Big|_{\tau_0}^{\tau_1} - 1.26 \, \ln t_\rho \Big|_{\tau_0}^{\tau_1}. \tag{5.42}$$

The value $t_\rho = \tau_0$ is found from equation (5.7) by using the value $X = 1$. This gives some value of $\tau_0 > 0$. We regard this as the time required for contamination to initially progress through the domain and then emerge at $X = 1$ (in this case $\tau_0 = 15.62$). Equation (5.41) is not valid for $t_\rho < \tau_0$ as no contamination is emerging at the water

table ($X \geq 1$) during this period, but for all intents and purposes we have integrated between $t_\rho = 0$ and $t_\rho = \tau_1$. For $\tau_0 = 15.62$ and $\tau_1 = 1.89 \times 10^7$ ($t_* = 89.997$ years), $\overline{Q} = 1.52 \times 10^6$. To dimensionalise this value, $\overline{Q}_*$, consider the steps carried out between equations (5.37) and (5.41). Simplified, this is

$$\overline{Q} = q_x \, X_\rho \, t_{\mathrm{A}}. \tag{5.43}$$

Recalling that q_x is the vertical component of the seepage velocity $\mathbf{u}$, substitute dimensional values into equation (5.43) from equations (5.3) and (5.4),

$$q_x \, X_\rho \, t_{\mathrm{A}} = \frac{q_{x*}}{K_*} \, \frac{X_{\rho*}}{d_*} \, \frac{t_* K_*}{\sigma d_*}. \tag{5.44}$$

Therefore,

$$\overline{Q}_* = q_{x*} \, X_{\rho*} \, t_*, \tag{5.45}$$

$$= \overline{Q} \, d_*^2 \, \sigma, \tag{5.46}$$

$$= 1.14 \times 10^7 \, \mathrm{m}^3. \tag{5.47}$$

5.5 Discussion

This chapter is a collation and extension of some aspects of the work carried out in Verrall et al. (2009b) (Chapter 2) and Verrall and Read (2012) (Chapter 4). The simplified approximate equations presented are only valid for domains that can be approximated as rectangular, with a constant hydraulic conductivity, and groundwater advection as a consequence of the height potential of the contaminated ponds. The purpose of these $1D$ equations is to simplify the modelling of the leaky pond problem, so it doesn't make sense to try to incorporate non-rectangular domains or variable hydraulic conductivity. Even if these infinite different scenarios could be included, the added complexity would render the resulting equations less intuitive, or practical, than a numerical modelling package. However, a useful future addition would be to incorporate an underlying horizontal flow of groundwater. This should be possible

using techniques similar to those presented in Chapters 2, 3 and 4, or alternatively, by using a numerical modelling package such as SUTRA (Voss and Provost, 2002).

It is important to note that the addition of an underlying horizontal flow would affect contaminant transport via hydrodynamic dispersion. The example in Section 5.4 made the same assumption as Chapter 4; that is, hydrodynamic dispersion reduces to molecular diffusion. This is because the advective flow of contamination is (more or less) perpendicular to diffusive movement within the domain, meaning we are only concerned with the transverse hydrodynamic dispersion coefficient. Given the domain considered in this chapter, the transverse coefficient should be of the same order of magnitude as molecular diffusion (Hunt, 1983). However, this assumption would fail if there were an underlying horizontal flow of groundwater in addition to the flow from the ponds. In such a case, the transverse coefficient could be orders of magnitude faster than molecular diffusion.

The domain analysed in this chapter (Figure 5.1) is a simplified version of a real scenario. In attempting to reduce the analysis of a leaky pond to a set of equations, the assumptions and simplifications stated in Section 5.1 were required. These equations aren't intended to replace a well posed problem, implemented properly in a numerical modelling package. Rather, they provide a reference to test these numerical solutions, or an approximation when numerical solutions are unavailable or impractical, for example, in the field, or as part of a decision support system. Finally, it is worth mentioning that, notwithstanding any simplifying assumptions, the approximate equations are derived from $2D$ models which are inherently conservative. That is, the vertical transect may be viewed as a channel that extends infinitely in the third dimension, whereas a real pond of finite surface area will likely be a less significant source in a $3D$ space.

6

Combined advection-diffusion-reaction

6.1 Introduction

The advection-diffusion-reaction (ADR) equation is important in a wide variety of fields. From air pollution modelling, to groundwater transport, to biological processes and beyond (Hundsdorfer and Verwer, 2003), the solution of this equation plays a fundamental role. Indeed, its analogue also plays a critical role in areas such as finance (as the Black-Scholes equation) and semiconductor physics (as the drift-diffusion equation). As such, solving the ADR equation accurately and efficiently is important to many areas of study.

Typically, when solving the ADR equation, numerical methods (such as finite difference or finite element (Strang, 1986)) are the default option, because for most practical problems, that is, multi-dimensional problems, the ADR equation is too difficult to solve analytically beyond the primary simplifying restriction of uniform flow. Analytical solutions that do overcome the above limitation are typically special cases that transform uniform flow solutions to a specific form of non-uniform flow field (for example, Broadbridge et al. (2000) and Zoppou and Knight (1999)). The difficulty (and non-generality) of this approach make numerical methods seem all the more attractive, despite fundamental problems associated with these techniques when applied to the ADR equation (Reddy and Trefethen, 1994). However, quasi-analytical techniques (for example, Craig and Heidlauf (2009) and Mehmani and Balhoff (2014)) combine aspects of both analytical and numerical methods, and provide a viable alternative by utilising the best aspects of each.

This chapter presents a novel quasi-analytical technique to solve the ADR equation for non-uniform flow fields. In the field of hydrology, analytical solutions of the flow field for arbitrary flow domains (Read, 1996a,b) have led to quasi-analytical solutions for the pure advection simplification of the ADR equation (Verrall et al., 2009a,b) (Chapters 2 and 3). These provide a fast, yet accurate alternative to numerical methods for dealing with variable velocities and non-parallel streamlines. Likewise, pure diffusion can be solved analytically for flow fields too complicated for combined advection-diffusion-reaction (see, for example, Verrall and Read (2012)) (Chapter 4). Finally, the reaction

subprocess of the ADR equation has always been the most amenable to analytic solutions, and can be solved for a wide variety of cases. Therefore, the advection, diffusion and reaction equations can all be solved either quasi-analytically or analytically when they are separated, in domains where the combined ADR equation is currently insoluble. As such, a natural question to ask is *Can we accurately combine these analytical solutions?*

In this chapter we present a split operator (SO) technique to combine analytical solutions of advection, diffusion and reaction. SO methods are a commonly used approach for combining numerical solutions of interacting physical phenomena, such as in groundwater transport. These methods replace a complicated model with a group of appropriately chosen subprocesses, described by the model, and solved successively in time (Csomos et al., 2005). The decoupled subprocesses, being simpler to solve than the original system, allow for the solution of otherwise intractable problems. Over the years three basic classes of SO methods (Gasda et al., 2011) have arisen in environmental transport problems: sequential SO (SSO); alternating SO; and iterative SO. As the type of SO method is not the salient aspect of our methodology, we restrict ourselves to the simplest and most common, the SSO, to demonstrate how to combine analytical solutions of advection, diffusion and reaction.

The SSO method divides a problem into two or more subproblems which are solved sequentially, with the solution of each subproblem used as the initial condition for the following subproblem. The most common approach is to split the whole problem into L ($l = 1...L$) discrete time intervals (Δt), where each group of subproblems is solved for $t^l = l\Delta t$, and the solution of the final subproblem is used as the initial condition of the first subproblem of $t^{l+1} = (l + 1)\Delta t$.

This chapter is organised as follows. In the next section we provide a mathematical description of the problem to be solved. Section 6.3 presents the analytical solution technique required to solve each decoupled subprocess, and the method used to combine these is proffered in Section 6.4. Section 6.5 examines potential sources of error in the SSO methodology, and the results of the combined technique, along with comparative solutions, are presented in Section 6.6. Finally, in Section 6.7 we present a discussion

and conclusions.

6.2 Mathematical description of the problem

As stated in Section 6.1, the problem to be solved is that of combined advection-diffusion-reaction, with the technique described in Section 6.4 applicable to a wide range of physical situations. In its general form, the governing ADR equation is

$$\frac{\partial C}{\partial t} = \nabla \cdot (D \nabla C) - \nabla \cdot (\mathbf{u} C) + R, \tag{6.1}$$

where C is the concentration (of whatever solute is being modelled), D is the diffusion coefficient, $\mathbf{u}$ is the bulk velocity of the solvent, and R is the reaction term (that is, a source or sink of solute). Note that each of the terms, D, $\mathbf{u}$ and R may vary with space, time, or the concentration C.

However, in this chapter, for the purposes of clarity and simplicity, we restrict ourselves to the relatively simple case of a one-dimensional ($1D$) velocity field, $u_* = \mathbf{u}(y)$, equal and constant latitudinal and longitudinal diffusion, $D_{x_*} = D_{y_*} = D_*$, and a simple linear decay term for reaction, $\lambda_* C_*$, where λ_* is a constant. The dimensionalised form of the ADR equation to be solved is then

$$\frac{\partial C_*}{\partial t_*} = D_* \frac{\partial}{\partial x_*} \left(\frac{\partial C_*}{\partial x_*} \right) + D_* \frac{\partial}{\partial y_*} \left(\frac{\partial C_*}{\partial y_*} \right) - u_* \frac{\partial C_*}{\partial x_*} - \lambda_* C_*, \tag{6.2}$$

with the asterisk subscripts representing the dimensionalised parameters of equation (6.1). Non-dimensionalising the above equation (refer to equations (A.20)–(A.26) in Appendix A.5 for details) results in the specific form of the ADR equation to be solved throughout this chapter,

$$\frac{\partial C}{\partial t} = \nabla \cdot (\nabla C) - \mathbf{u}(y) \frac{\partial C}{\partial x} - \lambda C. \tag{6.3}$$

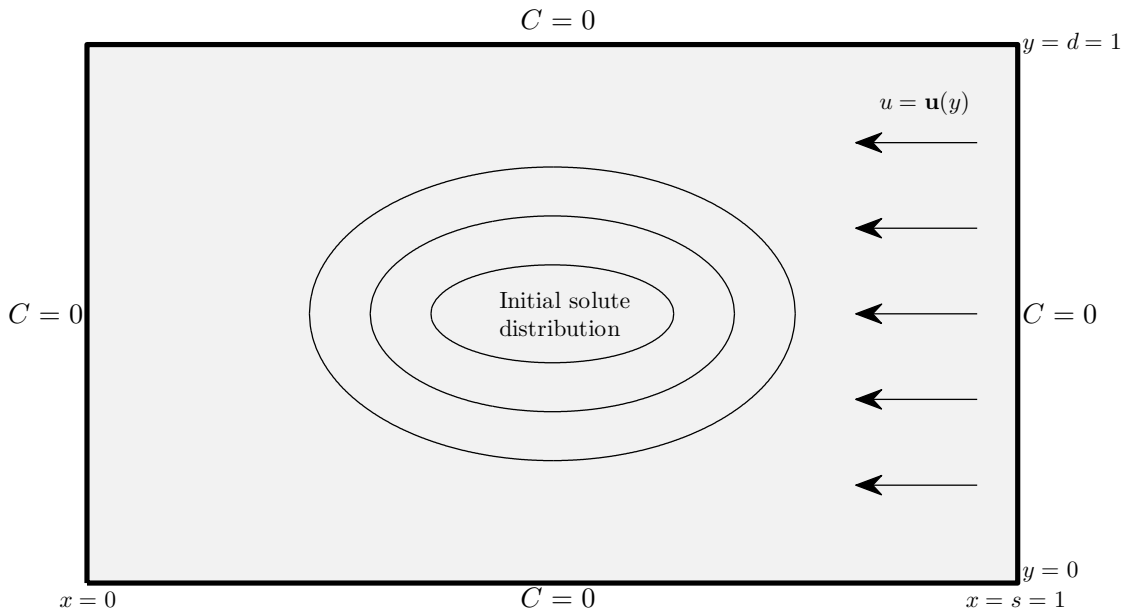

Figure 6.1: Domain being considered throughout this chapter.

Finally, we define an initial two-dimensional ($2D$) Gaussian distribution of solute,

$$C(x, y, 0) = \overline{c}e^{-(\frac{(x-x_0)^2}{2\sigma_x^2} + \frac{(y-y_0)^2}{2\sigma_y^2})} \tag{6.4}$$

(with the peak concentration $\overline{c} = 1$). This domain is seen in Figure 6.1, with s and d the lengths of the x and y axes respectively, and the domain scaled for the length of the y-axis, that is, $d = 1$. For convenience we will use a square domain, $s = 1$. All boundary conditions are Dirichlet (first-type) and set to $C = 0$.

6.3 Analytical solutions of the decoupled subprocesses

The SSO method can be viewed as an approximate technique to integrate equation (6.3) over an arbitrary time interval Δt (Valocchi and Malmstead, 1992). The method is

perhaps clearer when presented in the notation of Tompson and Dougherty (1990),

$$\Delta C = C(\mathbf{x}, t+\Delta t) - C(\mathbf{x}, t) = \int_t^{t+\Delta t} \nabla \cdot (\nabla C) dt - \int_t^{t+\Delta t} \mathbf{u}(y) \frac{\partial C}{\partial x} dt - \int_t^{t+\Delta t} \lambda C dt. \quad (6.5)$$

Solving the first integral gives a trial solution, henceforth $C^{(1)}(\mathbf{x}, t+\Delta t)$, which acts as the initial condition of the second integral. The solution of the second integral, henceforth $C^{(2)}(\mathbf{x}, t+\Delta t)$, acts as the initial condition of the third integral, the solution of which gives the final result $C(\mathbf{x}, t+\Delta t)$.

Decoupling the above equation gives the following system,

$$\frac{\partial C^{(1)}}{\partial t} = \nabla \cdot (\nabla C^{(1)}), \quad (6.6)$$

$$\frac{\partial C^{(2)}}{\partial t} = -\mathbf{u}(y) \frac{\partial C^{(2)}}{\partial x}, \quad (6.7)$$

$$\frac{\partial C}{\partial t} = -\lambda C, \quad (6.8)$$

each of which are solved separately in the subsections below.

6.3.1 Diffusion

For the domain of Section 6.2, we solve for diffusion (6.6) using analytic series methods (for a complete $2D$ solution similar to that used in this chapter, refer to Appendix A.2). When combined with a collocation approach (Trefethen, 2000), this technique produces fast, accurate results for any time period required. Moreover, the coefficients obtained for this solution can be used to evaluate any point in the domain. This is an important property of the solution, and indeed any analytical solution.

The diffusion problem (6.6) is formulated mathematically as follows. Inside the domain,

$$\frac{\partial}{\partial x}\left(\frac{\partial C^{(1)}}{\partial x}\right) + \frac{\partial}{\partial y}\left(\frac{\partial C^{(1)}}{\partial y}\right) = \frac{\partial C^{(1)}}{\partial t}, \quad (6.9)$$

where $C^{(1)}(x, y, t)$ is the concentration of solute at any point (x, y) in the domain at

time t. From Section 6.2 we observe the boundary conditions,

$$C^{(1)}(0, y, t) = C^{(1)}(s, y, t) = 0, \tag{6.10}$$

$$C^{(1)}(x, 0, t) = C^{(1)}(x, d, t) = 0. \tag{6.11}$$

Using separation of variables, and truncating after $m = M$, $n = N$ terms, the series solution of equation (6.9) at $t = t^{l+1}$ is

$$C^{(1)}(x, y, t^{l+1}) = \sum_{n=1}^{N} \sum_{m=1}^{M} A_{mn} \sin\left(\frac{m\pi x}{s}\right) \sin\left(\frac{n\pi y}{d}\right) e^{-\gamma_{mn}^2 \Delta t}, \tag{6.12}$$

where

$$\gamma_{mn}^2 = \left(\frac{m^2}{s^2} + \frac{n^2}{d^2}\right) \pi^2, \tag{6.13}$$

and A_{mn} are the series expansion coefficients. These can be obtained from an orthogonality relationship, or (as in the manner of this chapter) by using a theoretically equivalent collocation/discrete least squares approach (Trefethen, 2000). At $t = 0$,

$$C^{(1)}(x_i, y_j, 0) = \sum_{n=1}^{N} \sum_{m=1}^{M} A_{mn} \sin\left(\frac{m\pi x_i}{s}\right) \sin\left(\frac{n\pi y_j}{d}\right) \tag{6.14}$$

at $M'N'$ collocation points (x_i, y_j), $i = 1, \ldots, M'$; $j = 1, \ldots, N'$, where $M' \geq M$, $N' \geq N$. ($M' = M$, $N' = N$ for a 'pure' collocation or pseudo-spectral approach (Trefethen, 2000).) In this case, the solution process devolves into solving for A in the matrix equation

$$X^{\mathrm{T}} C^{(1)} Y^{\mathrm{T}} = \left(X^{\mathrm{T}} X\right) A \left(Y Y^{\mathrm{T}}\right), \tag{6.15}$$

where, for $i = 1, \ldots, M'$, $j = 1, \ldots, N'$, $m = 1, \ldots, M$, $n = 1, \ldots, N$,

$$[X]_{im} = \sin(m\pi x_i / s), \qquad [Y]_{nj} = \sin(n\pi y_j / d), \tag{6.16}$$

$$[C^{(1)}]_{ij} = C^{(1)}(x_i, y_j), \qquad [A]_{mn} = A_{mn}, \tag{6.17}$$

and the initial condition $C^{(1)}(x_i, y_j, 0)$ is obtained from equation (6.4).

6.3.2 Advection

The technique described in Section 6.4 (implicitly) requires knowledge of the path of any streamline within the domain. For the domain specified in Section 6.2, we note the simplicity of the velocity field, that is, $\mathbf{u} = \mathbf{u}(y)$. This indicates horizontal streamlines. Consider one such streamline, $y = a$ (where a is some constant). According to the above statement of the velocity field, along this streamline the velocity, $u = \mathbf{u}(a)$, is also constant. The technique described in Section 6.4 (conceptually) solves combined advection-diffusion on a point by point basis. Therefore, for any point in the domain, equation (6.7) reduces to the $1D$ advection equation with constant velocity,

$$\frac{\partial C^{(2)}}{\partial t} = -u\frac{\partial C^{(2)}}{\partial x}, \tag{6.18}$$

with an initial condition $C^{(2)}(x, a, t^l) = C^{(1)}(x, a, t^{l+1})$.

Solving the well known equation (6.18) gives

$$C^{(2)}(x, t^{l+1}) = C^{(2)}(x - u\Delta t, t^l). \tag{6.19}$$

6.3.3 Reaction

The final subprocess (6.8) of the decoupled system is the reaction (simple decay) term. Given an initial condition $C(x, y, t^l) = C^{(2)}(x, y, t^{l+1})$, the solution is trivially,

$$C(x, y, t^{l+1}) = C(x, y, t^l)e^{-\lambda\Delta t}. \tag{6.20}$$

6.4 Combined advection-diffusion-reaction

The majority of this section is devoted to combining the analytical solutions of advection and diffusion. This is the key to the technique outlined in this chapter, as reaction is a simple extension (at least in this case) to the methodology. However, in order to proceed, we first need to define a uniform grid of points over the domain described in Section 6.2. This uniform grid has two functions: firstly, the solution at these points is

the discrete representation of the continuous solution; and secondly, the grid points act as the collocation points required to solve for the series coefficients in equation (6.15). We define this set $\mathbb{G} = \mathbb{X} \times \mathbb{Y}$ where $\mathbb{X} = \{x' : x' \text{ is evenly spaced between } (0, s)\}$ and $\mathbb{Y} = \{y' : y' \text{ is evenly spaced between } (0, d)\}$.

To solve for advection, observe the form of equation (6.19). This indicates that at some point (x, y) after time $t = \Delta t$, the final value of concentration $C^{(2)}(x, y, \Delta t)$ is equal to the concentration of some upstream point $(x - \mathbf{u}(y)\Delta t, y)$ at $t = 0$. Since a function is available to find the initial concentration anywhere within the domain, equation (6.4), all that is required is the location of the upstream point.

Setting the uniform grid, $\mathbb{G} = (x', y')$, as the end points of the advection process after $t = \Delta t$, and using the velocity field $\mathbf{u}(y)$, the starting locations of advection are revealed as the set of points $\mathbb{A} = \{(\xi, \eta) : (x' - \mathbf{u}(y')\Delta t, y')\}$, that is, the coordinates of an advecting particle are transformed from $(\xi, \eta) \rightarrow (x', y')$ over the period $t = 0 \rightarrow \Delta t$ (or $t = t^l \rightarrow t^{l+1}$). For all intents and purposes, this is the Semi-Lagrangian scheme (or modified method of characteristics) sometimes used in numerical modelling (Hundsdorfer and Verwer, 2003). This result can be seen in Figure 6.2. The square markers represent the uniform grid, $\mathbb{G}$, while the cross markers represent the starting points of advection, $\mathbb{A}$. The dotted lines connecting these markers are the streamlines. We define the velocity field in this figure to be a Gaussian distribution in the y-axis,

$$\mathbf{u}(y) = \overline{u} e^{-\frac{(y-y_0)^2}{2\sigma_y^2}}. \tag{6.21}$$

To solve for combined advection-diffusion, all the required information is now at hand. Given the set $\mathbb{G} = (x', y')$, it is a simple matter to find the initial concentration on the uniform grid, $C^{(1)}(x', y', 0)$, utilising equation (6.4). This result is then used in equation (6.15) to obtain the series coefficients. The diffusion solution (6.12) is now available, but instead of solving for $C^{(1)}(x', y', \Delta t)$, we solve for the concentration field at $\mathbb{A}$, that is, $C^{(1)}(\xi, \eta, \Delta t)$. In doing so, diffusion is solved from $t = 0 \rightarrow \Delta t$ at the set of points that will then advect to the uniform grid over the period $t = 0 \rightarrow \Delta t$. This is the essence of the SSO scheme described in Section 6.1, with the result,

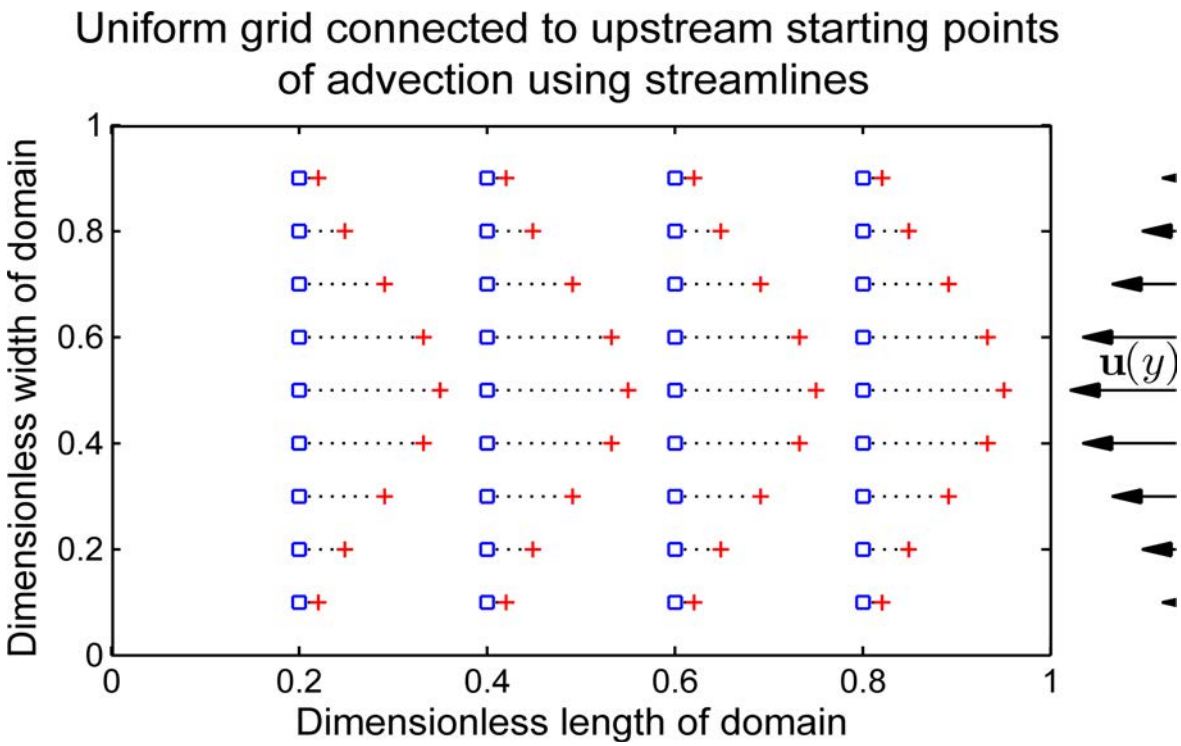

FIGURE 6.2: Upstream advection from the original uniform grid, $\mathbb{G}$ (square markers), to the starting locations of advection, $\mathbb{A}$ (cross markers). The dotted lines connecting the two are streamlines.

$C^{(2)}(x', y', \Delta t) = C^{(1)}(\xi, \eta, \Delta t)$, being combined advection-diffusion.

Finally, to get combined advection-diffusion-reaction, all that's required is to substitute the above result into equation (6.20). That is, $C(x', y', \Delta t) = C^{(1)}(\xi, \eta, \Delta t)e^{-\lambda \Delta t}$. The above procedure can then be repeated for L discrete split steps, as described in Section 6.1. For convenience, we refer to the method described in this section as the split analytical operator technique.

6.5 Split operator error and commutativity

Typically, when solving ADR problems, split operator techniques combine numerical solutions of each subprocess. In such cases, there are two sources of error: truncation error, that is, the error inherent to the numerical solution for that particular subprocess; and splitting error, the inherent numerical error caused by splitting the subprocesses in the first place (Gasda et al., 2011). In this chapter, by solving each subprocess

analytically, we remove (theoretically) the first of these sources of error. (Note that the analytic series solutions used in this chapter also have some associated truncation error, but this can be made as small as we choose.) This leaves splitting error to be considered.

In SO schemes there are certain special cases where splitting error disappears. These are when the subprocesses, advection, diffusion and reaction, are commutative (Csomos et al., 2005). That is, if the order in which we combine these subprocesses makes no difference to the solution, for example, advection-diffusion-reaction, as opposed to diffusion-reaction-advection, then the problem is commutative. Using the Lie operator formalism, Lanser and Verwer (1999) show that with exact integration of each subprocess, the problem is commutative if R is linear in C, and $\mathbf{u}$, D and R do not vary in space. Additionally, if the problem is commutative, the SO technique only requires one split step for an accurate solution, that is, $L = 1$. Increasing L (and therefore reducing Δt) does not improve the result. Given analytical solutions of each subprocess, if the problem is commutative then the split operator technique will give the exact solution of the ADR equation. In Section 6.6 we compare one such case (that meets the above requirements of commutativity) with a purely analytical solution.

However, for most practical situations splitting error exists and needs to be minimised. One technique is to reduce the size of the splitting step, Δt. As $\Delta t \to 0$, this splitting error has been formally shown to converge (Gasda et al., 2011), so in general, the smaller the splitting step, the more accurate the solution. In addition, the choice of SO technique can also reduce this splitting error. For example, second order Strang splitting (an alternating SO technique) is more accurate than the first order SSO method used in this chapter. Further insight into this splitting error can be found using the Lie operator formalism (Lanser and Verwer, 1999).

6.6 Results

In this chapter we present two examples: the first with a constant velocity throughout the domain; and the second with a variable velocity in the y-axis (the Gaussian velocity

field described in equation (6.21)). In the first of these, we compare the split analytical operator solution with a purely analytical solution of the coupled problem (details of the purely analytical solution can be found in Appendix A.5). In the second example (for which no closed form solution is available) we solve the split analytical operator problem for successively smaller split steps (that is, $\Delta t \to 0$ as L increases), and check for convergence of the solutions. In addition, given that the resolution of the grid will characterise the solution, we also test for RMS error convergence as the uniform grid is refined.

For the first example with constant velocity, the parameters used are: $s = 1$; $\sigma_x = \sigma_y = 1/16$; $u = -100$ (right to left); $\lambda = 10$ (sink term); $t = 0.002$; $\Delta t = 0.002$ (that is, one split step); $M' = N' = 100$ (uniform grid); and $M = N = 100$ (series coefficients). (Note that the problem has been non-dimensionalised for the diffusion coefficient.) We find the split analytical operator solution of combined advection-diffusion-reaction for our domain (Section 6.2), using the methods described in Sections 6.3 and 6.4. The above parameters meet the requirements of commutativity as discussed in Section 6.5, therefore, it follows that the result (Figure 6.3) should be the exact solution of the ADR problem. Comparing this result to the purely analytical solution found using series solutions (Appendix A.5), revealed that for the majority of the domain the difference between the two solutions is of the order 10^{-14}, that is, machine precision. However, close to the boundaries, $x = 0$ and $x = s$, this difference increases according to the proximity of concentration levels greater than zero (in this case, to approximately 10^{-5}). This difference appears to be largely a consequence of the advection subprocess of the SO technique. The coupled solution of Appendix A.5 enforces the boundary condition, $C = 0$, for both advection and diffusion, however the split analytical operator technique only enforces the boundary condition for diffusion, with the classical analytical solution of advection (6.19) having infinite boundaries. Even so, for this example a mass balance analysis (refer to Appendix A.6 for details) revealed that the two solutions agreed extremely well, with a mass balance ratio of 0.99999678.

The second example considered in this chapter will assume similar parameters as that of the first example, with the notable difference of a Gaussian velocity field in the

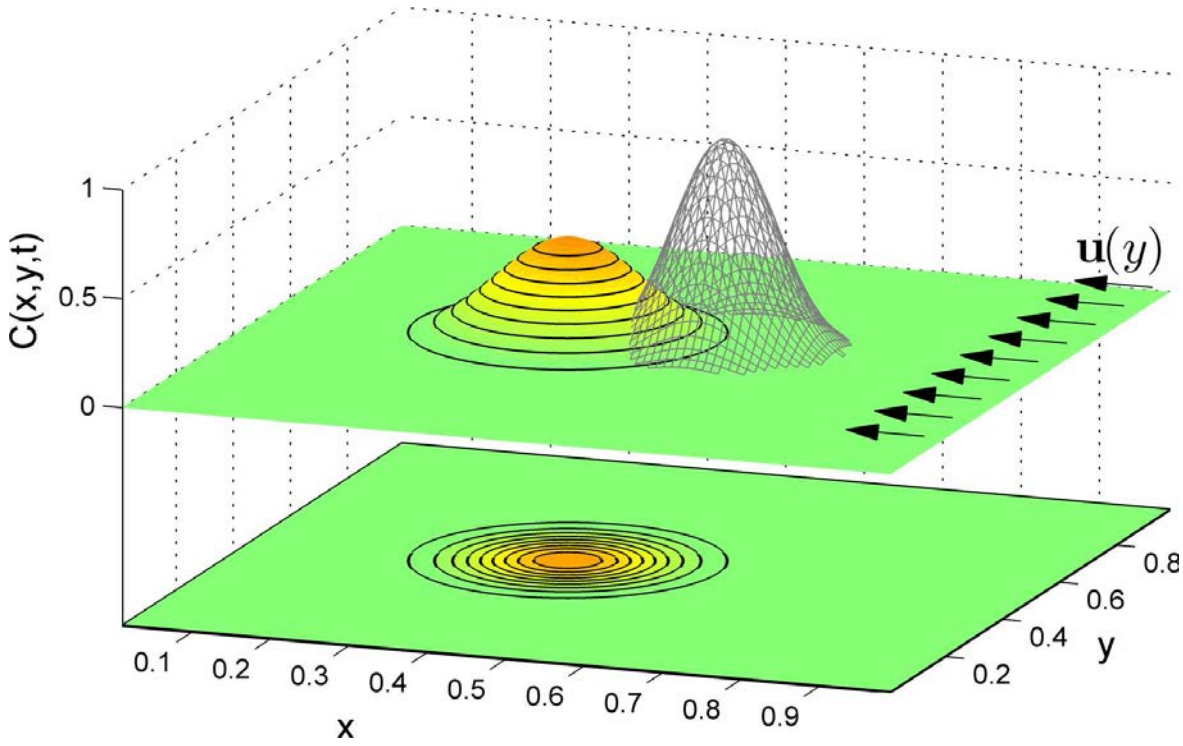

Figure 6.3: Split analytical operator solution of the ADR equation with a constant velocity field. Contours are projected onto a $2D$ (lower) plane to aid in visualisation. The grey wire mesh represents the initial concentration distribution. Concentration values are on the vertical axis, with the horizontal plane representing the $2D$ spatial domain.

y-axis, equation (6.21), with $\overline{u} = -100$ and $\sigma_y = 1/20$. Figure 6.4 shows the result after $t = 0.002$ with one split step. The introduction of an axis dependent velocity field violates the parameter requirements for commutativity, and therefore Figure 6.4 will vary from a purely analytical solution. As an analytical solution is unavailable for comparison, we solve for successively smaller split steps ($\Delta t \to 0$). Figure 6.5 is the final result of the split analytical operator solution after 50 split steps. (This result was achieved in (approximately) nine seconds on a standard PC (Intel Core 2 Duo CPU, 2.33GHz, 1.96GB RAM, Matlab), and compares more than favourably with most finite difference implementations that are only achieving modest accuracy.) The rate of convergence for the second example is shown in Figure 6.6 ($\overline{u} = -100$). For comparison, two similar examples varying only in velocity, $\overline{u} = -10$ and $\overline{u} = -1$, are also presented. As can be seen, as the peak velocity decreases, that is, the problem becomes more diffusion dominated, the convergence properties improve. For these

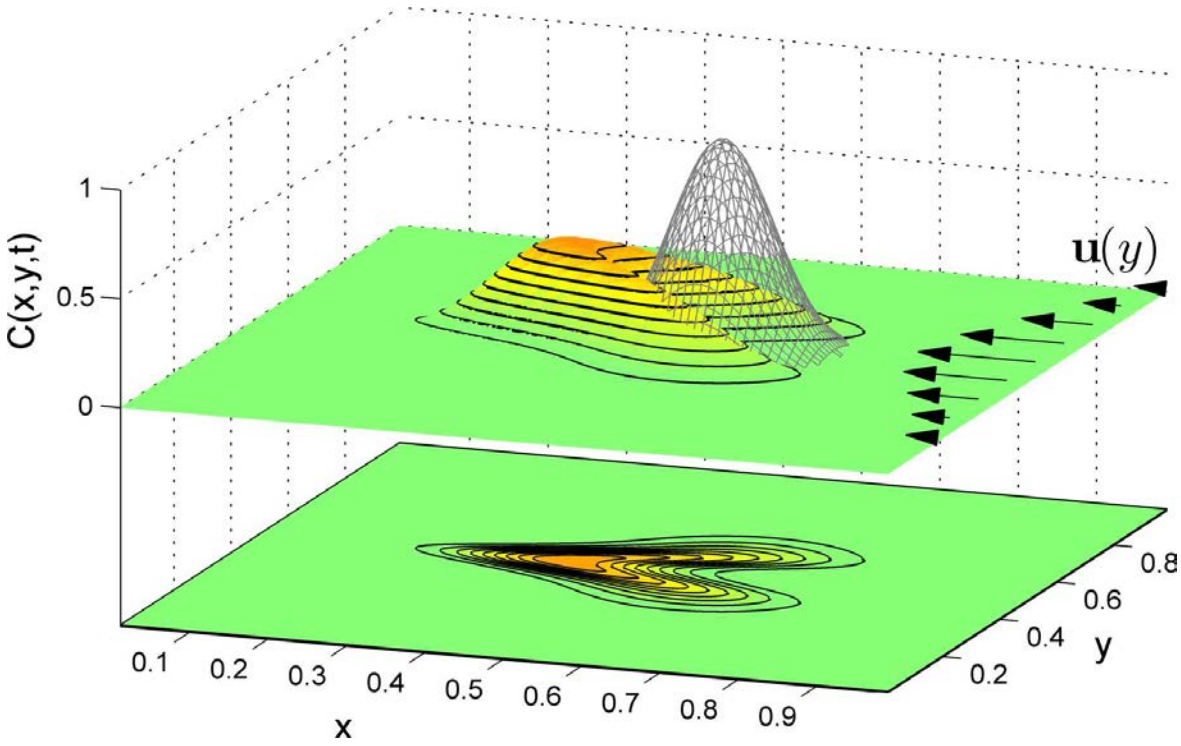

FIGURE 6.4: Split analytical operator solution of the ADR equation (with Gaussian velocity field) for 1 split step. Contours are projected onto a $2D$ (lower) plane to aid in visualisation. The grey wire mesh represents the initial concentration distribution. Concentration values are on the vertical axis, with the horizontal plane representing the $2D$ spatial domain.

examples, the convergence appears to be algebraic with the gradients of the curves in Figure 6.6 all approximately equal to two, that is, quadratic convergence. For our specific example, $\overline{u} = -100$, the solutions for one split step (Figure 6.4) and 50 split steps (Figure 6.5) vary by about 23% (RMS difference between the two solutions, divided by the RMS of the 50 split steps solution). The solutions for 49 split steps and 50 split steps vary by about 0.008%.

Finally, given that the number of grid points characterises the continuous solution, Figure 6.7 tests the effect of refining the grid against RMS error convergence. The number of grid points in each axis are continually doubled, $M' = N' = \{100, 200, 400, 800, 1600\}$, and the RMS error between successive solutions is plotted against the finer grid. All other parameters are those of the second example.

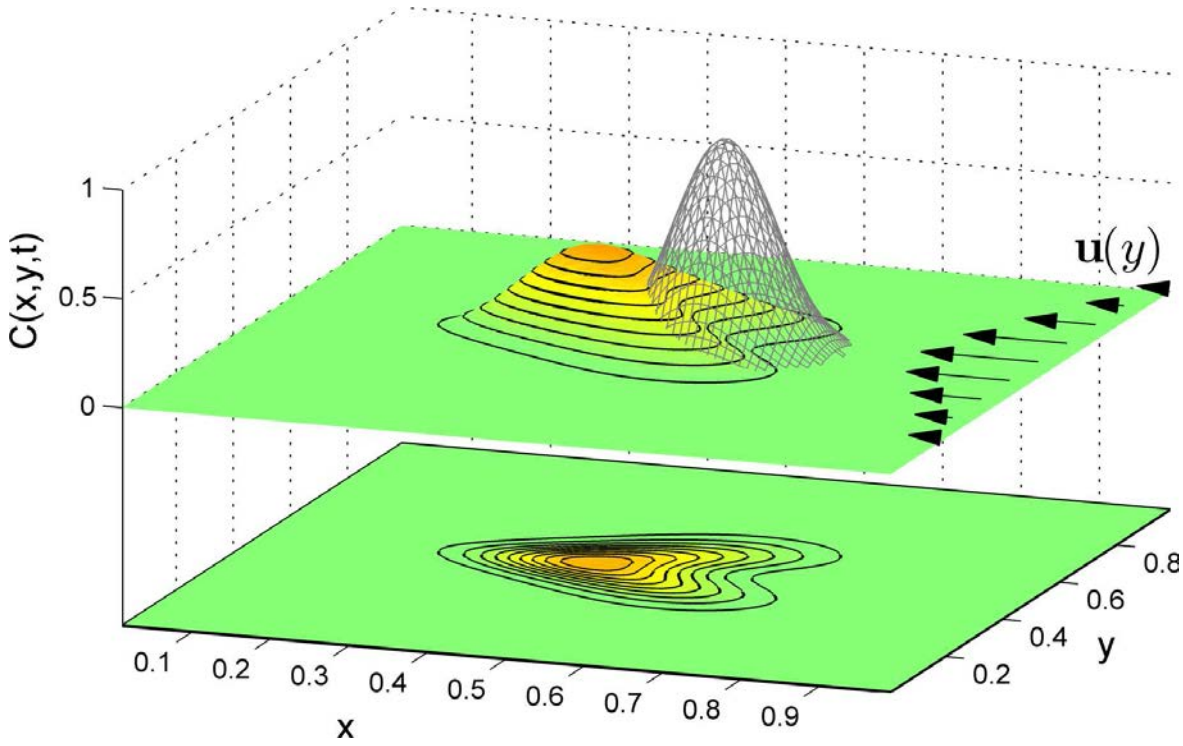

Figure 6.5: Split analytical operator solution of the ADR equation (with Gaussian velocity field) for 50 split steps. Contours are projected onto a $2D$ (lower) plane to aid in visualisation. The grey wire mesh represents the initial concentration distribution. Concentration values are on the vertical axis, with the horizontal plane representing the $2D$ spatial domain.

6.7 Discussion and conclusions

This chapter has presented a technique to combine analytical solutions of advection, diffusion and reaction, in a manner that is conceptually similar to the well known split operator methodology. Given an analytical solution for diffusion within the domain, the Semi-Lagrangian approach of connecting each final grid point with a calculated upstream starting location means advection becomes part of the diffusion calculation, by simply calculating diffusion at the upstream set of points. But unlike traditional implementations of Semi-Lagrangian schemes (that is, to numerical techniques), there is no interpolation required to merge advection and diffusion at these upstream locations. However, despite analytical solutions of each subprocess, Figure 6.7 demonstrates that the resolution of the grid plays a role in the accuracy of the solution.

The main advantage of the split analytical operator technique presented here is

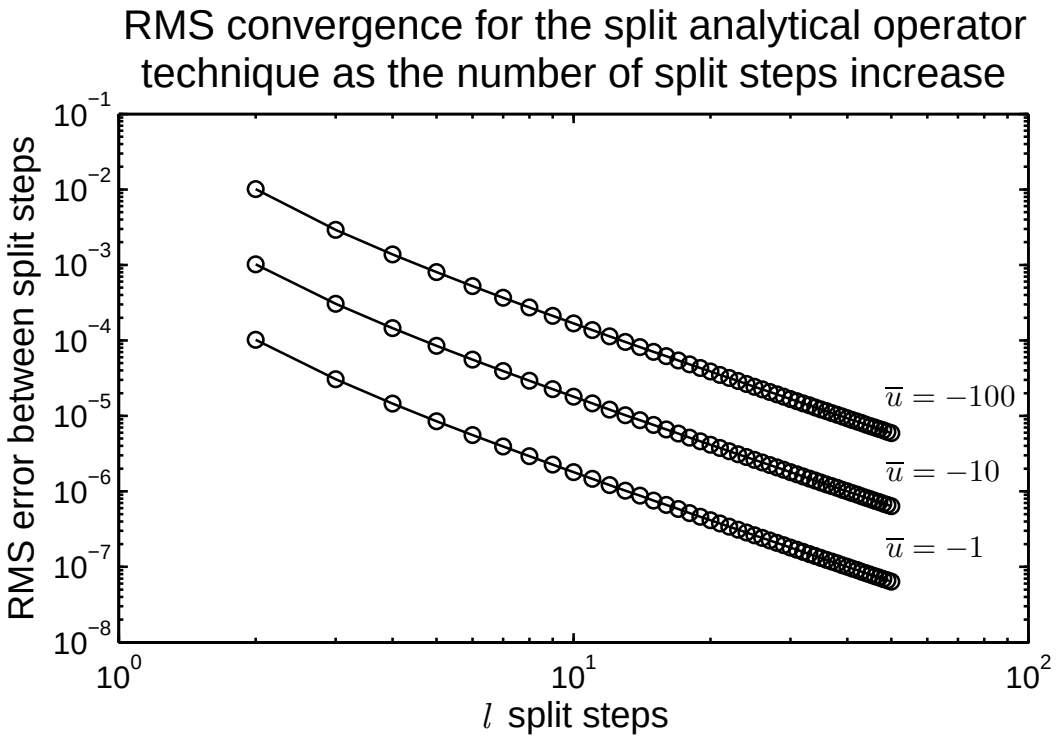

FIGURE 6.6: Rate of convergence for the split analytical operator technique as the number of split steps increase. The RMS error is between the l^{th} and the $(l-1)^{th}$ split steps.

improved accuracy; the same advantage as any analytical technique compared to its numerical equivalent. Using analytical solutions for each subprocess removes one of the two major sources of error of split operator methods, leaving only splitting error to be considered. As stated previously, this splitting error is not always present, but when it is, can be mitigated by reducing the size of the splitting step, Δt. In addition, there are other SO techniques available to reduce this splitting error further. Higher order schemes such as Strang splitting have been shown to improve results, as do iterative split operator methods, which attempt to eliminate or control splitting error through an iterative process. We leave the reduction of splitting error in the technique presented here for future consideration. However, we note that even when reductions to the size of the splitting step are required (effectively time discretisation), spatially, the solution $C(x, y, t)$ is a continuous function. (Although the resolution of the uniform grid in the split analytical operator technique affects the accuracy of the solution, it is not a spatial discretisation of the problem in the traditional sense.) This is in contrast

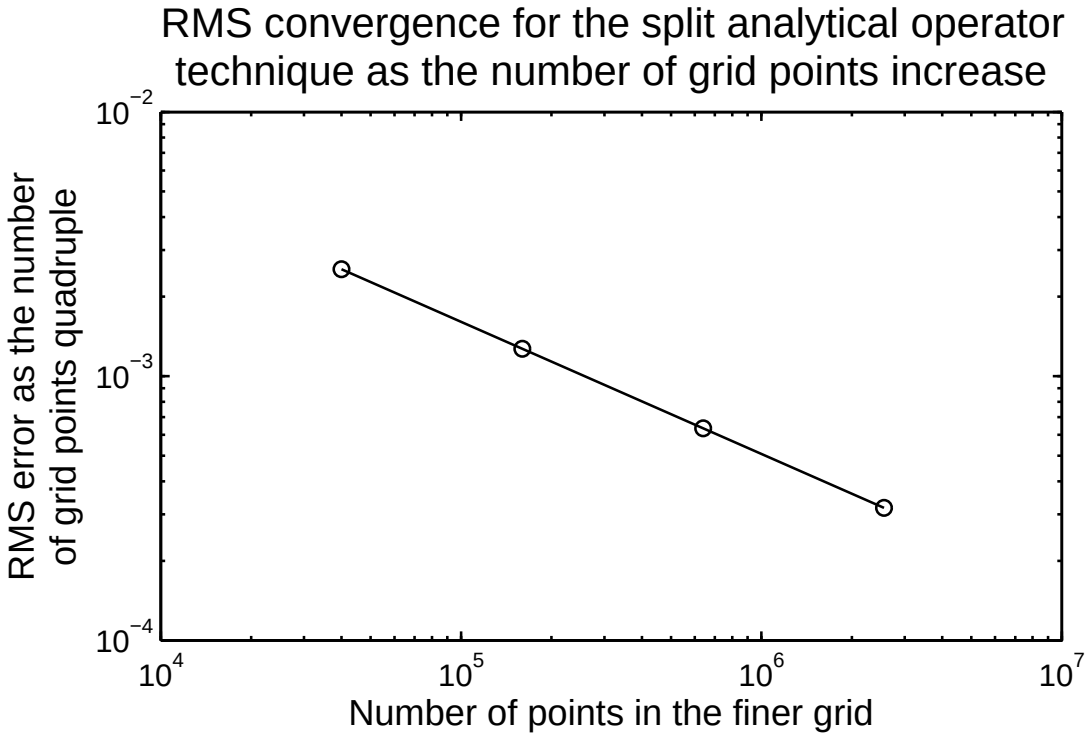

Figure 6.7: Rate of convergence for the split analytical operator technique as the number of grid points are quadrupled. The test cases are $M' = N' = \{100, 200, 400, 800, 1600\}$. The number of series coefficients are held constant at $M = N = 100$. All other parameters are as for the second example in Section 6.6.

to methods such as finite difference schemes that require both temporal and spatial discretisation.

The examples presented in this chapter were, for reasons of illustration, relatively simple. The uniform grid, $\mathbb{G}$, and constant time step, Δt, provide advantages, such as the efficient calculation of series coefficients using collocation, and the need for only one set of upstream locations, $\mathbb{A}$; but these conditions are not necessary. At the cost of increased complexity, the split analytical operator technique can accommodate non-uniform grids and variable time steps. However, the split analytical operator technique may be most useful in its potential application to non-uniform flow fields; an application that is difficult for other methods. For example, in Chapter 2 we solve analytically for the $2D$ flow field beneath saline aquaculture ponds. This type of implicit solution allows for the numerical calculation of any streamline in the domain to analytical accuracy. The technique described in this chapter is suitable for this type of problem,

as it requires only the final upstream location of an advecting particle after time Δt. The complexity of the streamline is irrelevant, so long as the upstream location is accurate.

This chapter has presented a technique to combine analytical solutions of advection, diffusion and reaction. Analytical solutions have been combined before using the split operator methodology (for example, Valocchi and Malmstead, 1992), but so far as the authors are aware, previous incarnations were $1D$ implementations only, simply added together for the purpose of investigating splitting error. The method presented here avoids interpolation for computed upstream concentrations, and shows some promise for providing accurate results for a range of problems hitherto restricted to purely numerical techniques. Indeed, it may also provide an alternative for some purely analytical solutions that meet the requirements of commutativity, such as that in Appendix A.5. Because of its exponential transform (A.28), when Appendix A.5 was applied practically it could not be solved over the equivalent range of values as the split analytical operator implementation.

7

Combined advection-diffusion for the leaky pond problem

7.1 Introduction

In this chapter we use the split analytical operator technique (Verrall and Read, 2015) (Chapter 6) to model advective-diffusive contaminant transport from leaky saline ponds throughout a freshwater aquifer below. The split analytical operator technique solves each transport subprocess analytically (or quasi-analytically), and combines the solutions sequentially; that is, the result of the first subprocess is used as the initial condition for the second subprocess. The accuracy of this technique is further improved by splitting the whole problem into L ($l = 1...L$) discrete time intervals (Δt), where each pair of subprocesses are solved for $l\Delta t$, and the solution of the second subprocess is used as the initial condition for the first subprocess of $(l + 1)\Delta t$.

This chapter is organised as follows. In Section 7.2 an overview of the specific problem to be solved is presented. Section 7.3 gives analytical (or quasi-analytical) solutions of the advection and diffusion subprocesses, with the combined advection-diffusion model presented in Section 7.4. Section 7.5 provides results for a given set of aquifer parameters, and finally, a discussion is presented in Section 7.6.

7.2 Hydrogeology and problem description

The problem to be modelled in this chapter is that of a leaky saltwater pond situated above a freshwater aquifer. The aquifer is assumed to be rectangular, with constant hydraulic conductivity. The bottom of the aquifer is impermeable bedrock, while the upstream (right) side boundary lies beneath the centre of the pond and hence acts as a line of symmetry for the purposes of advection and diffusion. The downstream (left) side boundary is placed well outside the area of interest and therefore assumed impermeable for convenience. Finally, the top boundary is the water table and the surface of the pond, with a smooth transition between the two. (Note, for simplicity we assume there is no unsaturated zone, that is, the water table coincides with the soil surface.) The height of the pond provides the driving potential of advective saltwater contamination. Outside the ponds the air/water interface precludes diffusion across

this top surface. At the saltwater/freshwater interface immediately beneath the ponds we assume no diffusion for convenience. (Note, this assumption will be discussed further in Section 7.6.) A schematic of the domain is presented in Figure 7.1.

We want to find the extent of contamination throughout the freshwater aquifer as a result of advective-diffusive transport from the saline pond. That is, we need to solve the advection-diffusion equation,

$$\frac{\partial C_*}{\partial t_*} = -\nabla_* \cdot (\mathbf{u}_* C_*) + \nabla_* \cdot (D_* \nabla_* C_*), \tag{7.1}$$

for the domain in Figure 7.1, where C_* is the concentration, D_* is the diffusion coefficient, and $\mathbf{u}_*$ is the bulk velocity of the solvent. Note that in the general equation above, the terms D_* and $\mathbf{u}_*$ may vary with space, time, or the concentration C_*. Also note that asterisk subscripts represent dimensional variables; these will later be dropped when the problem is non-dimensionalised.

7.3 Analytical/quasi-analytical solutions

As mentioned in the introduction, the model in this chapter is an application of the split analytical operator technique presented in Chapter 6. That is, analytical (or quasi-analytical) solutions of advection and diffusion are combined using the split operator methodology. Decoupling advection and diffusion from equation (7.1) gives the following system,

$$\frac{\partial C_*^{(1)}}{\partial t_*} = -\nabla_* \cdot (\mathbf{u}_* C_*^{(1)}), \tag{7.2}$$

$$\frac{\partial C_*^{(2)}}{\partial t_*} = \nabla_* \cdot (D_* \nabla_* C_*^{(2)}), \tag{7.3}$$

each of which are solved separately in the following subsections.

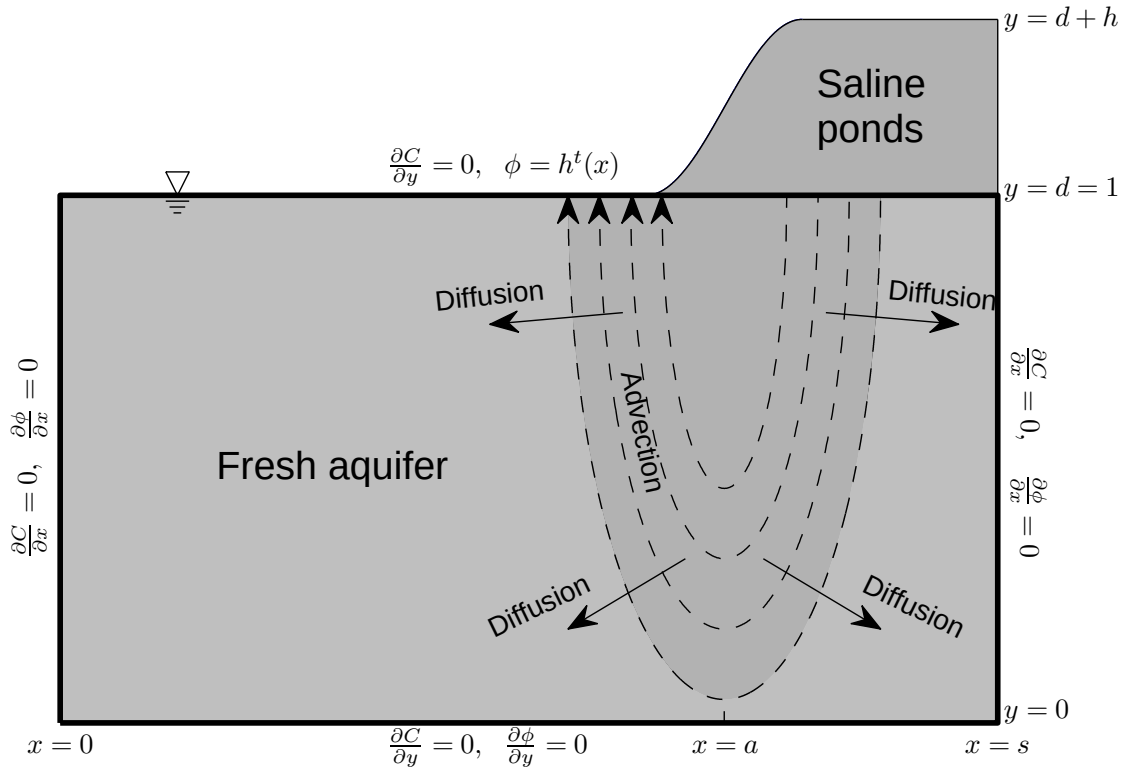

FIGURE 7.1: Domain being considered throughout this chapter.

7.3.1 Advection

Verrall et al. (2009b) (Chapter 2) describe a quasi-analytical Lagrangian approach to modelling advective contamination, which allows for the numerical tracing of any streamline within the domain to analytical accuracy. That is, the extent of contamination within the domain (Section 7.2) is found by numerically integrating (over time) along the streamlines of the analytically resolved flow domain. For the details of this quasi-analytical solution, we refer the reader to Chapter 2. However, for self-containedness, we present a brief outline and the relevant equations in the remainder of this subsection.

For the domain of Section 7.2, the solution is confined to an aquifer of constant hydraulic conductivity, K_*. Within the saturated aquifer, we assume the seepage

velocity $\mathbf{u}_* = (u_*, v_*)$ satisfies Darcy's law,

$$\mathbf{u}_* = -K_* \nabla_* \phi_*(x_*, y_*), \tag{7.4}$$

where $\phi_*(x_*, y_*)$ is the hydraulic head. Upon invoking the continuity condition, we obtain Laplace's equation for the saturated flow domain,

$$\nabla_*^2 \phi_*(x_*, y_*) = 0, \tag{7.5}$$

with the boundary conditions given by

$$v_*(x_*, 0) = -K_* \frac{\partial}{\partial y_*} \phi_*(x_*, 0) = 0, \tag{7.6}$$

$$u_*(0, y_*) = -K_* \frac{\partial}{\partial x_*} \phi_*(0, y_*) = 0, \tag{7.7}$$

$$u_*(s_*, y_*) = -K_* \frac{\partial}{\partial x_*} \phi_*(s_*, y_*) = 0, \tag{7.8}$$

$$\phi_*(x_*, d_*) = h_*^t(x_*), \tag{7.9}$$

where $h_*^t(x_*)$ is the height of the water surface along the top boundary. The boundary value problem is now fully defined and can be solved for $\phi_*(x_*, y_*)$. Once this is found, the stream function and the pore velocity become available.

The Cauchy-Riemann equations,

$$\frac{\partial \psi_*}{\partial y_*} = K_* \frac{\partial \phi_*}{\partial x_*}, \qquad \frac{\partial \psi_*}{\partial x_*} = -K_* \frac{\partial \phi_*}{\partial y_*}, \tag{7.10}$$

give the stream function $\psi_*(x_*, y_*)$, and allow the tracing of any streamline desired.

The pore velocity $\mathbf{U}_*(x_*, y_*)$ is related to the seepage velocity by the porosity σ, where $0 < \sigma < 1$ and σ is assumed constant, by

$$\mathbf{u}_* = \sigma \mathbf{U}_*. \tag{7.11}$$

Hence,

$$\mathbf{U}_* = (U_*, V_*) = -\frac{K_*}{\sigma}\left(\frac{\partial \phi_*}{\partial x_*},\ \frac{\partial \phi_*}{\partial y_*}\right). \tag{7.12}$$

At this point we non-dimensionalise the problem using the hydraulic conductivity K_*, and the depth of the aquifer d_*. That is,

$$x_* = d_* x,\ \ y_* = d_* y,\ \ a_* = d_* a,\ \ s_* = d_* s,\ \ h_* = d_* h, \tag{7.13}$$

$$h_*^t(x_*) = d_* h^t(x),\ \ \phi_*(x_*, y_*) = d_* \phi(x, y),\ \ \psi_*(x_*, y_*) = d_* K_* \psi(x, y), \tag{7.14}$$

$$t_* = \frac{\sigma d_*}{K_*} t_{\mathrm{A}},\ \ \mathbf{u}_* = K_* \mathbf{u},\ \ \mathbf{U}_* = \frac{K_*}{\sigma}\mathbf{U}, \tag{7.15}$$

where h_* is the height of the saltwater ponds above the water table, and t_{A} is dimensionless time (with the subscript denoting scaling for advection).

There are three points to note here. First, the dimensionless parameters can be obtained simply by removing the asterisk subscript from their dimensional equivalent. Second, since $d_* = d_* d$, the dimensionless depth d of the aquifer is $d = 1$. Finally, the dimensionless pore velocity $\mathbf{U}$ has been scaled by the (dimensionless) porosity σ.

The hydraulic head $\phi(x, y)$ is now solved using the classic separation of variables (Carrier et al., 1966) approach. The series solution obtained is truncated after $N + 1$ terms to give

$$\phi(x, y) = \sum_{n=0}^{N} A_n \cosh\frac{n\pi y}{s} \cos\frac{n\pi x}{s}, \tag{7.16}$$

which satisfies the bottom and side boundary conditions exactly, with the remaining boundary condition (7.9) (after being non-dimensionalised) used to evaluate the series coefficients $A_n,\ n = 0, 1, \ldots, N$. This is a standard cosine series, with

$$A_0 = \frac{1}{s}\int_0^s h^t(x)\, dx, \tag{7.17}$$

$$A_n = \frac{2}{s}\int_0^s h^t(x) \cos\frac{n\pi x}{s}\, dx, \quad n \neq 0. \tag{7.18}$$

Once the series solution for the hydraulic head $\phi(x, y)$ has been determined, the

pore velocity field $\mathbf{U} = (U, V)$ can be calculated by differentiating the series,

$$\mathbf{U} = (U, V) = -\left(\frac{\partial \phi}{\partial x}, \frac{\partial \phi}{\partial y}\right). \tag{7.19}$$

The pore velocity at any point is also given by

$$\mathbf{U} = \left(\frac{dx}{dt_{\mathrm{A}}}, \frac{dy}{dt_{\mathrm{A}}}\right), \tag{7.20}$$

where now the location at which the pore velocity is calculated is parameterised using (non-dimensional) time t_{A} as a parameter. That is, $x \equiv x(t_{\mathrm{A}}),\ y \equiv y(t_{\mathrm{A}})$. Thus, from equations (7.19) and (7.20), the time t_{A} taken for a neutrally buoyant particle to be advected along a stream line from (x_0, y_0) to $(x(t_{\mathrm{A}}), y(t_{\mathrm{A}}))$ is

$$t_{\mathrm{A}} = \int_{x_0}^{x(t_{\mathrm{A}})} \frac{dx}{U} = -\int_{x_0}^{x(t_{\mathrm{A}})} \frac{dx}{\partial \phi / \partial x} \tag{7.21}$$

$$= \int_{y_0}^{y(t_{\mathrm{A}})} \frac{dy}{V} = -\int_{y_0}^{y(t_{\mathrm{A}})} \frac{dy}{\partial \phi / \partial y}. \tag{7.22}$$

Rearranging equations (7.21) and (7.22) gives the (approximate) distances $(\delta x, \delta y)$ a particle is advected in the x and y directions over a small time interval δt_{A},

$$\delta x \approx -\frac{\partial \phi}{\partial x} \delta t_{\mathrm{A}}, \tag{7.23}$$

$$\delta y \approx -\frac{\partial \phi}{\partial y} \delta t_{\mathrm{A}}. \tag{7.24}$$

Consider at time $t_{\mathrm{A}} = \tau_0$ a discrete set of $I > 0$ points $(x_{i,0}, y_{i,0}),\ i = 1, \ldots, I$. Then, for any time $\tau_J = \tau_0 + J\delta t_{\mathrm{A}},\ J > 0$, the approximate location of the advection front $(x_{i,J}, y_{i,J})$ is found by calculating the intermediate points $(x_{i,j}, y_{i,j}),\ j = 1, \ldots, J-1$ using the difference equations

$$x_{i,j} \approx x_{i,j-1} - \left(\frac{\partial \phi}{\partial x}\right)_{i,j-1} \delta t_{\mathrm{A}}, \tag{7.25}$$

$$y_{i,j} \approx y_{i,j-1} - \left(\frac{\partial \phi}{\partial y}\right)_{i,j-1} \delta t_{\mathrm{A}}, \tag{7.26}$$

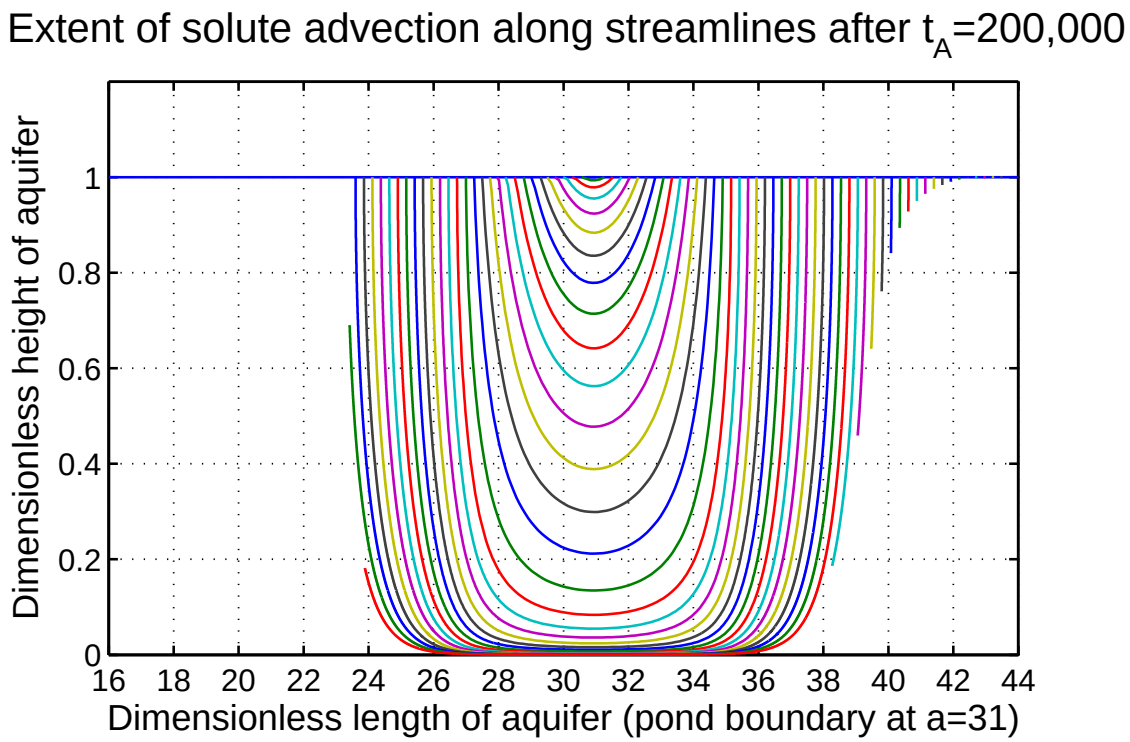

FIGURE 7.2: Extent of solute advection along streamlines after $t_{\mathrm{A}} = 200,000$.

where

$$\left(\frac{\partial \phi}{\partial x}\right)_{i,j} = \left(\frac{\partial \phi(x,y)}{\partial x}\right)_{\substack{x=x_{i,j} \\ y=y_{i,j}}}, \tag{7.27}$$

$$\left(\frac{\partial \phi}{\partial y}\right)_{i,j} = \left(\frac{\partial \phi(x,y)}{\partial y}\right)_{\substack{x=x_{i,j} \\ y=y_{i,j}}}. \tag{7.28}$$

For sufficiently small δt_{A} (that is, sufficiently large J), this will converge to the advection front at time τ_J. Using this algorithm, we can predict the advection of solutes from *any* initial location in the flow domain. Chapter 2 chose the initial location for solute advection as the water table, immediately below the aquaculture ponds ($a \leq x \leq s$). Figure 7.2 shows the result of such a process. As can be seen, many streamlines are incomplete, with the end points representing the final location of solute transport.

7.3.2 Final advection result

Now, let's consider the classical solution of the $1D$ advection equation (with constant velocity μ),

$$C(x,t) = C(x - \mu t, 0). \tag{7.29}$$

This indicates that at some point x after time t, the final value of concentration is equal to the concentration of some upstream point $x - \mu t$ at $t = 0$. To find this point (given known values of x, μ and t), all that's required is a trivial substitution. This $1D$ problem is essentially a single streamline, with the solution being the result of backtracking along this streamline to the initial upstream point. Tying this idea to the above analytical solution of the velocity field (U, V), and the numerical integration (over time) along the streamlines, then the final advection result is

$$C^{(1)}(x,y,t_{\mathrm{A}}) = C^{(1)}(x - \int_0^{t_{\mathrm{A}}} U(x(t_{\mathrm{A}}), y(t_{\mathrm{A}}))dt_{\mathrm{A}}\,, y - \int_0^{t_{\mathrm{A}}} V(x(t_{\mathrm{A}}), y(t_{\mathrm{A}}))dt_{\mathrm{A}}\,, 0). \tag{7.30}$$

7.3.3 Diffusion

For the domain of Section 7.2, we solve for the purely diffusive case (again) using analytic series methods. When applied to a regular (Eulerian) grid, this technique produces fast, accurate results for any time period required. Moreover, the coefficients obtained for this solution can be used to evaluate any point in the domain, not just on the original grid. This is an important property of the solution. For the details of this purely diffusive solution, we refer the reader to Verrall and Read (2012) (Chapter 4). However, for self-containedness, we present a brief outline and the relevant equations in the remainder of this subsection.

The diffusion problem is formulated mathematically as follows. Inside the aquifer,

$$\frac{\partial}{\partial x_*}\left(D_* \frac{\partial C_*^{(2)}}{\partial x_*}\right) + \frac{\partial}{\partial y_*}\left(D_* \frac{\partial C_*^{(2)}}{\partial y_*}\right) = \frac{\partial C_*^{(2)}}{\partial t_*}, \tag{7.31}$$

where $C_*^{(2)}(x_*, y_*, t_*)$ is the concentration of solute at any point (x_*, y_*) in the domain

at time t_*. From Section 7.2, there is no diffusion across any boundary, therefore,

$$D_* \frac{\partial}{\partial x_*} C_*^{(2)}(0, y_*, t_*) = D_* \frac{\partial}{\partial x_*} C_*^{(2)}(s_*, y_*, t_*) = 0, \tag{7.32}$$

$$D_* \frac{\partial}{\partial y_*} C_*^{(2)}(x_*, 0, t_*) = D_* \frac{\partial}{\partial y_*} C_*^{(2)}(x_*, d_*, t_*) = 0, \tag{7.33}$$

where s_* and d_* are the length and depth of the aquifer, respectively.

We non-dimensionalise the problem in terms of the depth of the aquifer, d_* (same as advection), the concentration of the ponds, C_*^0, and the diffusivity, D_*; that is,

$$s_* = d_* s, \quad x_* = d_* x, \quad y_* = d_* y, \quad C_*^{(2)} = C_*^0 C^{(2)}, \quad t_* = \frac{d_*^2}{D_*} t_{\mathrm{D}}, \tag{7.34}$$

where t_{D} represents dimensionless time (with the subscript denoting scaling for diffusion).

Equation (7.31) becomes the non-dimensional equivalent

$$\nabla^2 C^{(2)} = \frac{\partial C^{(2)}}{\partial t_{\mathrm{D}}}, \tag{7.35}$$

with boundary conditions

$$\frac{\partial}{\partial x} C^{(2)}(0, y, t_{\mathrm{D}}) = \frac{\partial}{\partial x} C^{(2)}(s, y, t_{\mathrm{D}}) = 0, \tag{7.36}$$

$$\frac{\partial}{\partial y} C^{(2)}(x, 0, t_{\mathrm{D}}) = \frac{\partial}{\partial y} C^{(2)}(x, d, t_{\mathrm{D}}) = 0. \tag{7.37}$$

Using separation of variables (refer to Appendix A.2 for details), and truncating after $m = M$, $n = N$ terms, the series solution of equation (7.35) is

$$C^{(2)}(x, y, t_{\mathrm{D}}) = \sum_{n=0}^{N} \sum_{m=0}^{M} B_{mn} \cos \frac{m\pi x}{s} \cos \frac{n\pi y}{d} e^{-\gamma_{mn}^2 t_{\mathrm{D}}}, \tag{7.38}$$

where

$$\gamma_{mn}^2 = (\frac{m^2}{s^2} + \frac{n^2}{d^2})\pi^2 \tag{7.39}$$

and B_{mn} are the series expansion coefficients. These can be obtained from an orthogonality relationship or (as in the manner of this chapter) by using a theoretically equivalent collocation/discrete least squares approach (Trefethen, 2000):

$$C^{(2)}(x_i, y_j, 0) = \sum_{n=0}^{N} \sum_{m=0}^{M} B_{mn} \cos\left(\frac{m\pi x_i}{s}\right) \cos\left(\frac{n\pi y_j}{d}\right) \tag{7.40}$$

at $M'N'$ collocation points $(x_i, y_j),\ i = 0, \ldots, M';\ j = 0, \ldots, N'$, where $M' \geq M + 1$, $N' \geq N + 1$. ($M' = M + 1,\ N' = N + 1$ for a 'pure' collocation or pseudo-spectral approach. This is the approach used in this chapter.) In this case, the solution process devolves into solving for B in the matrix equation

$$X^{\mathrm{T}} C^{(2)} Y^{\mathrm{T}} = \left(X^{\mathrm{T}} X\right) B \left(Y Y^{\mathrm{T}}\right), \tag{7.41}$$

where, for $i = 0, \ldots, M'$, $j = 0, \ldots, N'$, $m = 0, \ldots, M$, $n = 0, \ldots, N$,

$$[X]_{im} = \cos(m\pi x_i/s), \qquad [Y]_{nj} = \cos(n\pi y_j/d), \tag{7.42}$$

$$[C^{(2)}]_{ij} = C^{(2)}(x_i, y_j), \qquad [B]_{mn} = B_{mn}. \tag{7.43}$$

7.3.4 Final diffusion result

The spatial scaling, d_*, is the same for the dimensionless solutions of advection and diffusion; however, this is not true of the temporal scaling. In the following section we combine the dimensionless solutions of advection and diffusion, and these time scales need to be the same. The (dimensional) time for advection t_* is given in terms of the dimensionless advection time t_{A} by equation (7.15). This must be the same as the (dimensional) time for diffusion t_*, given in terms of the dimensionless diffusion time t_{D} by equation (7.34),

$$t_* = t_{\mathrm{A}} \frac{\sigma d_*}{K_*} = t_{\mathrm{D}} \frac{d_*^2}{D_*}. \tag{7.44}$$

Therefore, rearranging we obtain the relationship

$$t_{\mathrm{D}} = \frac{D_* \sigma}{K_* d_*} t_{\mathrm{A}} = \alpha t_{\mathrm{A}}, \tag{7.45}$$

where

$$\alpha = \frac{D_* \sigma}{K_* d_*}. \tag{7.46}$$

The dimensionless parameter α is used to scale the dimensionless solution of advection to the dimensionless solution of diffusion. This parameter would not be required if the advection and diffusion solutions were left dimensional; however, the advantages of a general non-dimensional solution outweighs this added complexity. We choose the dimensionless scaling for advection (as this is more convenient) as the time parameter for combining advection and diffusion. Therefore, equation (7.45) modifies equation (7.38) to

$$C^{(2)}(x, y, t_{\mathrm{A}}) = \sum_{n=0}^{N} \sum_{m=0}^{M} B_{mn} \cos \frac{m\pi x}{s} \cos \frac{n\pi y}{d} e^{-\gamma_{mn}^2 \alpha t_{\mathrm{A}}}. \tag{7.47}$$

7.4 Combining advection and diffusion

An analytical solution of the combined advection-diffusion problem stated in Section 7.2 is currently unavailable. This chapter doesn't attempt to find such a solution, but instead combines the preceding analytical solutions of advection and diffusion using a simple numerical technique. However, each solution is fundamentally different, with advection adhering to the Lagrangian approach (where a particle is followed as it moves through a porous medium), and diffusion following the Eulerian approach (where a point in space is observed while particles pass through it) (Bear, 1979). The problem is therefore, *how to combine these separate solutions?*

To proceed, we need to define a uniform grid of points over the domain described in Section 7.2. This uniform grid has two functions: firstly, the solution at these points is the discrete representation of the combined solution; and secondly, the grid points act as the collocation points required to solve for the series coefficients in equation (7.41). We define this set $\mathbb{G} = \mathbb{X} \times \mathbb{Y}$ where $\mathbb{X} = \{x' : x' \text{ is evenly spaced between } [0, s]\}$ and

$\mathbb{Y} = \{y' : y' \text{ is evenly spaced between } [0, d]\}$.

The $2D$ advection solution in Section 7.3.1 traces the path of contamination by numerically stepping along the streamlines of the domain. It starts at an initial set of points and progresses through time to the final location of transported contaminant. However, if we choose, it is just as easy to backtrack along streamlines over a given time period. That is, from any point in the domain, we can backtrack along the streamline over any time period to the initial upstream location, using a trivial modification to the technique in Section 7.3.1.

Setting the uniform grid, $\mathbb{G} = (x', y')$, as the end points of the advection process after some time $t_{\mathrm{A}} = \tau$, and backtracking along the streamlines using the quasi-analytical technique described in Section 7.3.1, the starting locations of advection are revealed as the set

$$\mathbb{A} = \{(\xi, \eta) \in \mathbb{R}^2 : \xi = x' - \int_0^\tau U(x(t_{\mathrm{A}}), y(t_{\mathrm{A}}))dt_{\mathrm{A}},\ \eta = y' - \int_0^\tau V(x(t_{\mathrm{A}}), y(t_{\mathrm{A}}))dt_{\mathrm{A}}\}.$$

That is, the coordinates of an advecting particle are transformed from $(\xi, \eta) \rightarrow (x', y')$ over the period $t_{\mathrm{A}} = 0 \rightarrow \tau$. For all intents and purposes, this is the Semi-Lagrangian scheme (or modified method of characteristics) sometimes used in numerical modelling (Hundsdorfer and Verwer, 2003). This result can be seen in Figure 7.3. The square markers represent the uniform grid, $\mathbb{G}$, while the cross markers represent the starting points of advection, $\mathbb{A}$. The lines connecting these markers are partial streamlines. Any point in the set $\mathbb{G}$ connected by a partial streamline to the salt/fresh interface becomes contaminated via advection over the period $t_{\mathrm{A}} = 0 \rightarrow \tau$. Therefore, it's a simple matter to define an initial concentration $C^{(1)}(\xi, \eta, 0)$. Any point in $\mathbb{A}$ at the salt/fresh interface is at the concentration of the ponds, and all other points are uncontaminated. The velocity field in this figure is defined by equation (7.19).

To solve for combined advection-diffusion all the required information is now at hand. As described by the split operator methodology, each subprocess is solved separately, with the result used as the initial condition for the subsequent subprocess. In our case, finding the set $\mathbb{A}$, and the initial advection concentration distribution

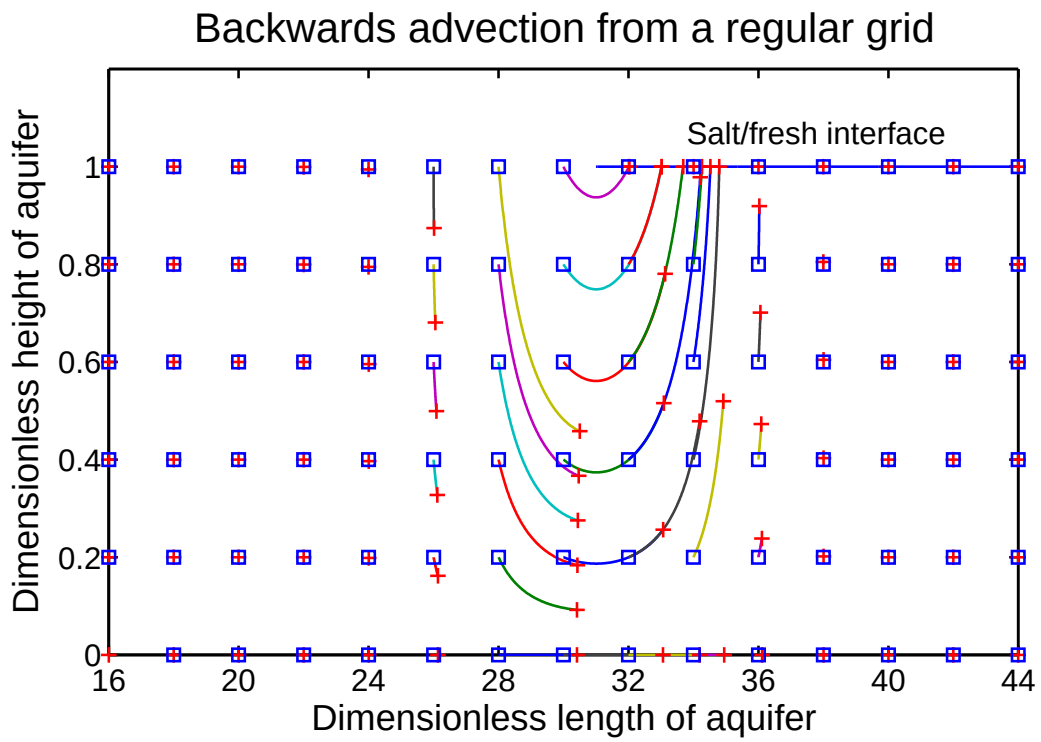

FIGURE 7.3: Upstream advection from the original uniform grid, $\mathbb{G}$ (square markers), to the starting locations of advection, $\mathbb{A}$ (cross markers). The lines connecting the two are streamlines.

$C^{(1)}(\xi, \eta, 0)$, is all that's required for the advection subprocess. That is, the initial diffusion concentration now becomes $C^{(2)}(x', y', 0) = C^{(1)}(\xi, \eta, 0)$ (since any contamination on $\mathbb{A}$, advects to $\mathbb{G}$, over the period $t_{\mathrm{A}} = 0 \rightarrow \tau$), and diffusion is solved using the technique described in Section 7.3.3. Combined advection-diffusion is therefore $C^{(2)}(x', y', \tau)$.

The above description demonstrates how to solve for advection, then diffusion, without any interpolation being required to merge the two processes. However, to improve the above result we can divide the time period, τ, into L ($l = 1...L$) discrete intervals, $\Delta t_{\mathrm{A}} = \tau / L$, and repeat the above procedure for each. That is, the starting locations of advection become

$$\mathbb{A} = \{(\xi, \eta) \in \mathbb{R}^2 : \xi = x' - \int_0^{\frac{\tau}{L}} U(x(t_{\mathrm{A}}), y(t_{\mathrm{A}}))dt_{\mathrm{A}},\ \eta = y' - \int_0^{\frac{\tau}{L}} V(x(t_{\mathrm{A}}), y(t_{\mathrm{A}}))dt_{\mathrm{A}}\},$$

and for each interval (excluding the final one), we solve for the diffusion process at

the starting points of advection, $C^{(2)}(\xi, \eta, \frac{l\tau}{L})$ (instead of $C^{(2)}(x', y', \frac{l\tau}{L})$). This effectively gives us the initial upstream concentration for each intermediate interval, $C^{(1)}(\xi, \eta, \frac{(l+1)\tau}{L}) = C^{(2)}(\xi, \eta, \frac{l\tau}{L})$. It follows that the initial diffusion concentration at each interval is therefore $C^{(2)}(x', y', \frac{(l+1)\tau}{L}) = C^{(2)}(\xi, \eta, \frac{l\tau}{L})$. Note, for the final interval, instead of solving the diffusion process at the starting points of advection, we instead solve for the regular grid, that is, $C^{(2)}(x', y', \frac{L\tau}{L})$.

7.5 Results

For the domain described in Section 7.2, we solve for combined advection-diffusion over a period of 7,610 years, and with the following dimensional parameters: $K_* = 10^{-5}$ m/s; $D_* = 2 \times 10^{-9}$ m^2/s; $\sigma = 0.3$; $d_* = 40$ m; $s_* = 1,760$ m; and $a_* = 1,240$ m (similar parameters to Model 1 in Chapter 2). Non-dimensionalising the above parameters means that K_*, D_* and σ disappear, with $d = 1$; $s = 44$; and $a = 31$. In addition, we choose a grid spacing of $\Delta x = 0.1$ in the horizontal plane, and $\Delta y = 0.005$ in the vertical plane. From equation (7.15), the time period for which we are solving (conveniently) becomes $t_{\mathrm{A}} = 200,000$ dimensionless time units. To numerically step along the streamlines for the advection component of the solution, we choose a discrete time step of $\delta t_{\mathrm{A}} = 10$ dimensionless units, which has been shown to produce accurate results for the advection only problem (Verrall et al., 2009a) (Chapter 3). The number of split steps chosen is $L = 250$ ($\Delta t_{\mathrm{A}} = 800$). This value of L was chosen for convenience, in that it was the optimal solution (in terms of computation time) for the problem and parameters described in this chapter, and the particular computer system on which the model was run. (Details on how this value of L was obtained can be found in Appendix A.7.) The result of combined advection-diffusion with the above parameters can be seen in Figure 7.4. The contributions from each process can be seen in the different colours in this figure. Red represents the contribution from advection, with blue and green representing diffusion. (It is important to note the difference between δt_{A} and Δt_{A}. The former is the size of the discrete time step used to step along the streamlines in the advection subprocess. The latter is the size of the temporal

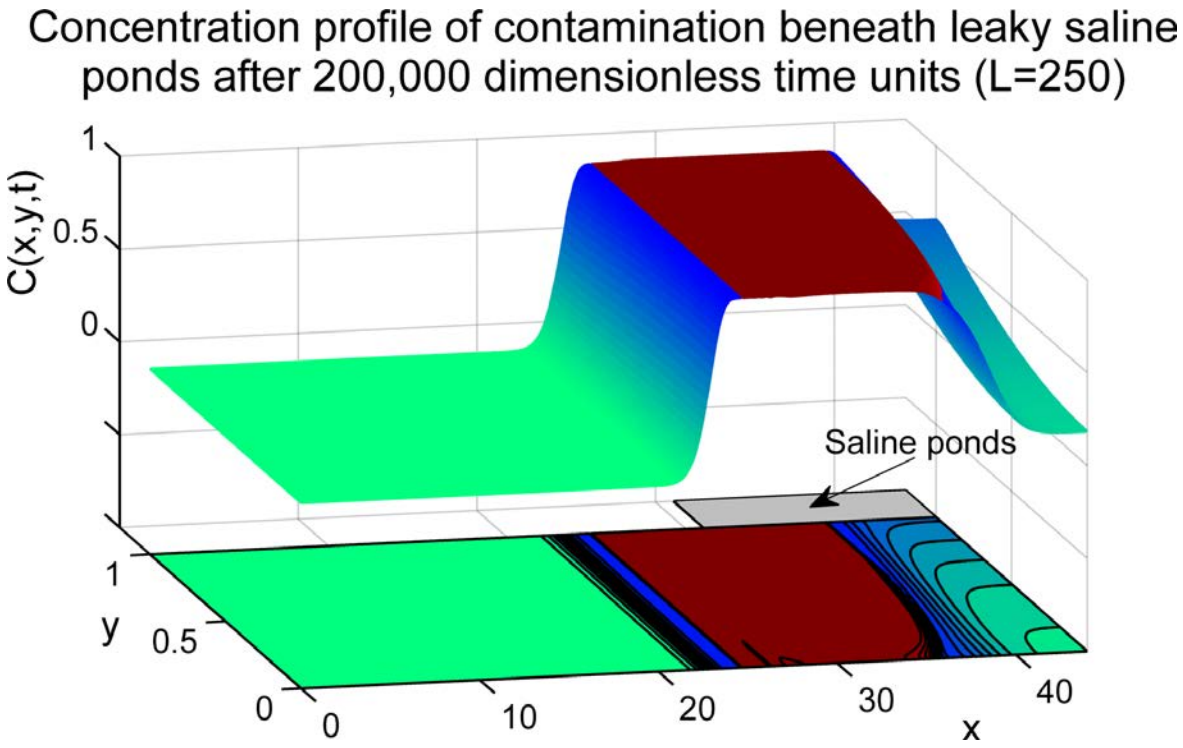

FIGURE 7.4: Split analytical operator solution with $L = 250$ (benchmark solution). Contours are projected onto a $2D$ (lower) plane to aid in visualisation. Concentration values are on the vertical axis, with the horizontal plane representing the $2D$ spatial domain.

discretisation of the split analytical operator technique described in Section 7.4.)

Using the above solution as a benchmark, we now halve the spacing of the grid points in both the horizontal and vertical axes. That is, with all else being equal, we solve for combined advection-diffusion with four times as many grid points (and therefore, four times as many series coefficients), and compare the solution to that of Figure 7.4. Figure 7.5 shows the actual difference between the two solutions. The extent of contamination is essentially the same, however, the wave between $x = 20$ and $x = 25$ indicates a steeper concentration gradient between the contaminated and non-contaminated regions for the solution with more grid points. That is, the benchmark solution seems slightly more diffusive than the finer grid solution. This is likely the result of numerical dispersion, as the slope of the concentration gradient able to be captured at the interface between the contaminated and non-contaminated regions depends on the relative spacing of the grid points. Between the two solutions there is a relative RMS error of 3.5%.

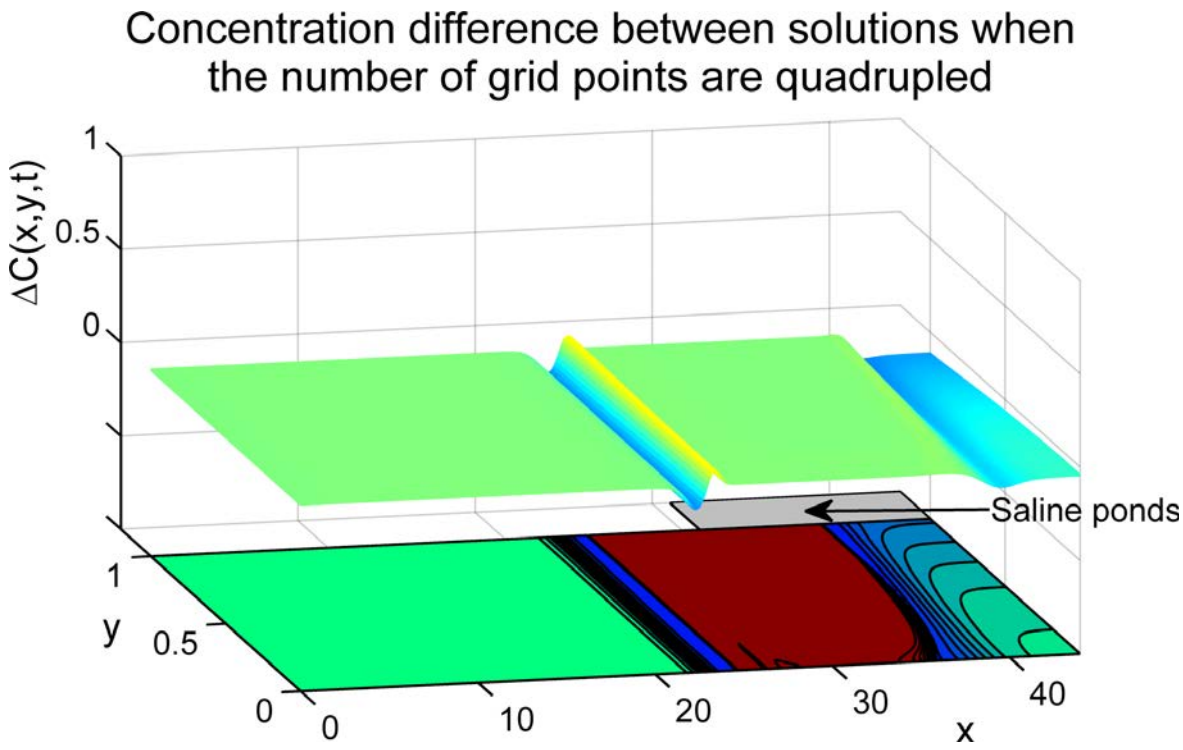

Figure 7.5: Difference between the benchmark solution and a solution with four times the number of grid points. The bottom projection is carried over from Figure 7.4 for ease of comparison. As can be seen, for most of the domain there is no difference between the solutions.

Next, again using the solution seen in Figure 7.4 as a benchmark, instead of increasing the number of grid points, we increase the number of split steps in the solution to $L = 2,000$. (As L increases ($\Delta t_{\mathrm{A}} \to 0$) the solution becomes increasingly accurate (Section 6.5).) Figure 7.6 shows the difference between the solutions for $L = 250$ ($\Delta t_{\mathrm{A}} = 800$) and $L = 2,000$ ($\Delta t_{\mathrm{A}} = 100$). Again, a wave appears between $x = 20$ and $x = 25$, indicating a steeper concentration gradient between the contaminated and non-contaminated regions for the solution with more split steps. This indicates more diffusion in the benchmark solution. With fewer split steps, the benchmark solution suffers from more splitting error than the more accurate solution (Section 6.5); furthermore, the final diffusion step in the benchmark solution is solved over a longer time period ($\Delta t_{\mathrm{A}} = 800$) than the more accurate solution ($\Delta t_{\mathrm{A}} = 100$). The relative RMS error between the two solutions is 8.0%. Figure 7.7 shows the actual solution for $L = 2,000$. We discuss this figure further in Section 7.6.

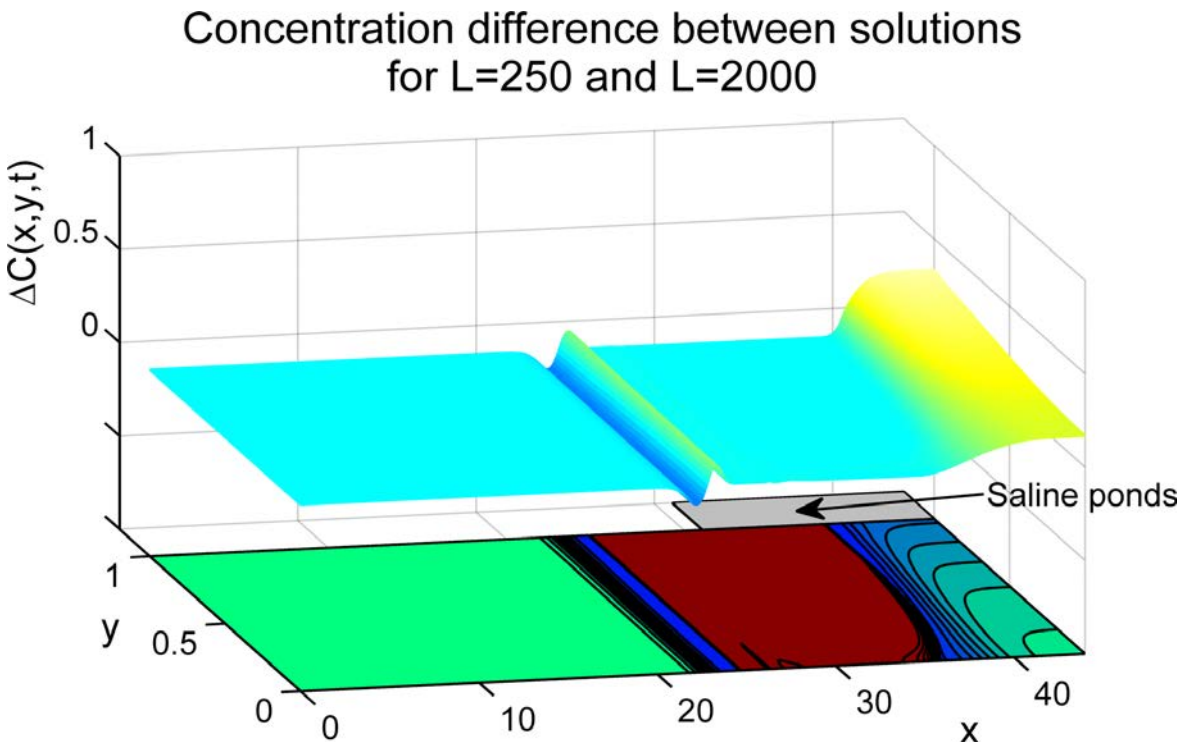

FIGURE 7.6: Difference between solutions where $L = 250$ (benchmark solution) and $L = 2,000$. The bottom projection is carried over from Figure 7.4 for ease of comparison. As can be seen, for most of the domain there is no difference between the solutions.

7.6 Discussion

This chapter investigated contamination, via combined advective-diffusive transport, from leaky saline ponds into a lower freshwater aquifer. It did so using the split analytical operator technique (Chapter 6), which combines analytical (or quasi-analytical) solutions of advection and diffusion by means of a simple numerical method. This combined analytical/numerical solution of the advection-diffusion equation requires a temporal discretisation, but unlike purely numerical methods, there is no spatial discretisation. There is, however, a discrete representation (in the form of a uniform grid) of the continuous spatial domain for practical reasons.

In Section 7.2 we defined separate boundary conditions (b.c.'s) for advection and diffusion. One of these b.c.'s employed a simplifying assumption of zero diffusion across the entire top surface of the domain, that is, a Neumann (or second-type) b.c. where

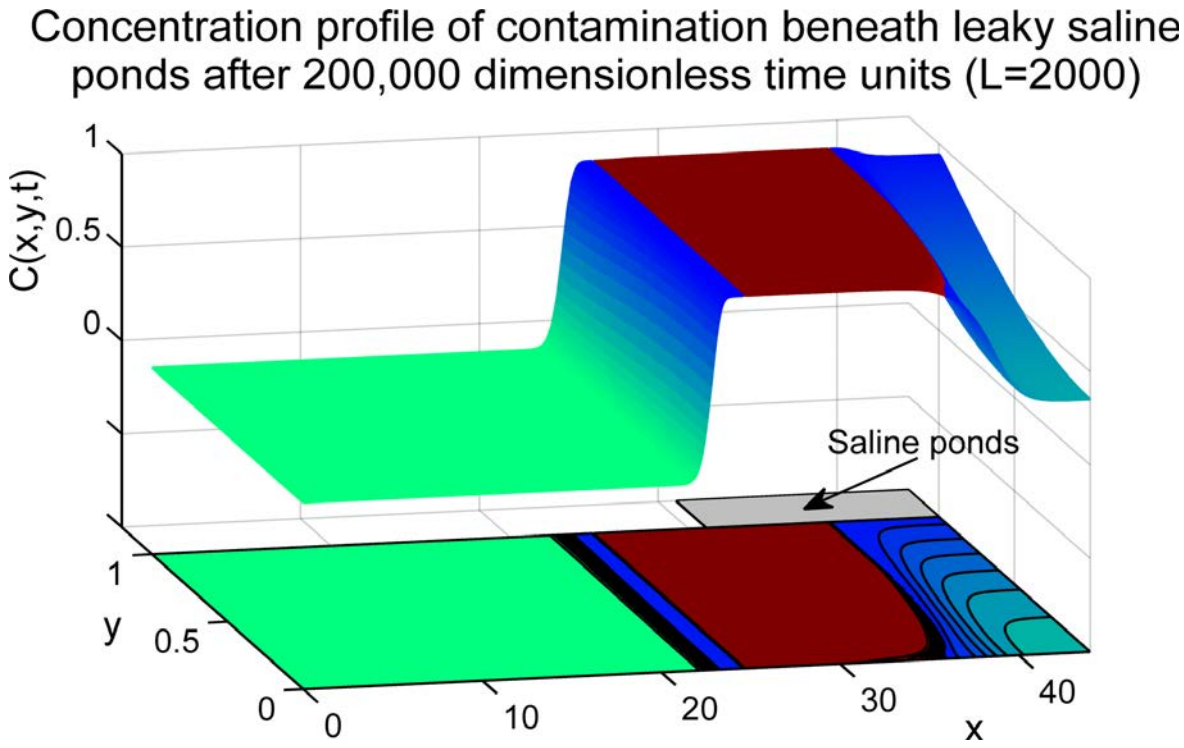

Figure 7.7: Split analytical operator solution with $L = 2,000$. Contours are projected onto a $2D$ (lower) plane to aid in visualisation. Concentration values are on the vertical axis, with the horizontal plane representing the $2D$ spatial domain.

$\frac{\partial C}{\partial y} = 0$. On closer inspection, a more accurate scenario is a mixed b.c. where

$$\frac{\partial C}{\partial y} = 0, \quad 0 \leq x \leq a,$$
$$C = 1, \quad a < x \leq s.$$

This indicates no diffusion across the air/water interface outside the ponds, but allows a constant strength source at the saltwater/freshwater interface immediately beneath the ponds. An analytical solution using the above mixed b.c. (similar to that described in Section 7.3.3) would indeed be preferable, but given the nature of the split analytical operator technique described in Section 7.4, is arguably unnecessary. Given a sufficiently small temporal discretisation, Δt_{A}, and grid points sufficiently close to the saltwater/freshwater interface, the alternating advection steps will deposit salt water from the ponds inside the boundary of the solution domain from where it can freely diffuse. This can be seen by comparing Figures 7.4 and 7.7 immediately beneath the

saline ponds near the right y-axis. In Figure 7.7 the contaminant concentration in this region is significantly higher than in Figure 7.4. This is also evident in the difference between the two solutions (Figure 7.6). It is expected that in the limit, $\Delta t_{\mathrm{A}} \rightarrow 0$, there is no difference between the Neumann b.c. used in this chapter and the mixed b.c. described above.

A true analytical solution of the advection-diffusion equation is currently unavailable for the problem defined in Section 7.2; however, as stated in Chapter 6, the split analytical operator technique will approach the true solution as the time discretisation approaches zero. Figure 7.7 shows the result of combined advection-diffusion using this methodology, with $L = 2,000$ split steps. It represents the realisation of the ultimate objective of this thesis; that is, a quasi-analytical technique to solve the advection-diffusion equation in the domain of Figure 7.1.

8

Comparison of quasi-analytical techniques

In Chapter 5, a set of $1D$ equations were presented that predict the extent of $2D$ advection-diffusion beneath leaky contaminated ponds. These equations separate the transport processes, and by doing so provide an insight into the relative progress and importance of advection and diffusion within this type of domain. However, $1D$ simplifications of the advection and diffusion processes cannot capture the full complexity of true $2D$ coupled advection-diffusion. To assess how accurate these $1D$ simplifications are, in this chapter we compare them to the most accurate solutions ($\Delta t_{\mathrm{A}} = 100$) of the split analytical operator (SAO) technique from Chapter 7.

To compare the two techniques, we choose a set of values for the parameters α, δ and h, and find the mean relative absolute error between the two methods for a range of breakthrough concentration levels along the water table. Given the work of Chapters 6 and 7, we assume that the split analytical operator technique will give the most accurate solution, therefore results from this technique will be the basis for comparison. Table 8.1 shows results for three sets of parameter values. These particular values were selected because they span a large range of the parameter sets tested, and they are representative of the relative error between the two techniques. The highlighted row in Table 8.1 represents the parameters $\alpha = 1.5 \times 10^{-6}$, $\delta = 4$, $h = 0.075$, and a breakthrough contaminant concentration level of 50%. This is the specific example used in Chapters 2, 3, 4 and 7.

To quantify the difference between the two methods, we first convert results from the split analytical operator technique to be similar in form to the equations from Chapter 5. That is, we track various breakthrough concentration fronts as they progress along the water table to obtain functions relating the distance, X, contamination has spread from the pond boundary versus the time taken to get there. Using these functions we then select a set of evenly spaced points along the water table, and find the time required to reach each of those points. These values of time are substituted into the functions from Chapter 5 to find the distance, X, predicted by the simplified $1D$ equations. The difference between the distances, ΔX, predicted by each technique is the absolute error.

As can be seen in Table 8.1, the error between the two techniques varies anywhere

$\alpha = 1.5 \times 10^{-6}$, $\delta = 4$, $h = 0.075$		$\alpha = 1.5 \times 10^{-4}$, $\delta = 2$, $h = 0.075$		$\alpha = 1.5 \times 10^{-8}$, $\delta = 1$, $h = 0.075$	
Concentration	Relative error	Concentration	Relative error	Concentration	Relative error
0.01	0.15	0.01	0.18	0.01	0.22
0.03	0.13	0.03	0.16	0.03	0.19
0.05	0.13	0.05	0.16	0.05	0.17
0.08	0.13	0.08	0.17	0.08	0.16
0.10	0.13	0.10	0.17	0.10	0.15
0.15	0.12	0.15	0.17	0.15	0.13
0.20	0.12	0.20	0.17	0.20	0.11
0.30	0.10	0.30	0.15	0.30	0.08
0.40	0.09	0.40	0.13	0.40	0.06
0.50	**0.08**	0.50	0.11	0.50	0.04
0.60	0.06	0.60	0.08	0.60	0.03
0.70	0.04	0.70	0.05	0.70	(0.04)
0.80	0.04	0.80	(0.06)	0.80	(0.07)
0.90	(0.05)	0.90	(0.12)	0.90	(0.11)

TABLE 8.1: 'Concentration' in the above table represents the breakthrough concentration front being tracked along the water table. Values vary between 0.01 (1%) and 0.9 (90%) of the original pond concentration. The 'Relative error' is the mean relative absolute error between the $1D$ equations and the SAO technique. In general, the $1D$ equations underestimate the amount of contamination, as demonstrated in Figure 8.1. However, when the $1D$ equations overestimate the amount of contamination, these relative error values are in brackets.

up to 22% (at least for all the various permutations of the parameters tested). This difference is largely attributable to the simplification (for the $1D$ equations) that advection and diffusion are dominant at different times and in different parts of the domain. While this is generally true, in the region where diffusion becomes dominant over advection, both transport processes will (for a time) be of the same order of magnitude. Therefore, in this region more transport is occurring than is being captured by the simple equations.

To get a visual representation of the difference between the two methods, in Figure 8.1 we plot each technique's predicted 50% breakthrough curve along the water table for the parameters $\alpha = 1.5 \times 10^{-6}$, $\delta = 4$ and $h = 0.075$ (the highlighted row from Table 8.1). This figure is an embellishment of Figure 4.5 from Chapter 4, which includes results from the numerical groundwater modelling package SUTRA (Voss and Provost, 2002). Figure 8.1 is composed of two parts, a general view (Figure 8.1a) and a magnified view (Figure 8.1b), each showing the comparison between the techniques. As can be seen, the curves produced by the simplified equations and the split analytical operator technique are the same basic shape. The difference between them (as measured from the pond boundary) appears to be fairly consistent, with the mean absolute

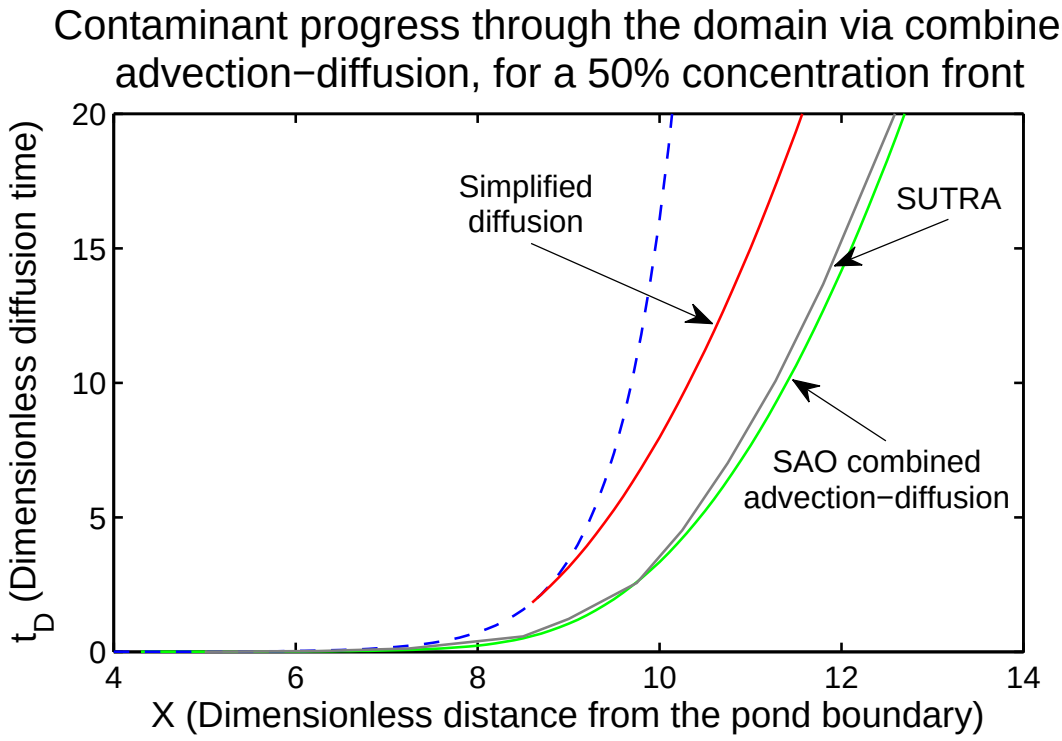

(a) Relative progress of contamination along the water table.

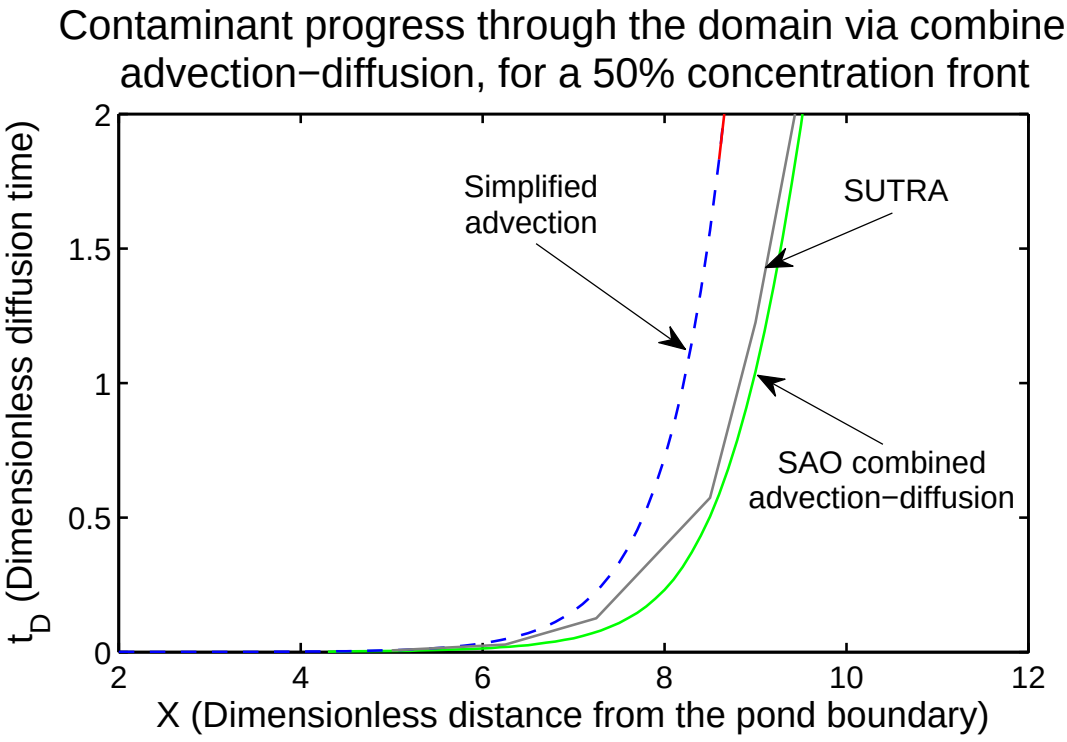

(b) Close up view: Relative progress of contamination along the water table.

FIGURE 8.1: Comparative contaminant progress along the water table via combined advection-diffusion, for the simplified $1D$ equations, the split analytical operator technique, and SUTRA.

relative error being 0.08 (8%). (As an aside, the numerical package SUTRA and the SAO technique are in good agreement, only varying by about 2%. As such, results from SUTRA for this type of domain are given further confirmation. That is, given its quasi-analytical nature, and in the absence of a true analytical solution, the SAO technique may prove useful in validating numerical simulations.)

The $1D$ simplified equations are derived from an idealised rectangular domain with constant hydraulic conductivity, and as such can only approximate a real domain. That is, any real domain will not be perfectly rectangular and will likely have heterogeneities in the soil matrix that will affect the advection and diffusion processes. Given this fact, the errors presented in Table 8.1 seem acceptable for the purposes of estimation or rapid calculation in the field. If a correction is desired, then the extent of the region predicted to be contaminated from the pond boundary can easily be modified via the error values found in Table 8.1. For example, Figure 8.2 demonstrates a correction of 8% for the simplified advection and diffusion curves in Figure 8.1. However, given that there is some variation in the errors presented in Table 8.1, perhaps an easier approach is to simply assign, let's say, a 25% correction across the board. That is, $X_{corrected} = X(1 + 0.25)$ for any set of parameters or breakthrough contaminant concentration levels. This correction could be incorporated into the coefficients of the simplified $1D$ equations, resulting in a conservative estimate of the contaminant front for any situation.

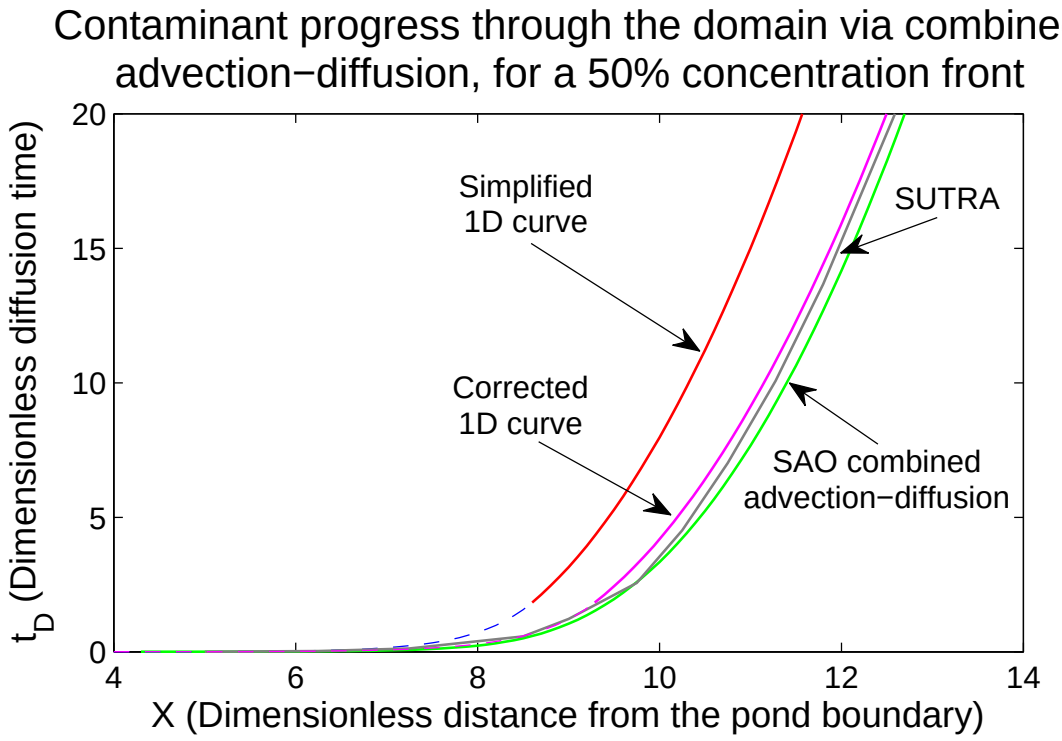

(a) Progress of contamination along the water table.

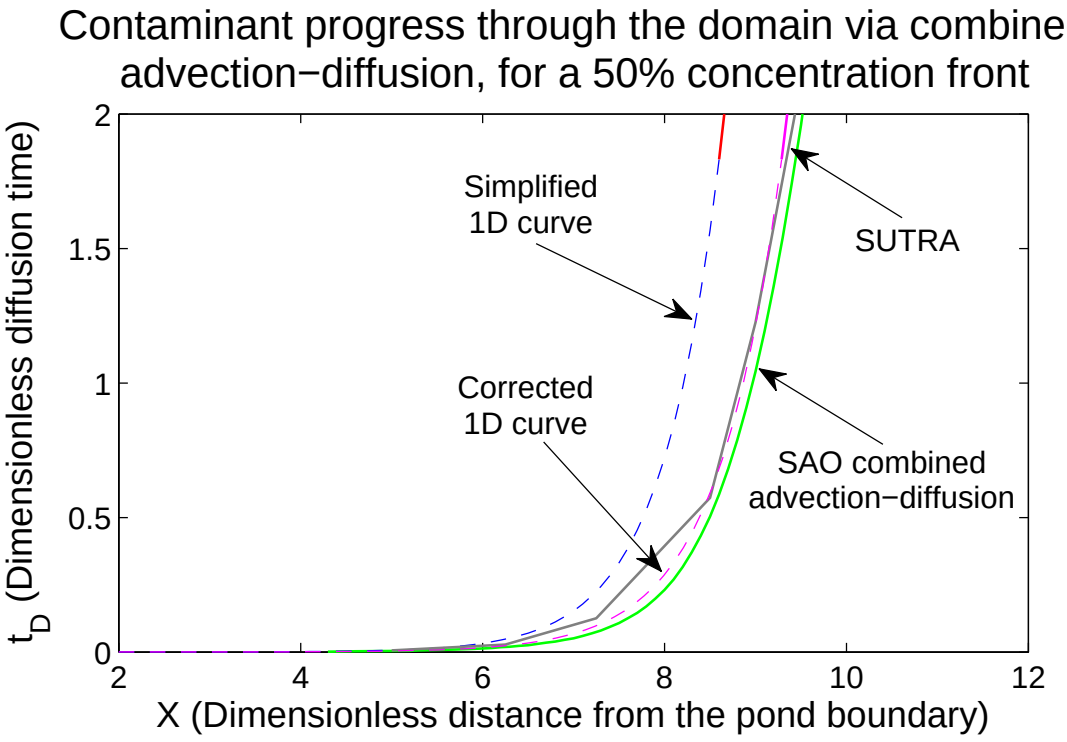

(b) Close up view: Progress of contamination along the water table.

FIGURE 8.2: Comparative contaminant progress along the water table via combined advection-diffusion, for the simplified $1D$ equations, corrected $1D$ equations, the split analytical operator technique, and SUTRA.

9

Discussion

9.1 Thesis summary

This thesis has explored quasi-analytical techniques for predicting contaminant transport via advection and diffusion beneath leaky saline ponds. In Chapter 2, the process of advection was considered, with a closed form solution for the potential function, stream function and velocity field derived via the series solutions method. Numerically integrating along different streamlines gave the location (or advection front) of salt water throughout the domain for any predefined upper time limit. The work of Chapter 2 was extended in Chapter 3 by introducing an improved numerical method for finding the advection fronts.

Chapter 4 examined the contribution of diffusion to contamination of groundwater from leaky saline ponds. A temporal discretisation was used to extend an analytical solution of pure diffusion to take into account a constant strength source condition. This was used to predict where and when diffusion becomes the dominant transport process over advection (using knowledge of the advection process gained in Chapter 2). A method was established to find when contamination occurs at any point in the aquifer, given knowledge of its physical parameters.

In Chapter 5, the quasi-analytical techniques from Chapters 3 and 4 were used to extensively model contamination beneath leaky saline ponds. From these results, useful simplified approximate equations were discovered which simplify the process of predicting the extent of contamination beneath leaky ponds. The equations incorporate both advection and diffusion, and provided the underlying simplifications (constant hydraulic conductivity, no density driven flow and a rectangular domain) are reasonable, the equations can accommodate ponds of variable height, aquifers of variable depth, and variable thresholds of contamination.

Chapter 6 combined the techniques developed in Chapters 2 and 4 to produce a novel quasi-analytical method for combined advection-diffusion. For ease of referral we called this the split analytical operator technique. This chapter departed from the familiar leaky contaminated pond problem in preference of a simpler domain; this was for demonstrative and explanatory purposes. The new method is based on the

split operator technique and the Semi-Lagrangian scheme, and combines analytical solutions of advection and diffusion. Using this technique it was also found that a reaction process of the contaminant could be easily incorporated.

Chapter 7 applied the split analytical operator technique derived in Chapter 6 to the leaky contaminated pond problem. This chapter realised the ultimate objective of this thesis, that is, an accurate solution for combined advection-diffusion beneath a leaky contaminated pond. Results from this quasi-analytical model were used in Chapter 8 to confirm the utility of the simplified $1D$ equations revealed in Chapter 5.

9.2 Future work

The results and techniques presented in this thesis have considerable scope for further investigation and/or development. The following suggestions are by no means exhaustive, but are ideas that occurred to the author during the course of this work.

Recall the simple $1D$ equations presented in Chapter 5. These equations only consider a rectangular domain with a constant hydraulic conductivity, and groundwater advection as a consequence of the height potential of the saline ponds. The point of these $1D$ equations is to simplify the modelling of the leaky pond problem, so it doesn't make sense to try to incorporate non-rectangular domains or variable hydraulic conductivity. Even if these infinite different scenarios could be included, the added complexity would render the resulting equations less intuitive, or practical, than a numerical modelling package. However, a useful addition would be to incorporate an underlying horizontal flow of groundwater. This should be possible using techniques similar to those presented in Chapters 2, 3 and 4.

For scenarios such as fresh groundwater sitting above a lower saline layer, described in Chapter 2, it should be possible to find empirical equations similar to those presented in Chapter 5. Such a situation would be complicated by diffusion from the lower saline layer; however, this lower (non-constant strength) diffusion source can be accommodated by the iterative diffusion technique from Chapter 4.

The split analytical operator method explored in Chapters 6 and 7 could potentially

be improved by using a different class of split operator technique. The sequential split operator method used in Chapters 6 and 7 is simple to understand and implement, but is only a 1st order scheme. The use of higher order schemes such as alternating or iterative split operator techniques should result in faster convergence towards the analytic solution.

So far, the split analytical operator technique has only been used with a constant diffusion coefficient. Recall that when applied to groundwater problems, the diffusion coefficient represents hydrodynamic dispersion, and is composed of two contributing factors: molecular diffusion (spatially constant) and mechanical mixing (spatially variable). By using a constant diffusion coefficient throughout this work, we assume that the contribution due to mechanical mixing is small. This is a reasonable assumption in groundwater problems with low flow rates (Hunt, 1983), such as that considered in this thesis; however, as this condition is not always met, it would be preferable to incorporate mechanical mixing into the general solution if possible. (Note, although there are high flow rates in some parts of the leaky pond domain, these are areas dominated by advective contamination which rapidly exits the boundary. The rest of the domain can be classed as having low flow rates.)

To incorporate mechanical mixing into the split analytical operator technique, recall that mechanical mixing occurs along the path of advective flow. As such, imagine the diffusion coefficient as having two components: a transverse component, D_T, which is perpendicular to the direction of advective movement; and a longitudinal component, D_L, which is along the direction of advective movement (Hunt, 1983). For uniform flow, that is, in the direction of one of the major axes, analytical solutions can be stretched to accommodate this scenario (see, for example, Appendix A.5), but for a $2D$ flow field such as that described by Figure 7.2, analytical solutions with spatially dependent diffusion are currently unavailable. However, considering the above definitions of D_T and D_L, let's define $D_T = D_*$ and $D_L = D_* + D_M$, where D_* is the molecular diffusion coefficient, and D_M is the contribution from mechanical mixing. Using this approach in conjunction with the split analytical operator technique, a potential method for solving spatially dependent diffusion presents itself.

In the split analytical operator technique, advection is solved along each streamline, then diffusion is solved globally using a constant coefficient. However, to incorporate spatially dependent diffusion, we need only add an additional diffusion step. That is, advection is solved along each streamline, then diffusion is solved globally using the constant diffusion coefficient, D_*, *then* diffusion is solved along each streamline using the diffusion coefficient, D_M. In this additional step, diffusion along each streamline is treated separately, and therefore becomes a $1D$ process, greatly simplifying the problem. However, the diffusion coefficient, D_M, is a function of velocity (Hunt, 1983), and therefore varies along the streamline. As such, the $1D$ diffusion process along each streamline will need to be solved for a variable diffusion coefficient, with all other required information, that is, the length, the concentration values, and velocity values along each streamline being obtainable from the previous steps of the split analytical operator technique.

9.3 Final remarks

This thesis has presented quasi-analytical techniques for solving advection and diffusion beneath leaky contaminated ponds. Quasi-analytical techniques are uncommon in mathematics, possibly because solutions are often exclusive to the particular problem being analysed; however, they provide a good option for improved accuracy when purely analytical methods are unavailable. The methods presented herein are potentially useful for validating traditional numerical techniques, or as solution schemes in their own right. In particular, the split analytical operator technique may provide a good alternative for solving the advection-diffusion equation, or its analogues, in fields such as hydrogeology, air pollution modelling, biology, semi-conductor physics, and even finance.

A

Appendices

A.1 Calculation of spline coefficients

$$\phi_*(x_*, d_*) = \begin{cases} d_*, & 0 \leq x_* \leq a_* \\ \alpha_3(x_*^3 - a_*^3) + \alpha_2(x_*^2 - a_*^2) & \\ \qquad +\alpha_1(x_* - a_*) + \alpha_0, & a_* < x_* \leq b_* \\ p_*, & b_* < x_* \leq r_* \end{cases} \tag{A.1}$$

A smooth transition from the water table to the pond height requires a gradient of zero at the points a_* and b_*, therefore,

$$\frac{d\phi_*}{dx_*} = 3x_*^2\alpha_3 + 2x_*\alpha_2 + \alpha_1 = 0.$$

Substituting $x_* = a_*$ and $x_* = b_*$ into the above equation gives

$$3a_*^2\alpha_3 + 2a_*\alpha_2 + \alpha_1 = 0, \tag{A.2}$$

$$3b_*^2\alpha_3 + 2b_*\alpha_2 + \alpha_1 = 0. \tag{A.3}$$

From the original equation (A.1) we also know that at $x_* = a_*$,

$$\phi_* = \alpha_3(a_*^3 - a_*^3) + \alpha_2(a_*^2 - a_*^2) + \alpha_1(a_* - a_*) + \alpha_0 = d_*.$$

Therefore,

$$\alpha_0 = d_*. \tag{A.4}$$

Substituting equation (A.4) into equation (A.1) at $x_* = b_*$,

$$\phi_* = \alpha_3(b_*^3 - a_*^3) + \alpha_2(b_*^2 - a_*^2) + \alpha_1(b_* - a_*) + d_* = p_*.$$

And rearranging,

$$(b_*^3 - a_*^3)\alpha_3 + (b_*^2 - a_*^2)\alpha_2 + (b_* - a_*)\alpha_1 = p_* - d_*. \tag{A.5}$$

From equations (A.2),(A.3) and (A.5), we now have a system of equations with unknowns α_1, α_2 and α_3,

$$\begin{bmatrix} 3a_*^2 & 2a_* & 1 \\ 3b_*^2 & 2b_* & 1 \\ (b_*^3 - a_*^3) & (b_*^2 - a_*^2) & (b_* - a_*) \end{bmatrix} \begin{bmatrix} \alpha_3 \\ \alpha_2 \\ \alpha_1 \end{bmatrix} = \begin{bmatrix} 0 \\ 0 \\ p_* - d_* \end{bmatrix}. \tag{A.6}$$

Solving the above system of equations using Cramer's rule gives

$$\alpha_3 = -2\frac{p_* - d_*}{(b_* - a_*)^3}, \qquad \alpha_2 = 3\frac{(b_* + a_*)(p_* - d_*)}{(b_* - a_*)^3},$$
$$\alpha_1 = -6\frac{a_* b_* (p_* - d_*)}{(b_* - a_*)^3}, \qquad \alpha_0 = d_*.$$

A.2 Analytic series solution for the diffusion problem

The solution to the diffusion equation (4.7) is assumed to be of the form

$$C(x, y, t) = X(x)Y(y)T(t), \tag{A.7}$$

which, after substitution into equation (4.7) and separating variables, leads to three ordinary differential equations in x, y and t:

$$X''(x) + \alpha^2 X(x) = 0, \quad Y''(y) + \beta^2 Y(y) = 0, \quad \dot{T}(t) + \lambda^2 T(t) = 0. \tag{A.8}$$

The homogeneous side boundary conditions in equation (4.8) become

$$X'(0) = X'(s), \qquad Y'(0) = Y'(1), \tag{A.9}$$

which, together with the differential equations (A.8) give eigenvalues

$$\alpha_m^2 = m^2\pi^2/s^2,\ m = 0, \ldots; \quad \beta_n^2 = n^2\pi^2,\ n = 0, \ldots; \quad \lambda_{mn}^2 = m^2\pi^2/s^2 + n^2\pi^2, \tag{A.10}$$

and eigenfunctions

$$X_m(x) = \cos\left(\frac{m\pi x}{s}\right); \quad Y_n(y) = \cos\left(n\pi y\right), \tag{A.11}$$

with

$$T_{mn}(t) = e^{-\lambda_{mn}^2 t}. \tag{A.12}$$

The analytic series solution to the diffusion equation (4.7) is the sum of the weighted modal solutions

$$\begin{aligned} C(x,y,t) &= \sum_{m=0}^{\infty}\sum_{n=0}^{\infty} a_{mn} X_m(x) Y_n(y) T_{mn}(t) \\ &= \sum_{m=0}^{\infty}\sum_{n=0}^{\infty} a_{mn} \cos\left(\frac{m\pi x}{s}\right) \cos\left(n\pi y\right) e^{-\lambda_{mn}^2 t}. \end{aligned} \tag{A.13}$$

A.3 Varying strength diffusion quadratics

Diffusive contamination will progress through an aquifer at different speeds, depending on what level of concentration is considered harmful. Below we present a plot of varying (quadratic) diffusion curves (from 1% to 90% of the pond concentration) for the domain of Figure 4.1. By considering each of the coefficients of these curves as a function of concentration (c^0), we generalise the equation of diffusion progress (4.19) to

$$t_{\mathrm{D}} = a_R(c^0)Z^2 + b_R(c^0)Z, \quad 0.01 \leq c^0 \leq 0.9, \tag{A.14}$$

where

$$a_R = e^{65.654(c^0)^5 - 147.446(c^0)^4 + 129.625(c^0)^3 - 53.062(c^0)^2 + 13.972(c^0) - 2.662} \tag{A.15}$$

and

$$b_R = e^{66.229(c^0)^5 - 148.716(c^0)^4 + 130.605(c^0)^3 - 53.374(c^0)^2 + 14.009(c^0) - 1.693}. \tag{A.16}$$

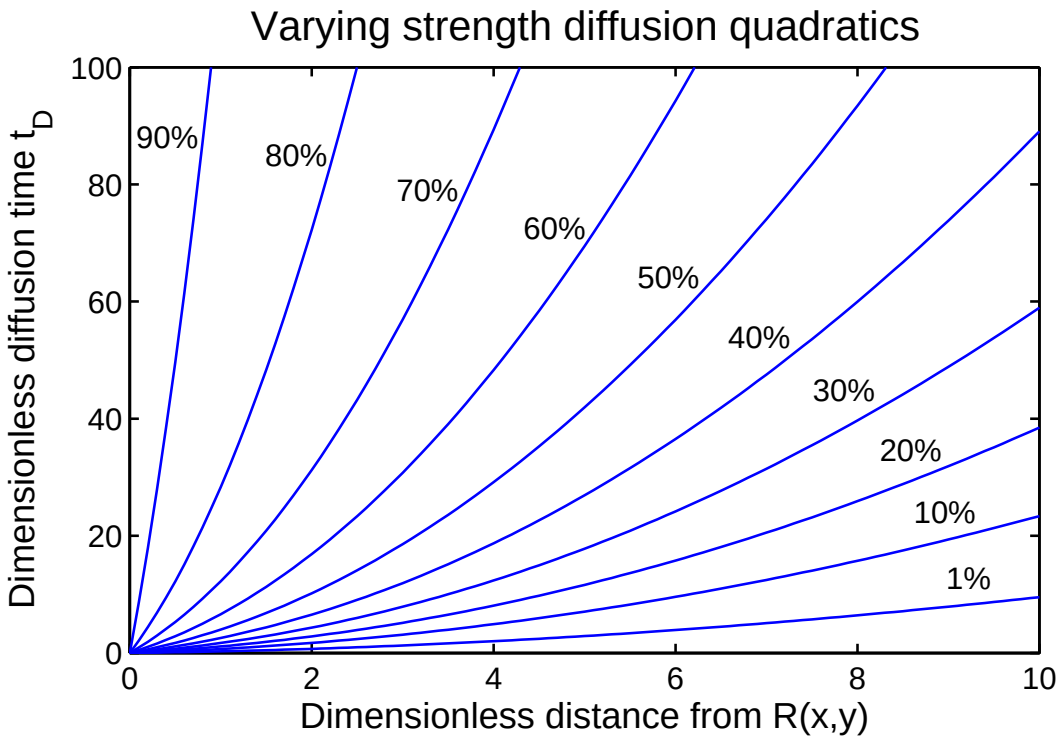

FIGURE A.1: Varying strength diffusion quadratics.

A.4 Advection coefficients as a function of δ

The advection equations found in the main body of this chapter assume a transition region between the water table and the height of the ponds of $X = \pm\delta$ (δ non-dimensionalised similarly to equation (5.3)). We wish to minimise the length of δ as much as possible. In this section, we explore the effect of changing the length of the transition region on the coefficients of equation (5.6), now rewritten with the coefficients as functions of δ,

$$t_{\mathrm{A}} = A(\delta)e^{B(\delta)X}. \tag{A.17}$$

Figure A.2 gives a schematic of the situation in question. The pond boundary ($X = 0$) is taken as the middle of the smooth transition zone, with the total length of this region being 2δ. Plotting the coefficients A and B (with $h = 1$) for various values of δ ($0.01 \leq \delta \leq 8$) produces Figure A.3. As can be seen, as δ decreases, the variation in the coefficients also decreases. Choosing the coefficients for the minimum value of δ available ($\delta = 0.01$) gives $A = 1.932$ and $B = 1.576$. For the sake of completeness, the following curves were fitted to the data:

$$A = \mathbf{Re}(1.95\, e^{-0.31(\delta-0.23)^{1.6}}), \tag{A.18}$$

where **Re** represents the real component of the complex number solution, and

$$B = -2.836 \times 10^{-4}\,\delta^3 + 2.301 \times 10^{-3}\,\delta^2 - 1.065 \times 10^{-2}\,\delta + 1.576. \tag{A.19}$$

There is an important point regarding the values of the coefficients in Figure A.3. They were calculated for streamlines emerging at the water table outside the influence of the transition region, that is, $X \geq \delta + 1$ (this is a conservative estimate of the lower bound). For $X < \delta + 1$, the effect of the transition region is to introduce a non-linearity into equation (A.17). (Investigation of this non-linearity is a potential future extension of the work in this chapter, with possible application to non-horizontal water tables.) An example of this non-linearity can be seen in Figure A.4. This is a plot of equation (A.17) for $\delta = 0.01$, that is, $A = 1.932$ and $B = 1.576$. As can be seen, the equation is

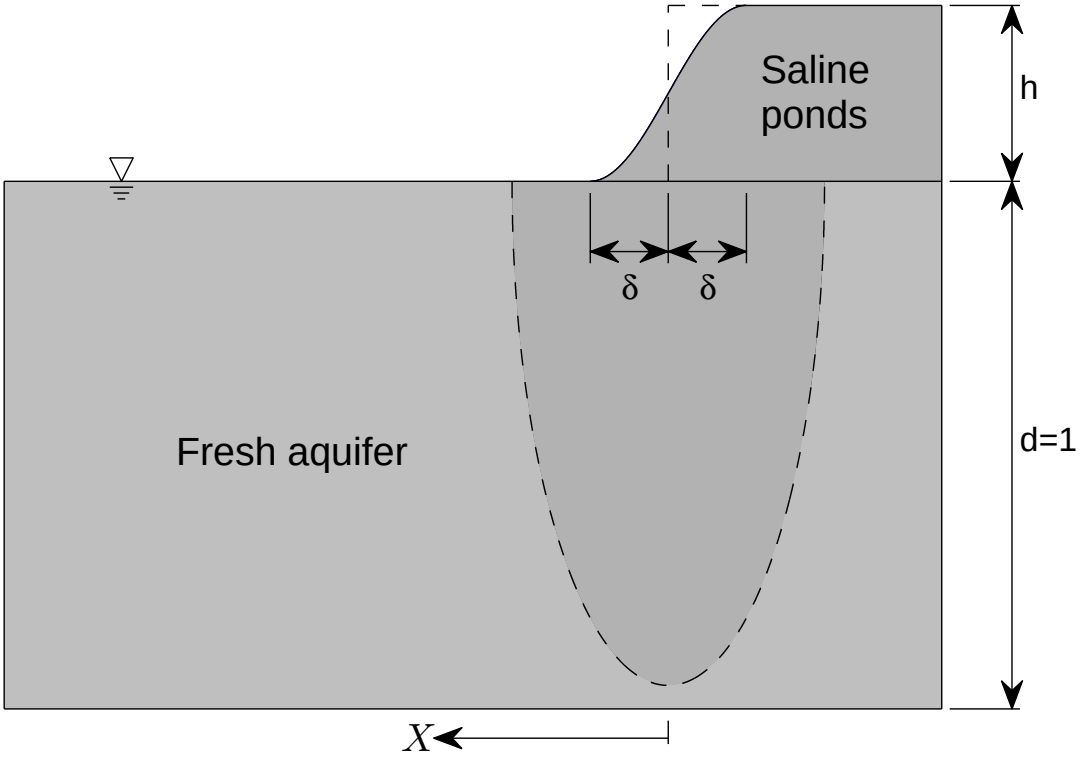

FIGURE A.2: Schematic showing the smooth transition between the height of the ponds and the water table.

only valid for $X \geq 1$.

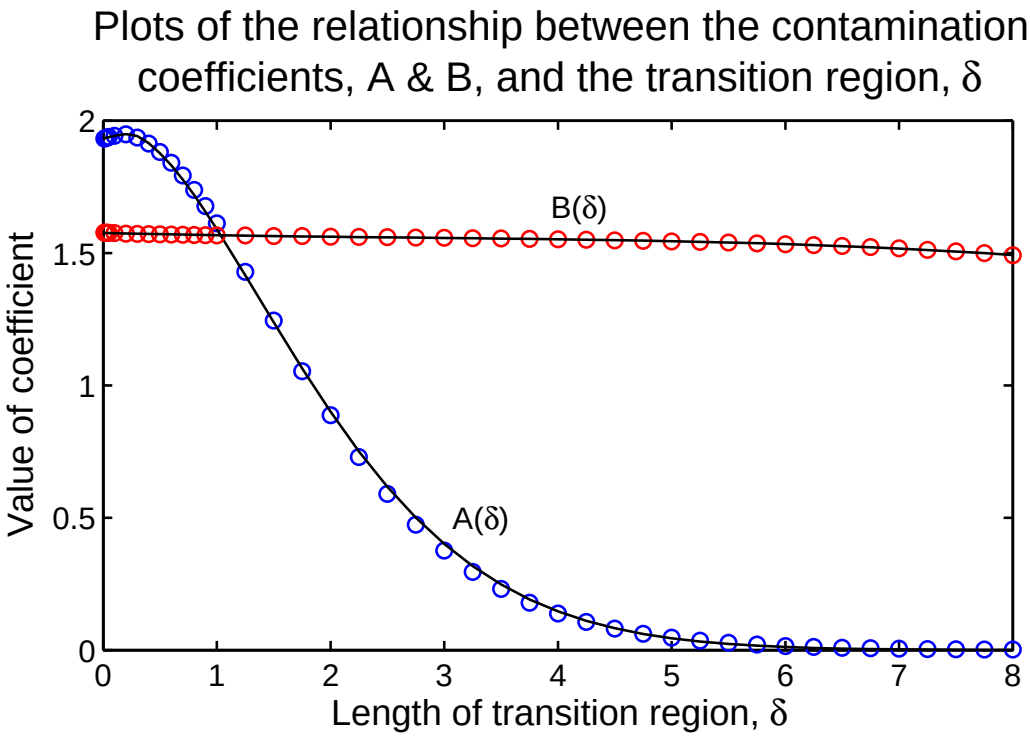

Figure A.3: Advection coefficients, A & B, and their relationship to the length of the transition region, δ.

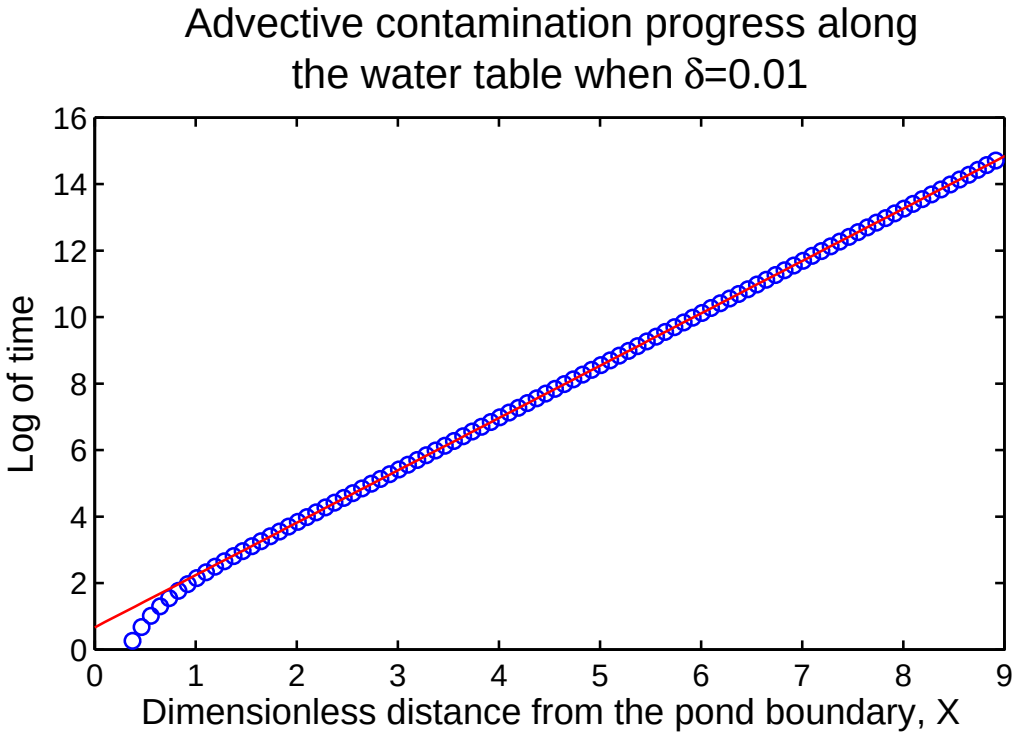

FIGURE A.4: Example demonstrating the lower bound of equation (A.17), as a result of the length of the transition region δ. The solid line is the fitted equation, with the data points representing the time and place each streamline emerges at the water table.

A.5 Analytic series solution of the ADR problem

$$\frac{\partial}{\partial x_*}\left(D_{x_*}\frac{\partial C_*}{\partial x_*}\right)+\frac{\partial}{\partial y_*}\left(D_{y_*}\frac{\partial C_*}{\partial y_*}\right)-u_*\frac{\partial C_*}{\partial x_*}-\lambda_* C_*=\frac{\partial C_*}{\partial t_*} \tag{A.20}$$

$$x_*=sx;\quad y_*=dy;\quad t_*=\tau t;\quad C_*=kC. \tag{A.21}$$

Therefore,

$$\frac{D_{x_*}k}{s^2}\frac{\partial^2 C}{\partial x^2}+\frac{D_{y_*}k}{d^2}\frac{\partial^2 C}{\partial y^2}-\frac{u_*k}{s}\frac{\partial C}{\partial x}-\lambda_* kC=\frac{k}{\tau}\frac{\partial C}{\partial t}. \tag{A.22}$$

Since k cancels, we can scale concentration C arbitrarily:

$$\frac{\partial^2 C}{\partial x^2}+\frac{s^2 D_{y_*}}{d^2 D_{x_*}}\frac{\partial^2 C}{\partial y^2}-\frac{s}{D_{x_*}}u_*\frac{\partial C}{\partial x}-\frac{s^2}{D_{x_*}}\lambda_* C=\frac{s^2}{D_{x_*}\tau}\frac{\partial C}{\partial t}. \tag{A.23}$$

We want

$$\frac{s^2}{d^2}\frac{D_{y_*}}{D_{x_*}}=1;\quad \frac{s^2}{D_{x_*}\tau}=1, \tag{A.24}$$

therefore,

$$s=\sqrt{\frac{D_{x_*}}{D_{y_*}}}d;\quad \tau=\frac{s^2}{D_{x_*}}=\frac{d^2}{D_{y_*}}. \tag{A.25}$$

Now, let

$$u=\frac{s}{D_{x_*}}u_*=\frac{d}{\sqrt{D_{y_*}D_{x_*}}}u_*;\quad \lambda=\frac{s^2}{D_{x_*}}\lambda_*=\frac{d^2}{D_{y_*}}\lambda_*. \tag{A.26}$$

Then equation (A.20) becomes

$$\nabla^2 C-u\frac{\partial C}{\partial x}-\lambda C=\frac{\partial C}{\partial t}. \tag{A.27}$$

Now, applying the transformation

$$C=ce^{\frac{ux}{2}} \tag{A.28}$$

into equation (A.27) gives the simplified form,

$$\nabla^2 c+\left(-\lambda-\frac{u^2}{4}\right)c=\frac{\partial c}{\partial t}. \tag{A.29}$$

The boundary conditions, $C = 0$ (as stated in Section 6.2) become $c = 0$ when substituted into equation (A.28), and likewise the initial condition becomes

$$c(x, y, 0) = C(x, y, 0)e^{-\frac{ux}{2}}. \tag{A.30}$$

Now, using the classic separation of variables approach, the solution of equation (A.29) is

$$c(x, y, t) = e^{-\left(\frac{u^2}{4}+\lambda\right)t} \sum_{n=1}^{N} \sum_{m=1}^{M} A_{mn} \sin\left(\frac{m\pi x}{s}\right) \sin\left(\frac{n\pi y}{d}\right) e^{-\gamma_{mn}^2 t}, \tag{A.31}$$

where

$$\gamma_{mn}^2 = \left(\frac{m^2}{s^2} + \frac{n^2}{d^2}\right) \pi^2, \tag{A.32}$$

and A_{mn} are the series expansion coefficients. These can be obtained in a similar manner as that described in Section 6.3.1, with the initial condition $c(x_i, y_j, 0)$ obtained from equations (6.4) and (A.30).

A.6 Calculation of mass within the system

The conservation of mass principle is often useful for testing the utility of numerical techniques. That is, a poor numerical scheme can artificially gain or lose significant mass within a system, affecting the accuracy of any results, and therefore subsequent conclusions. In Section 6.6 we presented results for the change in solute mass within the system for the constant velocity ADR problem, comparing the split analytical operator technique against a purely analytical solution. The calculation of mass within the system for the split analytical operator technique is simply the average of the concentration values at the grid points within the domain. The analytical calculation of mass follows on from Appendix A.5 and is presented below. The mass balance ratio is the analytical result divided by the split analytical operator result.

From Appendix A.5, we convert the solution (A.31) back to the original concentration variable $C(x, y, t)$ using equation (A.28):

$$C(x,y,t) = e^{-\left(\frac{u^2}{4}+\lambda\right)t} \sum_{n=1}^{N}\sum_{m=1}^{M} A_{mn}\left[e^{\frac{ux}{2}}\sin\left(\frac{m\pi x}{s}\right)\right]\sin\left(\frac{n\pi y}{d}\right)e^{-\gamma_{mn}^2 t}. \tag{A.33}$$

Next, find the integral of $\left[e^{\frac{ux}{2}}\sin\left(\frac{m\pi x}{s}\right)\right]$ using integration by parts:

$$\int e^{\frac{ux}{2}}\sin\left(\frac{m\pi x}{s}\right)dx = \frac{\frac{-s}{m\pi}\,e^{\frac{ux}{2}}\cos\left(\frac{m\pi x}{s}\right) + \frac{s^2}{m^2\pi^2}\frac{u}{2}\,e^{\frac{ux}{2}}\sin\left(\frac{m\pi x}{s}\right)}{1+\frac{s^2}{m^2\pi^2}\frac{u^2}{4}}. \tag{A.34}$$

We know the total solute within a system can be obtained by integrating the concentration function over the area of the domain,

$$m = \int_0^d\int_0^s C(x,y,t)\,dx\,dy. \tag{A.35}$$

Therefore, substituting and solving:

$$m = \int_0^d \int_0^s e^{-\left(\frac{u^2}{4}+\lambda\right)t} \sum_{n=1}^{N}\sum_{m=1}^{M} A_{mn}\left[e^{\frac{ux}{2}}\sin\left(\frac{m\pi x}{s}\right)\right]\sin\left(\frac{n\pi y}{d}\right) e^{-\gamma_{mn}^2 t}\, dx\, dy \tag{A.36}$$

$$= \int_0^d e^{-\left(\frac{u^2}{4}+\lambda\right)t} \sum_{n=1}^{N}\sum_{m=1}^{M} A_{mn} \cdots \times \left[\frac{\frac{-s}{m\pi}\, e^{\frac{ux}{2}}\cos\left(\frac{m\pi x}{s}\right) + \frac{s^2}{m^2\pi^2}\frac{u}{2}\, e^{\frac{ux}{2}}\sin\left(\frac{m\pi x}{s}\right)}{1+\frac{s^2}{m^2\pi^2}\frac{u^2}{4}}\right]\sin\left(\frac{n\pi y}{d}\right) e^{-\gamma_{mn}^2 t}\Bigg|_0^s dy \tag{A.37}$$

$$= \int_0^d e^{-\left(\frac{u^2}{4}+\lambda\right)t} \sum_{n=1}^{N}\sum_{m=1}^{M} A_{mn}\left(\frac{s}{m\pi}\right)\frac{\left[1-e^{\frac{us}{2}}\cos(m\pi)\right]}{\left(1+\frac{s^2}{m^2\pi^2}\frac{u^2}{4}\right)}\sin\left(\frac{n\pi y}{d}\right) e^{-\gamma_{mn}^2 t}\, dy \tag{A.38}$$

$$= e^{-\left(\frac{u^2}{4}+\lambda\right)t} \sum_{n=1}^{N}\sum_{m=1}^{M} A_{mn}\left(\frac{-sd}{mn\pi^2}\right)\frac{\left[1-e^{\frac{us}{2}}\cos(m\pi)\right]}{\left(1+\frac{s^2}{m^2\pi^2}\frac{u^2}{4}\right)}\cos\left(\frac{n\pi y}{d}\right) e^{-\gamma_{mn}^2 t}\Bigg|_0^d \tag{A.39}$$

$$= e^{-\left(\frac{u^2}{4}+\lambda\right)t} \sum_{n=1}^{N}\sum_{m=1}^{M} A_{mn}\left(\frac{sd}{mn\pi^2}\right)\frac{\left[1-e^{\frac{us}{2}}\cos(m\pi)\right]\left[1-\cos(n\pi)\right]}{\left(1+\frac{s^2}{m^2\pi^2}\frac{u^2}{4}\right)}\, e^{-\gamma_{mn}^2 t}. \tag{A.40}$$

Equation (A.40) gives the total mass within the domain at any time for the constant velocity ADR problem.

A.7 Optimised number of split steps

The split analytical operator method becomes more accurate as the number of split steps (discrete time intervals) is increased (Section 6.5). In general, this is also the case for any technique that discretises the solution domain, such as finite difference and finite element methods. Typically for these methods, as the discrete spacing is decreased, the computation time increases. That is, as the discrete interval approaches zero, the computation time tends to infinity. As such, computation time considerations often determine when a solution is 'good enough'.

However, the combined advection-diffusion solution in Chapter 7 is a little different. As the number of split steps, L, initially increase, the computation time actually decreases. This trend continues to a minimum, after which the computation time increases in the manner of the traditional discretised schemes described above. In the absence of an *a priori* estimate of when a solution is 'good enough', it seems reasonable to initially choose the solution with the minimum computation time.

For an advection only solution, the most computationally expensive aspect is stepping numerically (using δt_{A}) along the streamlines. For the combined advection-diffusion solution described in Section 7.4, after finding the endpoint of advection for the first interval, all the other intervals' advection components are incorporated into the diffusion process (refer to Section 7.4 for details). We wish to find the optimal (fastest) solution for combined advection-diffusion given that we must do a certain number of advection iterations, whether they are true numerical advection steps or diffusion substitutes.

Let N_t be the theoretical total number of advection iterations required (if diffusion wasn't part of the solution), N_a be the number of actual advection iterations, and N_d be the number of diffusion substitutes (or effectively, the number of intervals). Similarly, let T_t be the total computation time to solve the problem, T_a be the computation time for one numerical advection iteration, and T_d be the computation time for one diffusion iteration. We also know

$$N_d = \frac{N_t}{N_a} \; ; \quad T_d = \omega T_a, \tag{A.41}$$

where ω is the constant of proportionality (ratio) between the solution times of the two different processes. That is, once the algorithm is set up, we find the computation time to solve one advection iteration, T_a, and one diffusion iteration, T_d, with ω resulting from equation (A.41). So,

$$T_t = N_a T_a + N_d T_d \tag{A.42}$$

$$= N_a T_a + \frac{(N_t \omega T_a)}{N_a}. \tag{A.43}$$

Since we want to minimise the total computation time, let's differentiate with respect to the unknown, N_a, and equate to zero,

$$\frac{dT_t}{dN_a} = T_a - (N_t \omega T_a) N_a^{-2} = 0. \tag{A.44}$$

Therefore,

$$T_a = \frac{N_t \omega T_a}{N_a^2} \tag{A.45}$$

$$N_a = \pm\sqrt{\frac{N_t \omega T_a}{T_a}}, \qquad N_a \neq -ve \tag{A.46}$$

$$N_a = \sqrt{N_t \omega} \tag{A.47}$$

with equation (A.41) giving N_d.

If we wish to solve for an overall time period of, say, $t_{\mathrm{A}} = 200,000$ dimensionless time units using a numerical advection time step of $\delta t_{\mathrm{A}} = 10$ dimensionless units, then we would require $N_t = 20,000$ theoretical advection iterations (whether actual or diffusion substitutes). N_t is therefore a known quantity. Likewise, T_a and T_d (and therefore ω) can be quickly calculated before attempting to solve the combined advection-diffusion problem. It is a simple matter then to work out the number of intervals, N_d, for the fastest possible solution. (Of course, the practical value of N_d used will have to be the closest factor of N_t.) Finally, if the value of t_{A} required is not a convenient number such as $200,000$, then N_t can be made factorisable by simply choosing a smaller (less rounded) numerical advection time step (hypothetically, for example, $\delta t_{\mathrm{A}} = 9.23874$).

List of symbols

The following list is neither exhaustive nor exclusive, but may be helpful. Note that variables/parameters with an asterisk subscript are dimensional, while those without are non-dimensional.

K_* ..... hydraulic conductivity

ϕ, ϕ_*, h^t, h^t_* .... hydraulic head

ψ, ψ_* ..... stream function

$\mathbf{u}$, $\mathbf{u}_*$ ..... seepage velocity

$\mathbf{U}$, $\mathbf{U}_*$ ..... pore velocity

σ ..... porosity

r, r_*, s, s_* ..... length of domain

d, d_* ..... height of domain

h, h_* ..... height of ponds above water table

D_* ..... diffusion/dispersion coefficient

C^0_* ..... concentration of the saline ponds

α ..... characteristic aquifer parameter

q_x, q_{x*} ..... specific discharge at X

Q_x ..... average flux of contaminated outflow

$\overline{Q}$, $\overline{Q}_*$ ..... total volume of contaminated outflow

δ ..... half length of transition region between the surface of the ponds and the water table

References

Anderson, M. P., Woessner, W. W. & Hunt, R. J. (2015). *Applied groundwater modeling: Simulation of flow and advective transport* (Second). Academic Press. ISBN: 0120581035.

Arunakumaren, N. J., McMahon, B. A. & Bajracharya, K. (2000). *Water management in the lower Burdekin: Groundwater model conceptualisation*. Dept Natural Resources and Mines, Qld, Australia.

Bear, J. (1972). *Dynamics of fluids in porous media*. New York: American Elsevier. ISBN: 0486656756.

Bear, J. (1979). *Hydraulics of groundwater*. New York: McGraw-Hill. ISBN: 0486453553.

Bear, J. (Ed.). (1999). *Seawater intrusion in coastal aquifers*. Springer.

Bennett, B. (1998). Rising salt: a test of tactics and techniques. *ECOS*, *96*, 10–13.

Bouwer, H. (2000). Integrated water management: emerging issues and challenges. *Agricultural Water Management*, *45*(3), 217–228. DOI: 10.1016/S0378-3774(00)00092-5

Bristow, K. L., Narayan, K. A., Kemei, J. K. & Charlesworth, P. B. (2006). *Groundwater level and salinity in the Trent Road area, North Burdekin Water Board: An update to June 2005*. CSIRO Land and Water.

Broadbridge, P., Hill, J. M. & Goard, J. M. (2000). Symmetry reductions of equations for solute transport in soil. *Nonlinear Dynamics*, *22*(1), 15–27. DOI: 10.1023/A:1008309107295

Carrier, G. F., Krook, M. & Pearson, C. E. (1966). *Functions of a complex variable*. McGraw-Hill.

Craig, J. R. & Heidlauf, T. (2009). Coordinate mapping of analytical contaminant transport solutions to non-uniform flow fields. *Advances in Water Resources*, *32*(3), 353–360. DOI: 10.1016/j.advwatres.2008.11.013

Csomos, P., Farago, I. & Havasi, A. (2005). Weighted sequential splittings and their analysis. *Computers & Mathematics with Applications*, *50*(7), 1017–1031. DOI: 10.1016/j.camwa.2005.08.004

Farlow, S. J. (1993). *Partial differential equations for scientists and engineers*. Mineola, New York: Dover Publications. ISBN: 048667620X.

Fetter, C. W. (2001). *Applied hydrogeology*. Upper Saddle River, N.J: Prentice-Hall. ISBN: 0130882399.

Gasda, S. E., Farthing, M. W., Kees, C. E. & Miller, C. T. (2011). Adaptive split-operator methods for modeling transport phenomena in porous medium systems. *Advances in Water Resources*, *34*(10), 1268–1282. DOI: 10.1016/j.advwatres.2011.06.004

Hamming, R. W. (1977). *Digital filters*. Englewood Cliffs: Prentice-Hall.

Hundsdorfer, W. & Verwer, J. G. (2003). *Numerical solution of time-dependent advection-diffusion-reaction equations*. Springer. ISBN: 3540034404.

Hunt, B. (1983). *Mathematical analysis of groundwater resources*. London, Boston: Butterworths. ISBN: 0408013990.

Jakeman, A. J., El Sawah, S., Guillaume, J. H. A. & Pierce, S. A. (2011). Making progress in integrated modelling and environmental decision support. In J. Hrebicek, G. Schimak & R. Denzer (Eds.), *Environmental software systems: Frameworks of eEnvironment* (Vol. 359, pp. 15–25). IFIP Advances in Information and Communication Technology. Springer-Verlag Berlin.

Lanser, D. & Verwer, J. G. (1999). Analysis of operator splitting for advection-diffusion-reaction problems from air pollution modelling. *Journal of Computational and Applied Mathematics*, *111*(1-2), 201–216. DOI: 10.1016/S0377-0427(99)00143-0

Liu, C. W., Lin, K. H., Chen, S. Z. & Jang, C. S. (2003). Aquifer salinization in the Yun-Lin coastal area, Taiwan. *Journal of the American Water Resources Association*, *39*(4), 817–827.

Mehmani, Y. & Balhoff, M. T. (2014). Generalized semi-analytical solution of advection-diffusion-reaction in finite and semi-infinite cylindrical ducts. *International Journal of Heat and Mass Transfer*, *78*, 1155–1165. DOI: 10.1016/j.ijheatmasstransfer.2014.07.082

Philip, J. R. (1984). Travel-times from buried and surface infiltration point sources. *Water Resources Research*, *20*(7), 990–994. DOI: 10.1029/WR020i007p00990

Powers, W. L., Kirkham, D. & Snowden, G. (1967). Orthonormal function tables and the seepage of steady rain through soil bedding. *Journal of Geophysical Research*, *72*(24), 6225–6237. DOI: 10.1029/JZ072i024p06225

Read, W. W. (1996a). Hillside seepage and the steady water table. 1: Theory. *Advances in Water Resources*, *19*(2), 63–73. DOI: 10.1016/0309-1708(95)00034-8

Read, W. W. (1996b). Hillside seepage and the steady water table. 2: Applications. *Advances in Water Resources*, *19*(2), 75–81. DOI: 10.1016/0309-1708(95)00035-6

Read, W. W. & Volker, R. E. (1993). Series solutions for steady seepage through hillsides with arbitrary flow boundaries. *Water Resources Research*, *29*(8), 2871–2880.

Reddy, S. C. & Trefethen, L. N. (1994). Pseudospectra of the convection-diffusion operator. *Siam Journal on Applied Mathematics*, *54*(6), 1634–1649.

Simmons, C. T. & Narayan, K. A. (1998). Modelling density-dependent flow and solute transport at the Lake Tutchewop saline disposal complex, Victoria. *Journal of Hydrology*, *206*(3-4), 219–236.

Stoessell, R. K. & Hanor, J. S. (1975). Nonsteady state method for determining diffusion-coefficients in porous-media. *Journal of Geophysical Research-Oceans and Atmospheres*, *80*(36), 4979–4982.

Strang, G. (1986). *Introduction to applied mathematics*. Wellesley-Cambridge Press. ISBN: 0961408804.

Tompson, A. F. B. & Dougherty, D. E. (1990). Particle-grid methods for reacting flows in porous media: Application to Fisher's equation. In G. Gambolati, A. Rinaldo, C. A. Brebbia, W. G. Gray & G. F. Pinder (Eds.), *Computational methods in*

subsurface hydrology (Vol. 1, pp. 393–398). Computational Mechanics Publications.

Trefethen, L. N. (2000). *Spectral methods in Matlab*. Philadelphia: Siam.

USGS. (2005). MODFLOW, the U.S. Geological Survey modular ground-water model. USGS, Reston, VA.

Valocchi, A. J. & Malmstead, M. (1992). Accuracy of operator splitting for advection-dispersion-reaction problems. *Water Resources Research*, *28*(5), 1471–1476. DOI: 10.1029/92WR00423

Verrall, D. P. & Read, W. W. (2012). Predicting diffusion in aquifers beneath saline ponds. *Journal of Hydrology*, *475*, 150–157. DOI: 10.1016/j.jhydrol.2012.09.046

Verrall, D. P. & Read, W. W. (2015). A quasi-analytical approach to the advection-diffusion-reaction problem, using operator splitting. *Applied Mathematical Modelling*. DOI: 10.1016/j.apm.2015.07.023

Verrall, D. P., Read, W. W. & Narayan, K. A. (2009a). Computational aspects of accurately modelling salt advection beneath aquaculture ponds. In W. W. Read, J. W. Larson & A. J. Roberts (Eds.), *Proceedings of the 13th biennial computational techniques and applications conference, CTAC-2006* (Vol. 48, pp. C1075–C1089). ANZIAM J.

Verrall, D. P., Read, W. W. & Narayan, K. A. (2009b). Predicting salt advection in groundwater from saline aquaculture ponds. *Journal of Hydrology*, *364*(3-4), 201–206. DOI: 10.1016/j.jhydrol.2008.10.022

Voss, C. I. & Provost, A. M. (2002). SUTRA, a model for saturated-unsaturated variable-density ground-water flow with solute or energy transport. Water Resources Report 02-4231. USGS, Reston, VA.

Zoppou, C. & Knight, J. H. (1999). Analytical solution of a spatially variable coefficient advection-diffusion equation in up to three dimensions. *Applied Mathematical Modelling*, *23*(9), 667–685. DOI: 10.1016/S0307-904X(99)00005-0